structure of the stopping atoms introduce great theoretical complications, the empirical energy-loss behavior is best described by a smooth deviation from formula (9.2.5).

For the lowest velocities of importance, another approach has been taken to obtain reliable stopping data for emulsion. Whaling (W 58) has compiled empirical data from many sources for the stopping cross section of low-energy protons in various elements. When expressed as cross sections per electron these data yield rather smooth curves as functions of atomic number and velocity. Interpolating as necessary, Whaling's data were used to construct a rate of energy-loss curve for protons in a material having the composition of standard emulsion. The information from these various sources has been combined to yield the data of Table 9.2.2. The averaging effect of the several elements in emulsion probably increases the reliability of the low-energy data, and it joins smoothly to that measured at higher velocities.

It will be noticed that $w_{\max}$, as given by Eq. (9.1.2), depends explicitly on the particle mass. In order to produce a table independent of mass, the approximation $w_{\max} = 2mc^2\beta^2\gamma^2$ was used in calculating Table 9.2.2. At the highest particle velocities this begins to introduce an appreciable error for mesons which, however, is to a large extent compensated by the radiation energy-loss experienced by these particles.

Different solid phases of an element, or compounds of it with different chemical binding energies, are expected to have different stopping powers, especially for low-energy particles. There is a theory (LS 53, B 60.3) of this effect and also some experimental results. In a recent experiment of Softky (S 61.2) it was found that the atomic stopping power of graphite exceeds that of diamond by 6% for 1.1 Mev protons.

The energy-loss rate of charged particles in an absorbing material and the attenuation of electromagnetic radiations in the same absorber are fundamentally the same process. Therefore, the processes discussed in Chapter 5 (Volume II) and these of Chapter 9 are closely related.

9.3 Energy-Loss Rates of Electrons and Positrons

The electron-electron and positron-electron collision cross sections deviate significantly from Eq. (9.1.1) for large-energy transfers. The meaning of $w_{\max}$ must also be modified for electrons because incident and target electrons are indistinguishable. In an electron-electron collision the original kinetic energy, T, is divided between two electrons, so that one has energy w and the other $T - w$.

The differential energy-transfer cross section calculated by Møller (M 32) for this process is:

$$\frac{d\sigma}{dw}\,dw = \frac{2\pi r_0^2 mc^2}{\beta^2}\left[\left(\frac{T}{w(T-w)} - \frac{1}{T}\right)^2 + \frac{1-2\gamma}{\gamma^2 T}\left(\frac{T}{w(T-w)} + \frac{1}{T}\right)\right] dw \tag{9.3.1}$$

Here $0 < w < T/2$, since the electron of lower energy is defined to be the delta ray. When γ is large the second term inside the square brackets is generally neglected. The integral $\mathscr{I}_2$ (Section 9.2) for the electron is

$$\mathscr{I}_2 = \frac{2\pi n r_0^2 mc^2}{\beta^2}\left[\ln\left(\frac{2mc^2\beta^2\gamma^2 w_0}{I^2}\right) - \beta^2 - 2C\right] \tag{9.3.2}$$

—the same as for a heavy particle. For the high energy approximation:

$$\mathscr{I}_1 = \frac{2\pi r_0^2 mc^2 n}{\beta^2}\int_{w_0}^{T/2}\left(\frac{1}{w} + \frac{w}{T(T-w)}\right)^2 w\,dw \tag{9.3.3}$$

When $\beta \to 1$:

$$\mathscr{I}_1 \approx \frac{2\pi r_0^2 mc^2 n}{\beta^2}\left[\ln\frac{T}{4w_0} + \frac{9}{8}\right] \tag{9.3.4}$$

Therefore, with $\beta^2 \approx 1$ the ionization energy-loss rate of an electron is:

$$\mathscr{I} \approx \frac{2\pi r_0^2 mc^2 n}{\beta^2}\left[\ln\frac{2mc^2\beta^2\gamma^2 T}{I^2} + \frac{1}{8} - 2(\ln 2) - 2C\right] \tag{9.3.5}$$

On the other hand, the energy-transfer cross section from a positron to an electron in the high-energy approximation is:

$$\frac{d\sigma}{dw}\,dw = \frac{2\pi r_0^2 mc^2 n}{\beta^2}\left[1 - \frac{w}{T} + \left(\frac{w}{T}\right)^2\right]^2 \frac{dw}{w^2} \tag{9.3.6}$$

In close collisions, the positron may sustain any energy loss from w_0 to T. We then find that for a positron:

$$\mathscr{I}_1 \approx \frac{2\pi r_0^2 mc^2 n}{\beta^2}\left[\ln\left(\frac{T}{w_0}\right) - \frac{11}{12}\right] \tag{9.3.7}$$

so that with $\beta \approx 1$:

$$\mathscr{I} \approx \frac{2\pi r_0^2 mc^2 n}{\beta^2}\left[\ln\left(\frac{2mc^2\beta^2\gamma^2 T}{I^2}\right) - \frac{23}{12} - 2C\right] \tag{9.3.8}$$

The differences in the ionization energy-loss rates for various fast singly charged particles all arise from differences in the cross sections for large energy transfer.

For standard emulsions the quantity $2\pi r_0^2 mc^2 n$ is 0.2663 Mev/cm and $I \approx 331$ ev. The quantity C is obtained from Table 9.2.1.

The proportion of the electron energy that is lost in the form of radiation rises rapidly as the electron energy increases, and at all high energies the radiation loss dominates. This affects the appearance of the electron track hardly at all, however. Occasional positron-electron pairs are observed adjacent to the track, and tridents on the trajectory itself are sometimes seen. Additional processes by which the energy of a fast electron or positron is dissipated are treated in Chapter 5 (Volume II).

All the known energy-loss effects in emulsion were added to obtain the electron and positron range tables given in Chapter 10.

9.4 Energy-Loss Rate of a Heavy, Multiply Charged Ion

An ion of net charge $z'e$ and nuclear charge ze has a radius R outside of which the electric field of the ion (except for electric multipole terms) resembles that of a point charge of magnitude $z'e$. Within this radius, the field rises more than in proportion to the inverse square of the radius, and near the nucleus the field approximates that of a point charge, ze. Consequently, the differential cross section, Eqs. (9.1.1) and (9.1.5), must be modified for ionic collisions with electrons. Rather a separate question is the distribution of z' at each velocity. This topic is briefly treated below.

For modifying the differential collision cross section to the required accuracy, it may suffice to use the Born approximation. Following Mott and Massey (MM 49) one introduces a parameter K given by

$$K = (2/\lambda\!\!\!^{-}) \sin(\chi/2) \tag{9.4.1}$$

where $\lambda\!\!\!^{-}$ is the electron radian length, $\lambda/2\pi$.

To describe the screening effect of the electron cloud on the scattering of an electron, an ionic form-factor is defined. It is:

$$F(K) = \frac{4\pi}{K} \int_0^R r\rho(r) (\sin Kr)\, dr \tag{9.4.2}$$

in which $\rho(r)$ is the electron density in the ion.

Suppose we take the origin in the rest frame of the ion. Then, particularly if the stopping material is of low atomic number, the stopping

electrons can be assumed to make free collisions with the ion as a scattering center. The cross section for scattering an electron through angle χ into the interval $d\chi$ is then:

$$2\pi(\sin\chi)\,\sigma(\chi)\,d\chi = \frac{\pi r_0^2}{2\beta^4}(z-F)^2\csc^4(\chi/2)\sin\chi\,d\chi \tag{9.4.3}$$

The energy in the laboratory frame absorbed by the electron in the scattering event is $w = 4t\sin^2(\chi/2)$, where t is the kinetic energy of the electron in the rest frame of the ion. Therefore, the energy lost per unit path in close collisions is:

$$\mathscr{J}_1^* = \frac{4\pi r_0^2 nmc^2}{\beta^2}\int_{\chi_1}^{\pi}(z-F)^2\cot(\chi/2)\,d(\chi/2) \tag{9.4.4}$$

The angle χ_1 is related to the energy transfer, w_1, to an electron whose distance of closest approach is just equal to the ion radius [$w_1 = 4t\sin^2(\chi_1/2)$].

A fairly well-established principle of Bohr (B 48.1) is that the most loosely bound electron in the ion has a velocity about equal to that of the ion itself with respect to the absorbing material. This is the velocity $\beta = (2t/mc^2)^{1/2}$. From the virial theorem, the kinetic energy, $(mc^2/2)\beta^2$, of the most loosely bound electron in the ion also is about $z'e^2/2R$, so that $R \approx z'r_0/\beta^2$, where $r_0 = e^2/mc^2$, and β is neither very small nor very large.

Therefore $w_1 = t = (mc^2/2)\beta^2$, and the lower limit of integration is $\pi/3$.

$$\mathscr{J}_1^* \approx \frac{4\pi n r_0^2 mc^2}{\beta^2}\int_{(\chi=\pi/3)}^{\pi}(z-F)^2\cot(\chi/2)\,d(\chi/2) \tag{9.4.5}$$

The form factor, F, can be fitted approximately (TU 57) by the following function: $F = (z-z')/(1+a\xi)$, where ξ is the Bethe variable, $\xi_1\sin(\chi/2)$, with $\xi_1 = (10^8\lambda z^{1/3})^{-1}$. The magnitude of a is about six. Then also, $\cot(\chi/2)d(\chi/2) = d\xi/\xi$. With this substitution, Eq. (9.4.5) is readily integrated:

$$\mathscr{J}_1^* = \frac{4\pi z'^2 n r_0^2 mc^2}{\beta^2}\left[\ln 2 + \left(\frac{z^2}{z'^2}-1\right)\left(\ln\frac{1+a\xi_1}{1+(a\xi_1/2)}\right) - \left(\frac{z}{z'}-1\right)^2\frac{a\xi_1}{(2+a\xi_1)(1+a\xi_1)}\right] \tag{9.4.6}$$

This formula is to be compared with Eq. (9.2.2) for $\mathscr{J}_1'$ evaluated for a point charge $z'e$ and with $w_0 = t$. The limits on χ correspond to $w_{\max}/w_0 = 4$. The difference $\mathscr{J}_1^* - \mathscr{J}_1'$ is

$$\mathscr{J}_1^* - \mathscr{J}_1' \approx \frac{4\pi z'^2 n r_0^2 mc^2}{\beta^2}\left[\left(\frac{z^2}{z'^2} - 1\right)\left(\ln\frac{1 + a\xi_1}{1 + (a\xi_1/2)}\right)\right.$$

$$\left. - \left(\frac{z}{z'} - 1\right)^2 \frac{a\xi_1}{(2 + a\xi_1)(1 + a\xi_1)}\right] \quad (9.4.7)$$

This expression also is equal to the difference $\mathscr{J}^* - \mathscr{J}'$ of the total rates of energy loss because the formula for the distant collisions is the same for an ion and a point particle of equal net charge.

When $a\xi_1 \gg 1$, we can write

$$\mathscr{J}^* - \mathscr{J}' \approx \frac{4\pi n r_0^2 mc^2 (z^2 - z'^2) \ln 2}{\beta^2}$$

which is independent of $a\xi_1$.

In emulsion the difference is

$$\mathscr{J}^* - \mathscr{J}' \approx \frac{0.37(z^2 - z'^2)}{\beta^2} \text{ Mev/cm} \quad (9.4.8)$$

As a numerical example, we may apply this estimate to an argon ion. Consider the rate of energy loss of argon near its maximum at $\beta^2 \approx 0.0048$. Here $a\xi_1 \approx 7.3$ and $\mathscr{J}^* \approx 5 \times 10^4$ Mev/cm (H-B 60). At this velocity $\mathscr{J}^* - \mathscr{J}' \approx 1.2 \times 10^3$ Mev/cm—only 2.4% of $\mathscr{J}^*$. Because the difference is this small, it is often unnecessary to distinguish between z' and z^*, the effective charge for energy loss. In treating problems of electron capture, nonrelativistic formulas are applicable because for capture to occur, the ion velocity must be low.

Equation (9.4.5) contains no terms corresponding to electron inelastic and exchange scattering on the ion. Such effects certainly exist, but it is argued that they will always be small because the electrons remaining with the ion have binding energies exceeding the kinetic energy of the incident electron in the ionic frame of reference. One must not forget, however, that at low velocities of the incident electron, the Born approximation is unreliable. Equation (9.4.7), therefore, must be applied with caution until it is more completely verified by experiment. At present it is known only to be correct in order of magnitude.

As mentioned above, Bohr considered z' to be determined by the condition that the slowest electrons retained by the ion must have

root-mean-square velocities relative to the ion higher than the ion velocity in matter. Knipp and Teller (KT 41) used this assumption along with a statistical ion model to calculate z'. Bohr's hypothesis appears to be reasonably good irrespective of what the stopping material is. It is now known, however, from the work of Lassen (L 51.1) that the average charge carried by an ion is lowered when the stopping material is a gas of low density, for then excited electrons may go to the ground state by radiation between collisions. More electrons, then, tend to be carried by the ion.

Papineau (P 56.1) collected data on the effective charge of ions with $3 \leqq z \leqq 10$ measured at various velocities. He found that the ratio of the effective charge to the nuclear charge is about the same function of $\beta/z^{2/3}$ irrespective of the ion or the stopping material. In his analysis, the mean-square effective charge for energy loss was assumed to be equal to the mean-square net charge carried by the ion. Here we distinguish between these quantities. They are designated z^{*2} and $\langle z'^2 \rangle$, respectively. In Papineau's work and the earlier work of Lonchamp (L 53.1), the fractional charge on the ion was assumed to be determined by the independent variable $\beta/z^{2/3}$, following Knipp and Teller. In the Thomas-Fermi atom model, the mean electron velocity varies with $z^{2/3}$, and Knipp and Teller used this statistical model in their early theoretical paper on the ranges of fission fragments.

In the velocity interval where K electrons are being captured, β/z, rather than $\beta/z^{2/3}$, is the governing variable. For light nuclei, this is an important region, being the major portion of the range interval in which electron capture takes place. For heavy ions with $\beta \ll z/137$, the dependence of z^*/z on β and z is expected to be about as $\beta/z^{2/3}$. For almost-stripped nuclei, which have velocities $\beta \approx z/137$, the independent variable, as noticed by Barkas (B 53) and Heckman *et al.* (H-B 60), approaches β/z.

Precise energy-loss measurements on heavy ions were made by Heckman *et al.* (H-B 60). They found empirical rates of energy loss for C,N,O,Ne, and A ions in emulsion. Their momentum analyzer was the double focusing 180° magnetic spectrometer shown in Fig. 9.4.1. The momentum resolution obtained was better than one part in 1000. Various ionic charge states of the same magnetic rigidity were passed through the spectrometer simultaneously. Therefore, the ions incident on the detecting emulsion had momenta that were integral multiples of the minimum momentum. Figure 9.4.2 shows the observed charge states of neon at various magnetic rigidities.

A set of discrete particle ranges corresponding to these momenta were measured. Alpha particles, as well as other helium and hydrogen isotopes

of the same magnetic rigidity, also were sent through this analyzing system, so that each range could be measured and used in calibration. The method eliminated most types of systematic error. Details are given in the original paper. Least-squares fitting of a power series in

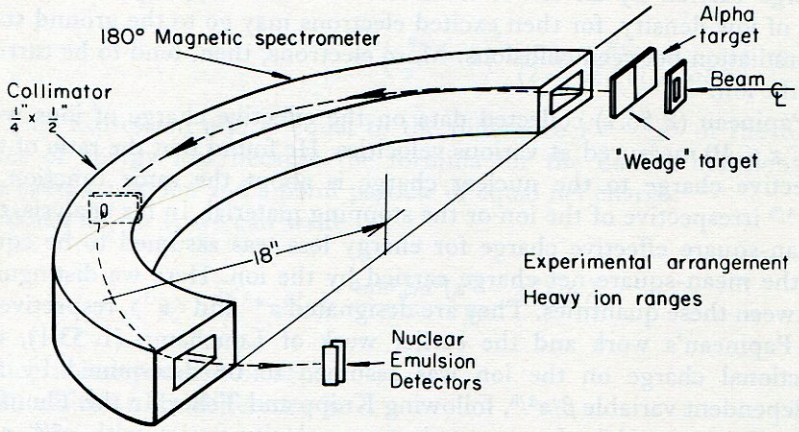

FIG. 9.4.1. Magnetic spectrometer used for heavy ions (IDLRL).

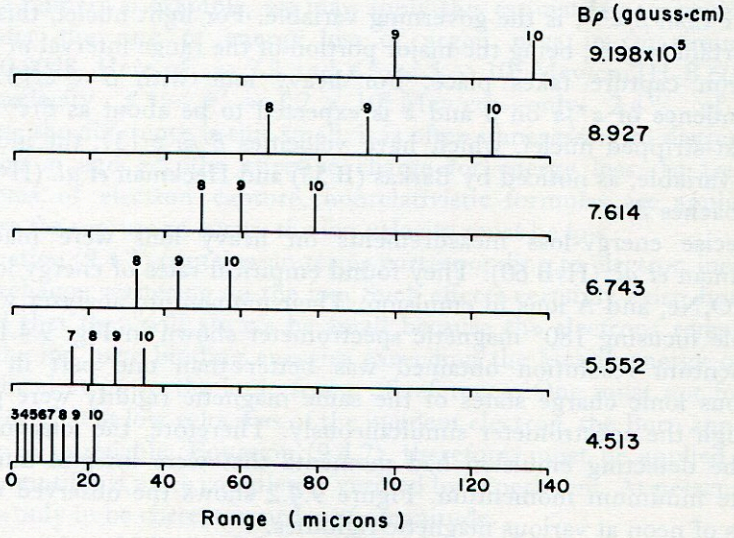

FIG. 9.4.2. Charge states of neon observed to be present at 6 magnetic rigidities. The states appeared as resolved range groups which are indicated in the diagram (IDLRL).

(ln R) to the empirical data by machine methods gave analytic functions for the range-energy data that are more reliable than any single measurement. On differentiating these functions, the rates of energy loss shown in Fig. 9.4.3 were calculated.

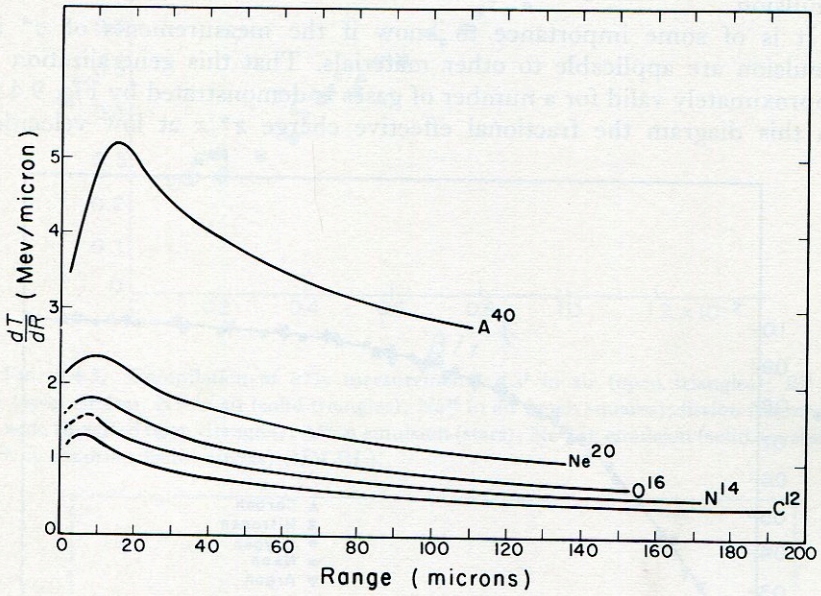

FIG. 9.4.3. Energy-loss rates of heavy ions in emulsion as functions of residual range (IDLRL).

If $\iota(\beta)$ is the rate of energy loss of an ideal proton at velocity βc, and $\mathscr{J}^*(z,\beta)$ that of an ion, then $z^{*2} = \mathscr{J}^*/\iota$ is defined to be the mean-square effective charge for energy loss.

In Fig. 9.4.4 the fractional effective charge z^*/z for all the ions studied in emulsion is graphed against $\beta/z^{2/3}$. It can be seen that, over a considerable range of $\beta/z^{2/3}$, it is the correct variable to provide a universal representation of the data.

The following empirical function fits the data to about the accuracy that it is known:

$$z^* = z[1 - \exp(-125\beta/z^{2/3})] \tag{9.4.9}$$

The energy-loss rate of any heavy ion is then found from $\mathscr{J}^* = z^{*2}\iota(\beta)$ where ι is the rate of energy loss of a proton at velocity β. For β in the interval $0.05 - 0.2$, an important region for the capture process, $\iota \approx 8.0 \times 10^{-4}\beta^{-4/3}$ Mev/μ in emulsion.

Therefore:

$$\mathscr{S}^* \approx 8 \times 10^{-4}\beta^{-4/3}z^2[1 - \exp(-125\beta/z^{2/3})]^2 \quad \text{Mev}/\mu \quad (9.4.10)$$

is a rough expression of the energy-loss rate of a low-velocity ion in emulsion.

It is of some importance to know if the measurements of z^* in emulsion are applicable to other materials. That this generalization is approximately valid for a number of gases is demonstrated by Fig. 9.4.5. In this diagram the fractional effective charge z^*/z at low velocities

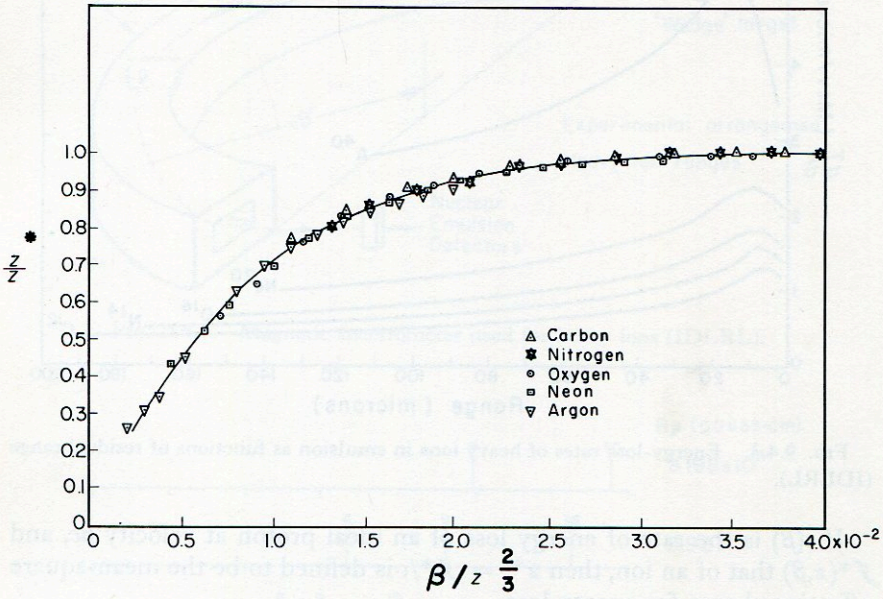

FIG. 9.4.4. The fractional effective charge z^*/z, required to produce the observed rates of energy loss as a function of the reduced velocity, $\beta/z^{2/3}$, of the ion (IDLRL). (Reference H-B 60.)

is plotted against $\beta/z^{2/3}$ for various ions in air, neon, and emulsion. A locus is defined and only a slight variation with stopping material is indicated. At low gas pressures this rule, of course, fails.

At higher velocities it is possible to compare the measurements in emulsion with data from solid materials. Figure 9.4.6 shows the curve derived for emulsion along with the dashed curves of Knipp and Teller (KT 41), and of Papineau (P 56.1). The points shown are empirical data obtained for various ions in a number of materials by several groups.

Owing to processes of electron capture and loss in dense matter, the

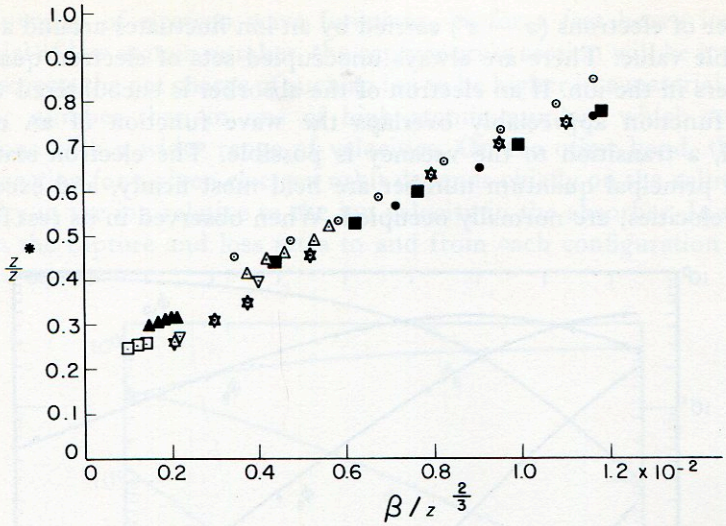

FIG. 9.4.5. Compilation of z^*/z measurements: Li^7 in air (open triangles); B^{11} in air (open circles); N^{14} in air (solid triangles); Ne^{20} in air (open squares); fission fragments in neon (inverted open triangles); A^{40} in emulsion (stars); Ne^{20} in emulsion (solid squares); O^{16} in emulsion (solid circles) (IDLRL).

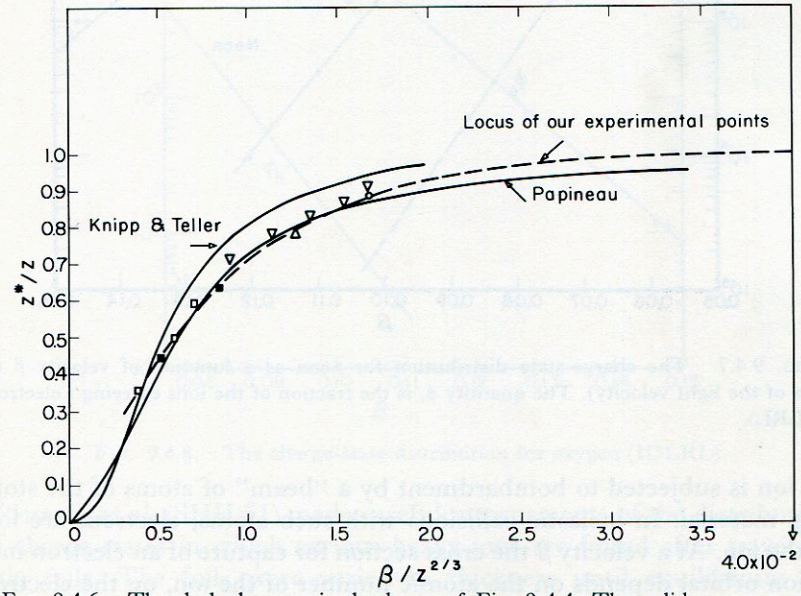

FIG. 9.4.6. The dashed curve is the locus of Fig. 9.4.4. The solid curves are the theoretical calculations of Knipp and Teller and the semi-empirical curve of Papineau. The points represent various measurements made by five experimental groups for several ions in a number of materials (IDLRL).

number of electrons ($z - z'$) carried by an ion fluctuates around a most probable value. There are always unoccupied sets of electron quantum numbers in the ion. If an electron of the absorber is encountered whose wave function appreciably overlaps the wave function of an empty orbital, a transition to the vacancy is possible. The electron states of lowest principal quantum number are held most firmly, and except at high velocities, are normally occupied. When observed in its rest frame,

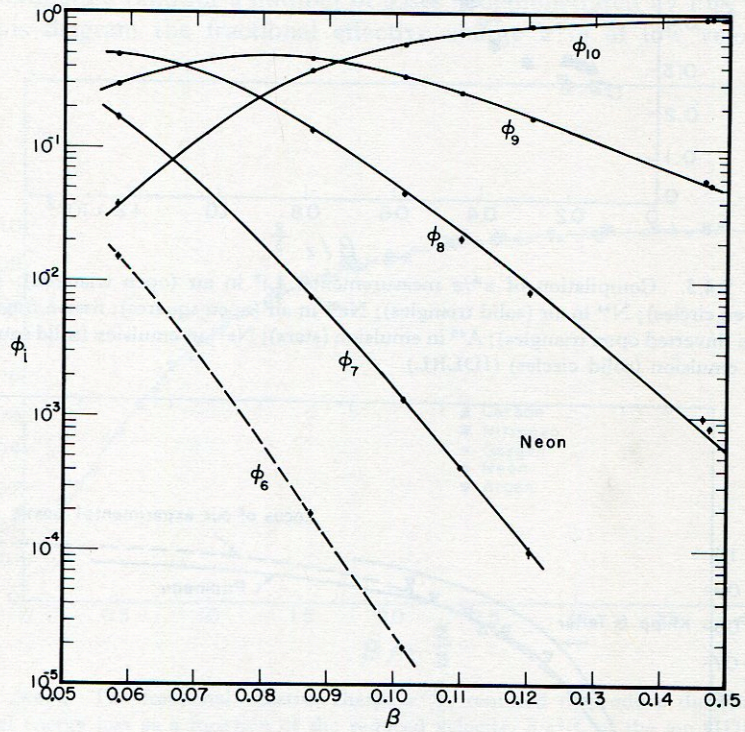

FIG. 9.4.7. The charge-state distribution for neon as a function of velocity β (in units of the light velocity). The quantity ϕ_i is the fraction of the ions carrying i electrons (IDLRL).

the ion is subjected to bombardment by a "beam" of atoms of the stopping material. In inelastic collisions with such atoms, electrons are lost by the ion. At a velocity β the cross section for capture of an electron into an ion orbital depends on the atomic number of the ion, on the electron quantum numbers, and on the quantum numbers already filled. It may not vary much, however, with the stopping material if the electrons in the absorber are rather uniformly distributed in velocity. When there is

little overlap of electron wave functions, as for a fast heavy ion in a material of low atomic number, the capture cross section will be lowered. One expects the net charge of such an ion to be higher in a material of low atomic number than in one of high atomic number, which contains electrons with a wider range of velocities. On the other hand, the loss cross section for a given electron orbit depends chiefly on the value of its velocity in the ion relative to the ion velocity in the absorber. In equilibrium the capture and loss rates to and from each configuration of the ion are equal.

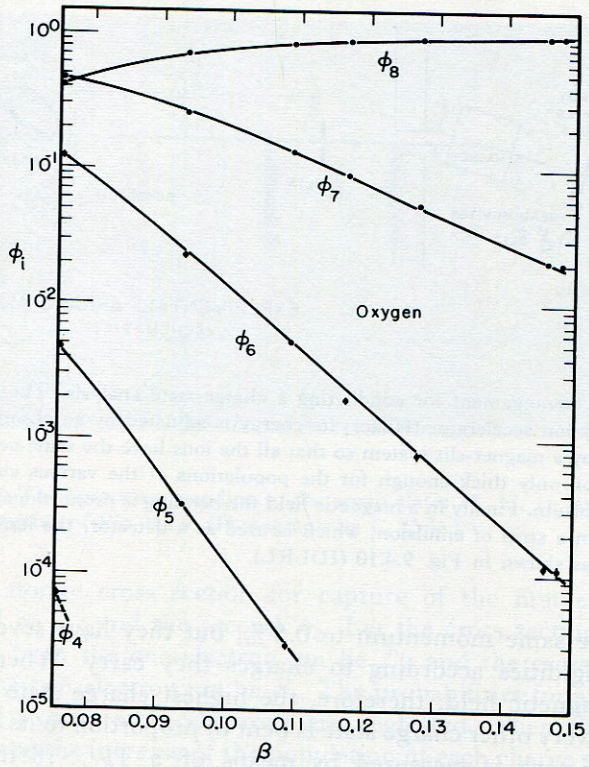

FIG. 9.4.8. The charge-state distribution for oxygen (IDLRL).

Simon *et al.* (SHH 61) made careful measurments of the distributions of charge states in which various heavy ions are found after traversing thin foils. The foils were varied in thickness until equilibrium was reached. The curves shown in Fig. 9.4.7 are of the equilibrium proportions of various charge states of neon ions in a zapon foil. In Fig. 9.4.8 the charge-state distribution of oxygen is shown.

The experimental arrangement for making such measurements is shown in Fig. 9.4.9. The heavy-ion linear accelerator (Hilac) is used to give the ions kinetic energy of 10.2 Mev/nucleon. Then degrader foils lower the velocity as much as desired, and a monitor foil measures the beam intensity by the current of secondary electrons that are projected from this foil. The collimated beam is then analyzed by a magnet and a slit system. A particular charge state is selected and the beam has a very precise momentum when it reaches the equilibrium foil. On emerging from it, the ions exist in the equilibrium distribution of charge states.

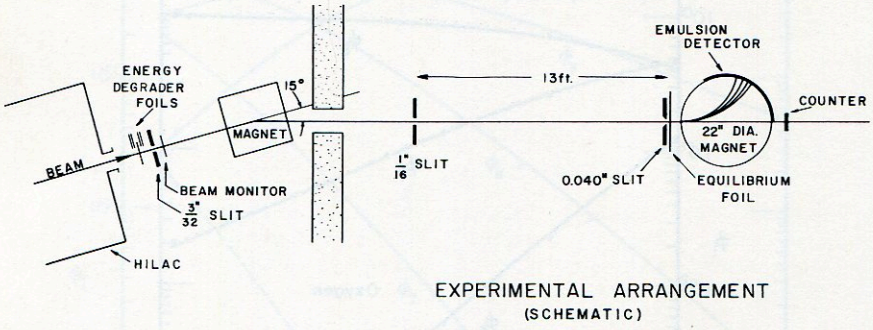

FIG. 9.4.9. Arrangement for conducting a charge-state analysis. The beam energes from the heavy-ion accelerator (Hilac); its energy is adjusted by an absorbing foil; and it is analyzed by a magnet-slit system so that all the ions have the same velocity. It then penetrates a foil only thick enough for the populations of the various charge states to come to equilibrium. Finally in a magnetic field the bending is proportional to the charge state so that on a strip of emulsion, which is used as a detector, the ions are found in discrete lines as shown in Fig. 9.4.10 (IDLRL).

All have the same momentum to 0.5%, but they have several discrete magnetic rigidities according to charges they carry. When the beam enters a magnetic field, therefore, the highest charge state is bent the most, and every other charge state is bent in proportion to its charge. The intensity of each is measured by means of a $1\frac{1}{2} \times 18$ inch acetate-backed emulsion strip in a circular arc so that the ions enter it approximately perpendicular to its surface. After processing the emulsion, the populations of the states are found by counting the tracks in the well-resolved focal spots produced by each charge state. Each track appears as an opaque column of silver. By varying the exposure times, relative intensities through a range of five orders of magnitude or more can be measured. A photographic reproduction of one of the emulsion strips is shown in Fig. 9.4.10.

The behavior of curves such as those of Fig. 9.4.7 can be understood on introducing the elementary capture and loss cross sections. In order to study the physics of the process without requiring an excessive number of terms in the equations, we confine this analysis to neon ions with $\beta > 0.12$. Then ions carrying three or more electrons are present with abundances of less than 10^{-4}. The process is reduced to one of capture into the K-shell and loss from the K-shell, because occupation of the L-shell or higher shells is very unlikely. Let the normalized populations of ions carrying 0, 1, and 2 electrons be ϕ_{10}, ϕ_9, ϕ_8, respectively.

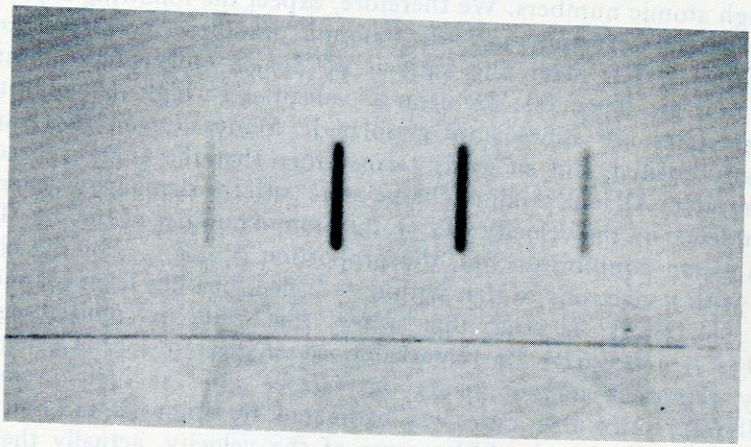

FIG. 9.4.10. The lines corresponding to the argon states 18, 17, 16, and 15 observed using the apparatus of Fig. 9.4.9. (Photograph by C. Cole.)

Let the atomic cross section for capture of the first electron into the K-shell be σ_1; and the second, σ_2. Let the cross section for loss of an electron from the one-electron ion be Σ_1, and the cross section for loss from the two-electron ion be Σ_2. The probabilities for simultaneous transfers of two or more electrons are neglected. Then the following terms describe the increase of the population of each charge state in path lengths dx, when the equilibrium foil has N atoms per unit volume:

$$d\phi_{10} = N(\phi_9\Sigma_1 - \phi_{10}\sigma_1)\,dx$$

$$d\phi_9 = N[\phi_{10}\sigma_1 + \phi_8\Sigma_2 - \phi_9(\sigma_2 + \Sigma_1)]\,dx$$

$$d\phi_8 = N(\phi_9\sigma_2 - \phi_8\Sigma_2)\,dx$$

If at $x = 0$ the beam consists of a known distribution of charge states, the solutions of these equations can be used to measure the cross sections.

For example, if initially $\phi_{10} = 1$, then $N\sigma_1$ is equal to the initial value of $(d\phi_9/dx)$. At equilibrium: $\phi_9/\phi_{10} = \sigma_1/\Sigma_1$ and $\phi_8/\phi_9 = \sigma_2/\Sigma_2$.

Because of the screening produced by the first electron, the first and second electrons captured are not quite equivalent. If this effect is neglected, we notice that two spin states can contribute to the cross section σ_1, and only one to σ_2. For this reason, the cross section σ_1 is doubled compared to σ_2. When the ion carries two equivalent electrons, the probability of electron loss is twice as great as when it carries only one. Screening effects on the K electrons are relatively less important for high atomic numbers. We therefore, expect the following expression to approach exactness as the atomic number increases: $(\sigma_1/\sigma_2)(\Sigma_2/\Sigma_1) = 4$. For neon, this ratio is $\phi_9^2/(\phi_8\phi_{10})$. Only small deviations from four are detectable for neon at velocities so high that only three charge states are appreciably populated. Many-electron ions can be similarly treated, but so many terms enter that the analysis becomes complicated. All ions produce charge-state patterns that have a systematic dependence on the velocity and on the atomic number of the ion. Thus, for a zapon equilibrium foil, the proportion ϕ_{z-n}/ϕ_{z-n-1} of the charge state with n electrons to that with $n - 1$ electrons has been graphed in Fig. 9.4.11. It is seen that when this ratio is plotted against $137\beta/(z - n - 0.62)^{0.70}$ a remarkable set of discrete loci is generated. They represent measurements on various ions at many velocities (HHS 62). Since this ratio was estimated by Bohr (B 48.1) to vary approximately with the fifth power of the velocity, actually the fifth root of the ratio is the ordinate.

The mean square value $\langle z'^2 \rangle$ of the charge carried by the ion is given by $\langle z'^2 \rangle = \Sigma_1^z i^2 \phi_i$. For zapon this is observed to have a value about equal to the value z^{*2} found in emulsion of higher mean Z.

Elastic collisions of heavy ions with whole atoms can become a significant energy-loss process. Collisions in which considerable energy is transferred are detectable, however, and these tracks can be eliminated. In such a collision the ion will be deflected, and if the energy transfer is large enough, a visible track will be produced by the knock-on nucleus. Relatively long tracks of protons projected elastically are not infrequently seen to start on the tracks of heavy ions.

Inelastic collisions of heavy ions with emulsion nuclei are virtually always recognizable in emulsion. A star of several prongs, or a least a sharp deflection, is produced. The tracks of particles that have suffered violent nuclear collision are not included when ranges are measured, and the derived energy-loss rates do not include such processes. They do include losses up to the maximum set by whatever the criterion for track rejection is.

The appearance of the track of a carbon ion colliding with a proton in emulsion is shown in Fig. 9.4.12. At nonrelativistic velocities the right angle between the tracks emerging from the collision of particles having equal masses is characteristic. Figure 9.4.13 is the photomicrograph of a collision of an 0^{16} ion with an oxygen nucleus of the emulsion.

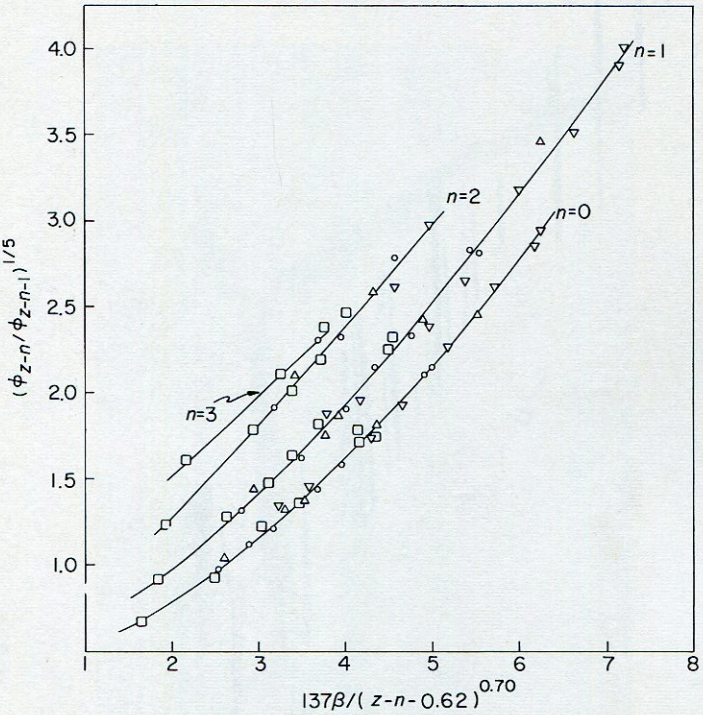

FIG. 9.4.11. Relative populations of charge states as functions of velocity and atomic number. Triangles are nitrogen points; inverted triangles, carbon points; circles, oxygen points; and squares, neon points. Note that universal curves are produced. The loci for $n = 0, 1, 2$ corresponding to 0, 1, or 2 K electrons are clearly resolved. The locus for $n = 3$ corresponding to an L electron in addition is more poorly resolved. This effect is not surprising in view of the reduced binding energy of an L electron (IDLRL).

The average energy loss in elastic collisions with atoms can be estimated as follows: let the momentum absorbed by an atom in an elastic collision with a particle of momentum **P**, be **p**. The vector **p** will most frequently be almost perpendicular to **P**, with components p_y and p_z, the primary particle being directed along the x axis. The energy absorbed will then be $(p^2/2M) = (p_y^2/2M) + (p_z^2/2M)$, where M is the atomic mass.

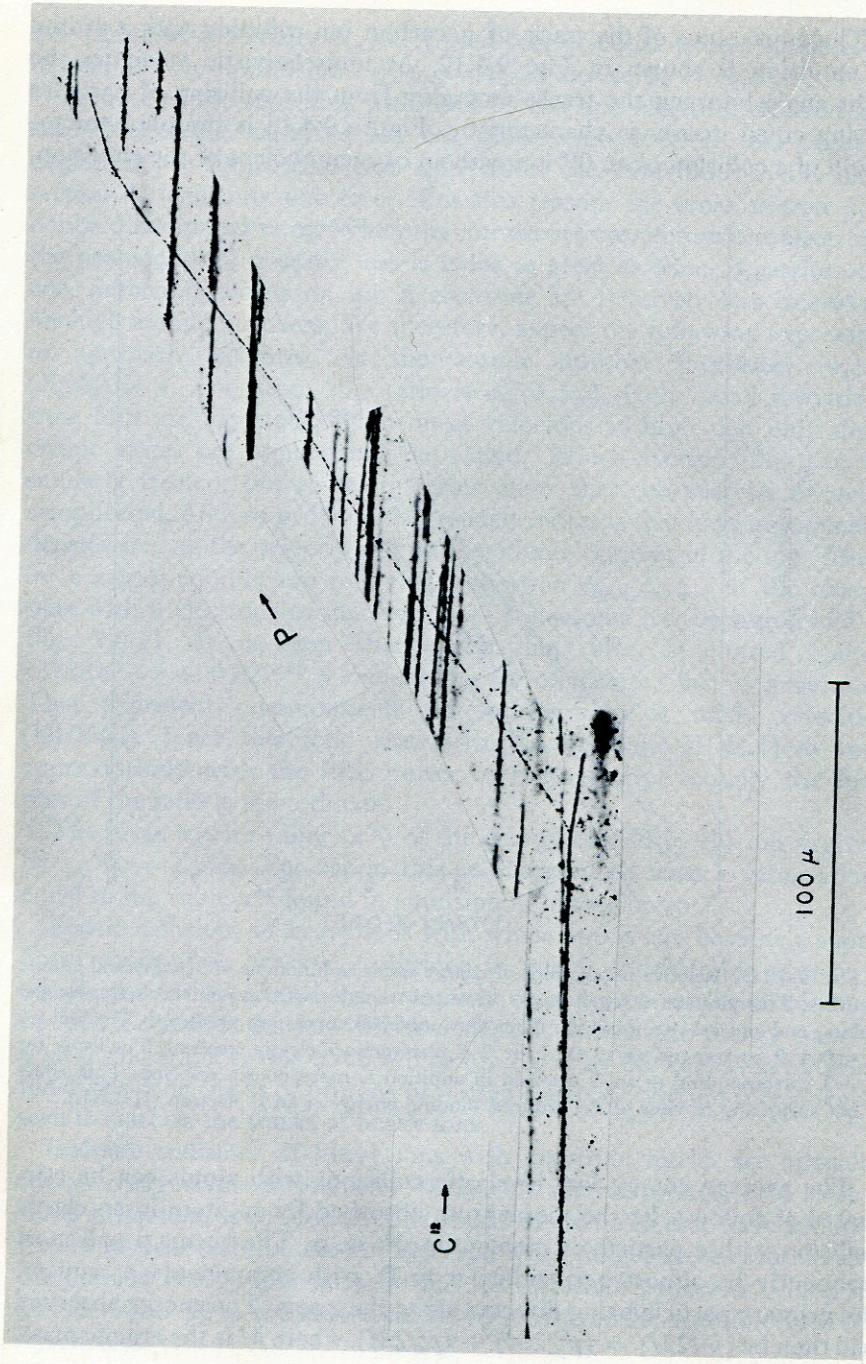

FIG. 9.4.12. Track of a proton projected forward from point of collision with a C^{12} ion. Such an event can be completely analyzed (IDLRL).

The projected angle of deflection ω is related to p_y by $p_y = \omega P$. Then the average value, $\langle p^2 \rangle$, of p^2 is found as follows:

$$\langle p^2 \rangle = 2\langle p_y^2 \rangle = 2P^2 \langle \omega^2 \rangle \tag{9.4.11}$$

In unit path there will be an average number of collisions $N\sigma$ (see Chapter 8). The energy loss $\mathscr{J}_N$ to atoms in such elastic collisions then is

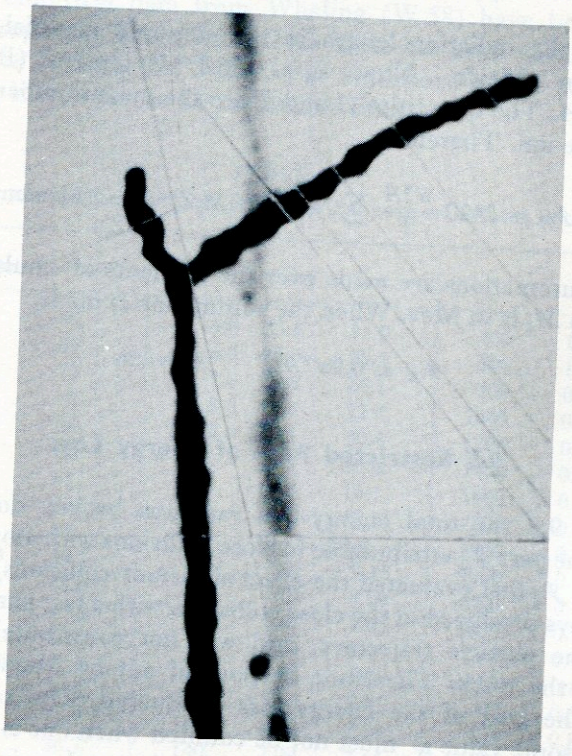

FIG. 9.4.13. Characteristic 90° angle between tracks of equal-mass nonrelativistic collision partners. (Photomicrograph by C. Cole.)

$\mathscr{J}_N = N\sigma P^2 \langle \omega^2 \rangle / M$ per unit path. The mean-square projected angle of scattering in a path length t is given by $\langle \phi^2 \rangle = N\sigma t \langle \omega^2 \rangle$. Therefore, we may express $\mathscr{J}_N$ directly in terms of multiple scattering of the particle:

$$\mathscr{J}_N = P^2 \langle \phi^2 \rangle / Mt \tag{9.4.12}$$

In emulsion this energy-loss term normally is not large, and has almost the same dependence on β as the electronic stopping formula. It

may become important, however, at low velocities when their binding causes many of the electrons to become ineffective in stopping. Then the atomic stopping effect becomes dominant.

We can roughly evaluate this energy-loss rate in emulsion as follows by Eq. 8.4.4:

$$\langle \phi^2 \rangle = \frac{225 z'^2 t}{P^2 \beta^2 x_0}$$

where x_0 is the radiation length in the stopping material, and $P\beta$ is measured in Mev/c. Now $x_0 \approx 166 Z^{-0.76}$ gm/cm^2 (BR 61), and $\beta^2 \approx T/469A$. The quantities A and T are the mass number and kinetic energy of the ion. Therefore,

$$\mathscr{J}_N \approx 2420 \frac{z'^2 A}{T} \sum N_i \Big/ \sum N_i M_i Z_i^{-0.76} \qquad \text{Mev/cm}$$

where the summations are made over the elements of emulsion, and the atomic mass M_i is in Mev. When the summation is made,

$$\mathscr{J}_N \approx 0.9 z'^2 A/T \qquad \text{Mev/cm} \tag{9.4.13}$$

9.5 Restricted Rate of Energy Loss

In Section 9.2 the total energy-loss rate was broken down into two portions, the part $\mathscr{J}_1$ attributable to close collisions with atomic electrons, and a term $\mathscr{J}_2$ that evaluated the effect of distant collisions. In emulsion the delta rays produced in the close collisions with a fast particle will tend to leave the particle trajectory, and will not contribute to the grain density in the track. Therefore, as pointed out by Messel and Ritson (MR 50), the part of the energy loss producing delta rays of energy exceeding some value w' must not be counted when one is attempting to evaluate the energy loss that produces the observed grain density. The energy dissipated in the gel also has little effect on the grain density of the track. It is assumed that only energy that remains in the silver bromide crystals traversed by the particle can be responsible for producing the latent image in the primary grains.

One may indeed go farther, and suggest that it is not obvious that the effect of one act of energy loss in which an amount of energy w is transferred to an electron is the equivalent for production of a track latent image to n acts of energy loss "at different places" in the crystal in which a total energy transfer w is involved.

We shall leave this question for the moment, and calculate the

restricted rate of energy loss. By its definition this is energy that is in the right place to produce the primary latent image, irrespective of the efficiency of its utilization.

In calculating the restricted rate of energy loss, i', expressed in Mev gm^{-1} cm^2, I and C are evaluated for silver bromide—not for all the emulsion components.

When w_{max} falls below w', the smaller value is applicable. At very low velocities, empirical data from Whaling (W 58) have been used as a guide in preparing Table 9.5.1. This table has been calculated for two choices of w', 2 Kev and 5 Kev. For emulsions of the usual range of grain sizes, these seem to be reasonable limits.

TABLE 9.5.1

RESTRICTED ENERGY-LOSS RATE FOR PROTONS IN SILVER BROMIDE[a]

τ	i'_{2000}	i'_{5000}	τ	i'_{2000}	i'_{5000}	τ	i'_{2000}	i'_{5000}
1.2	83	90	5.4	25.6	31.0	400	1.12	1.24
1.4	73	83	6.0	23.6	28.5	500	1.02	1.12
1.6	66	77	7.0	20.9	25.1	700	0.902	0.993
1.8	60	72	8.0	18.8	22.4	1000	0.824	0.904
2.0	56	68	9.0	17.1	20.4	1200	0.799	0.875
2.2	52	64	10	15.8	18.6	1400	0.784	0.857
2.4	49	61	12	13.6	16.1	1600	0.775	0.846
2.6	46	57	16	10.9	12.7	1800	0.769	0.839
2.8	43	54	20	9.13	10.6	2000	0.766	0.834
3.0	41.0	50.7	24	7.91	9.16	3000	0.761	0.826
3.2	38.9	48.0	28	7.01	8.09	4000	0.772	0.836
3.4	37.1	45.6	30	6.65	7.65	5000	0.781	0.844
3.6	35.4	43.4	40	5.31	6.08	10^4	0.814	0.876
3.8	33.9	41.5	50	4.47	5.09	2×10^4	0.848	0.910
4.0	32.5	39.8	70	3.45	3.91	3×10^4	0.864	0.926
4.2	31.3	38.2	100	2.65	2.99	10^5	0.897	0.959
4.4	30.1	36.7	140	2.09	2.34	2×10^5	0.907	0.968
4.6	29.1	35.4	200	1.65	1.84	3×10^5	0.910	0.972
4.8	28.1	34.2	260	1.41	1.57	5×10^5	0.913	0.975
5.0	27.3	33.0	300	1.30	1.44	∞	0.915	0.977

[a] τ is in Mev; i'_{2000} and i'_{5000} are in Mev gm^{-1} cm^2.

At high velocities the table was constructed using the formula:

$$i' = \frac{2\pi r_0^2 mc^2 (n/\rho)}{\beta^2} \left[\ln \left(\frac{2mc^2}{I^2} \beta^2 y^2 w' \right) - \beta^2 - 2C \right] \qquad (9.5.1)$$

and at low velocities it was obtained from empirical data corrected for the

delta-ray energy loss. The quantity C was calculated from Sternheimer's (S 56.1) and Walske's (W 56) papers, and is given in Table 9.5.2. A mean ionization potential of $I = 450$ ev, and a constant $2\pi r_0^2 mc^2(n/\rho) = 0.06705$ Mev cm^2/gm were adopted for AgBr. The quantity n/ρ is, of course, the number of electrons per gram of AgBr(2.63×10^{23}).

TABLE 9.5.2

THE CORRECTION TERM $C(\beta)$ FOR SILVER BROMIDE

τ	$C(\beta)$	τ	$C(\beta)$
3.0	0.025	70	0.048
3.2	0.034	100	0.037
3.4	0.041	140	0.027
3.6	0.050	200	0.019
3.8	0.055	260	0.015
4.0	0.060	300	0.013
4.2	0.064	400	0.009
4.4	0.069	500	0.007
4.6	0.071	700	0.004
4.8	0.075	1000	0.002
5.0	0.077	1200	0.002
5.4	0.081	1400	0.001
6.0	0.087	1600	0.001
7.0	0.094	1800	0.004
8.0	0.099	2000	0.011
9.0	0.102	3000	0.056
10	0.104	4000	0.109
12	0.104	5000	0.171
16	0.101	10000	0.431
20	0.095	20000	0.792
24	0.089	30000	1.058
28	0.083		
30	0.080		
40	0.069		
50	0.060		

The restricted rate of energy loss of all singly charged particles reduces to Eq. (9.5.1) when an upper limit, w', less than the maximum energy transfer is applied. This means that the primary ionization, and therefore the primary grain density, for all singly charged fast particles *at the same velocity* is expected to be the same. No exception to this law has been found.

9.6 Energy-Loss Rate in Nonstandard Emulsion

The composition of emulsion is variable. Even the density of emulsion of a standard type depends on the relative humidity. The stopping power of the emulsion changes with its composition, and often one must allow for such changes.

A straightforward way to determine the stopping power of the emulsion is to calculate it from the individual elements present, assuming that their effects are additive. This assumption usually introduces a negligible error except at extremely low velocities.

Let $\mathscr{J}_i$ be the energy-loss rate at a particular velocity in Mev gm^{-1} cm^2 for the ith element in the emulsion, and let ρ_i be the concentration, expressed in grams per cubic centimeter, of that element in the emulsion. Then

$$\mathscr{J} = \sum_i \rho_i \mathscr{J}_i \qquad \text{Mev/cm} \tag{9.6.1}$$

This is the rate of energy loss in the nonstandard emulsion at the velocity assumed. [The quantity $\mathscr{J}$ is equal to $z^{*2}\iota$, where ι is the energy-loss rate of a singly charged particle and z^{*2} is the mean square effective charge for energy loss (see Section 9.4).]

Sometimes one does not have accurate energy-loss data for every element in the emulsion, but data for standard emulsion, water, and silver bromide are available (see Tables 9.2.2 and 9.7.1). If a material not normally present is used for loading the emulsion, its stopping power also must be known. Let the rate of energy loss in Mev gm^{-1} cm^2 for standard emulsion be $z^{*2}i(= \mathscr{J}/3.815)$; for water, $z^{*2}i_w(= \mathscr{J}_w)$; for silver halide, $z^{*2}i_h(= \mathscr{J}_h/6.473)$; and for the loading material, $z^{*2}i_l/d_l$. Here d_l is the specific gravity of the loading material.

Now consider the nonstandard emulsion to be a linear combination of the four components mentioned above. Let their concentrations in grams per cubic centimeter be ρ_e, ρ_w, ρ_h, and ρ_l, respectively, so that the nonstandard emulsion density is $\rho = \rho_e + \rho_w + \rho_h + \rho_l$. Some of the concentrations may be negative. In particular ρ_h will be negative if the emulsion contains an excess of gel, and ρ_w will be negative if the emulsion is drier than normal.

The rate of energy loss then is:

$$\mathscr{J}_n = z^{*2}(\rho_e i_e + \rho_w i_w + \rho_h i_h + \rho_l i_l) \qquad \text{Mev/cm} \tag{9.6.2}$$

The most frequently occurring problem of nonstandard composition is encountered when nominally standard emulsion has a density different

the change in volume when a sample of the emulsion absorbs a mass, Δw, of water, we can write:

$$\mathcal{J}_n = \frac{\rho r - 1}{\rho_0 r - 1}\mathcal{J} + \frac{\rho_0 - \rho}{r\rho_0 - 1}\mathcal{J}_w \quad \text{Mev/cm} \qquad (9.6.3)$$

In this equation, $\mathcal{J}_n$ is the rate of energy loss in the nonstandard emulsion, while $\mathcal{J}$ and $\mathcal{J}_w$ refer to standard emulsion and water, respectively. The standard density of emulsion is taken to be ρ_0 (= 3.815 gm/cm³), while ρ_1 is the actual density of the sample. If ρ_w is the concentration of water in the emulsion (the concentration in standard emulsion being zero), then $\rho = \rho_0 + \rho_w(1 - r\rho_0)$ (We have taken the density of water to be 1 gm/cm³.) For emulsion with a high water concentration $r = 1$ ml/gm (GBFG 53), so that then $\rho = \rho_0 - \rho_w(1 - \rho_0)$. In Section 3.8 we have described the behavior of r.

In Table 9.2.2 the energy-loss rate for standard emulsion has been given. Table 9.6.1 gives the rate of energy loss i_w, computed (B 58.3) for water, and, i_h, for silver bromide. The latter was prepared using the same constants as those employed for the calculation of the restricted rate of energy loss in silver bromide (see Section 9.5). With these tables the rate of energy loss in any combination of silver halide, gel, and water can easily be found.

9.7 The Grain Density and Linear Track Structure

The most obvious way to measure the density, g_0, of developed grains in the track of a charged particle is to count their number in a measured length of track. At low grain densities the error in such a measurement may not be great, but as the grain density rises, adjacent grains become unresolvable with the microscope, and it becomes impossible to know how many grains are in a clump. It has not been unusual then to adopt a simple convention which equates the number of grains in a clump to the length of the clump in units of a mean developed grain diameter. This gives a measure, D, of the grain density. For an uninclined track D differs from g_0 in two respects. It is always less than g_0 and its variance is less in per cent than that of g_0. The measurement of D has subjective aspects, and it is tedious because many decisions must be made. A more objective counting procedure is merely to determine the linear density, B, of resolvable clumps, known as "blobs," consisting of one or more developed grains. This is equivalent to determining the density of gaps in the track, and counting of gaps may be preferred when the grain density is high, but in this region only poor statistical accuracy can be obtained.

As the ionization increases, D rises asymptotically toward a maximum equal to the reciprocal developed grain diameter, α^{-1}, whereas the blob density passes through a maximum $(e\alpha)^{-1}$ and becomes very small where the ionization is large. (It should be noted that the common nuclear-track emulsions are remarkably free of totally insensitive grains. The grains therefore must contain many sensitivity centers. At sufficiently high rates of energy loss, the gap densities approach limits that are very low. Since grains enlarge on development, and secondary grains develop, a small fraction of the grains nevertheless probably are inert.)

The grain density, g_0, is not correctly determined by counting except when every developed grain is resolved. What one usually measures directly is only a function of the true grain density. For convenience we shall use the general expression ionization parameter for any measure of the grain density, and designate g_0 as the true grain density. The quantity measured should be chosen to give either the maximum amount of information, or the most information per unit of effort, depending on the problem.

For complete consistency in the measurement of granularity it is also necessary to make operational definitions.

A particle track is seen as a more or less continuous series of grain images. These are roughly circular in projection, but their centers, in general, are displaced around the particle trajectory both vertically and horizontally. They may occult each other or be too close for resolution with the optical equipment employed. They vary in size.

Suppose the length between the centers of two grain images is considered. Let it be projected on a plane perpendicular to the line of sight. The projection is a distance a when the grains can just be resolved into two objects. Then if c is the distance projected on the particle trajectory between the centers of two such grains, and the projected image of no other grain comes between them, a gap of length c-a is said to exist in the track. Since a varies for different pairs of grains, an expectation value $\langle a \rangle = \alpha$ is defined which describes in one combined parameter the emulsion, the optical equipment, and the observer characteristics. The blob density, B, is defined as the linear density of gaps, or of clusters of unresolved grains, in the track. A quantity $H = H(l)$ is the density of gaps exceeding the length l. It is, of course, also equal to the density of clusters of grains in which are found no no gaps exceeding l. The blob density is, therefore, the special case of a cluster density in which $l = 0$, so that $B = H(0)$. If different values of l, namely l_1, l_2, etc., are considered, several values of H, H_1, H_2, H_3, etc., are introduced.

Although blob counting (or gap counting) is the easiest measurement technique, a maximum in the blob density as a function of g_0 limits the

usefulness of this quantity. Over a large interval B is insensitive to the ionization, and when the grain density becomes very high, the blob density falls toward zero.

The *lacunarity* L is the linear fraction of a track that consists of gaps. Thus $L = -\int_0^\infty l(dH/dl)dl$. The track *opacity*, 0, is simply $(1 - L)$.

Hodgson (H 50) was one of the first to study the lacunarity, which he called "gap density." He analyzed the tracks of alpha particles, protons, τ mesons, and μ mesons in a particular sample of G.5 emulsion. In 70 μ the integrated lacunarity completely resolved individual μ mesons and τ mesons, while groups of τ mesons and protons were separated if 150 μ of residual range were available. The lacunarity integrated over the residual range was called the "integrated emptiness" of the track by Bowker *et al.* (BGB 51); they also found it to be a useful measure of the ionization.

An ionization parameter that is not directly related to the linear structure of the track is the mean track width, *MTW*. It is studied in Section 9.10.

A very important discovery was made by O'Ceallaigh (O 54.1), who observed that the gap lengths have an exponential frequency distribution. The negative slope, g, of the distribution on a log frequency versus gap-length diagram is a measure of the grain density. It is called the gap-length coefficient. The mean gap length $\bar{l}$ is statistically equal to the reciprocal of the gap-length coefficient. O'Caellaigh found these quantities to be less sensitive than other measures of the grain density to the grain diameter. There seems to be a plateau during the period of development during which no new silver halide crystals are reduced to metallic silver, but only physical development proceeds. (With very prolonged development, all the crystals eventually are reduced.) On this development plateau, α increases but g changes only very slowly. When there is a gradient of development through the thickness of an emulsion layer, the mean gap length and the gap-length coefficient tend to remain stable ionization parameters.

This can be understood from the theory of the exponential gap distribution. If all gaps are shortened by the same amount, the mean gap length remains unaltered. It follows from this that whatever the distribution of the amounts by which gaps are shortened, the mean gap length is unaffected. It means, for example, that the growth of grains in development and displacements produced by crowding do not affect the mean gap lenth. Only an increment in g changes it. The law of gap lengths is as follows: The density, H, of gaps exceeding length, l, is

$$H = B \exp(-gl) \tag{9.7.1}$$

Here B is the blob density, and g is a measure of the grain density. A further result is that the blob density, B, is related to g, by the equation

$$B = g \exp(-g\alpha) \tag{9.7.2}$$

The relations (9.7.1) and (9.7.2) were given in this form by Fowler and Perkins (FP 55), who regarded g as a useful ionization parameter, but did not identify it with the true grain density.

Recently (B 59.1*, B 60*, B 61), the writer has been able to show theoretically that the gap coefficient and the reciprocal mean gap length are more than functions of the grain density, but each is itself an estimate of the true grain density, g. These statements have also been verified experimentally (H 60, PB 61).

It was further found (B 59.1, B 60) that the lacunarity is given by

$$L = e^{-g\alpha} \tag{9.7.3}$$

An important new connection was found relating an ionization parameter —the mean blob length, $\bar{b}$—with g. The equation (B 61) is:

$$\bar{b} = (e^{\alpha g} - 1)/g \tag{9.7.4}$$

The mean blob length, $\bar{b}$, and the mean gap length for a given α depend only on the blob density and the lacunarity, which are directly measurable averages for a track segment:

$$\bar{l} = L/B \quad \text{and} \quad \bar{b} = (1 - L)/B \tag{9.7.5}$$

Therefore, $B = (\bar{l} + \bar{b})^{-1}$ and $L = \bar{l}(\bar{l} + \bar{b})^{-1}$.

It is interesting also that

$$\bar{b} = \frac{1}{B} - \frac{1}{g} \tag{9.7.6}$$

The length α is a parameter that is determined largely by the average developed grain size. It is also affected by the optical resolution of the microscope, and by observer conventions, among other things. Alvial *et al.* (A-O 56), however, have shown that it is not sensitive to grain density. It is defined mathematically by Eq. (9.12.18).

It is essential, of course, that the measured g not vary with the optical

* These progress reports are less than perfect treatments in various respects. They were, therefore, not offered to a journal for formal publication. Both are now superseded by references (B 61), (PB 61), and particularly by this book, which treats some aspects of the grain-density problem most exactly. The discussion of this chapter draws heavily on all these writings.

resolution. The definition of α insures that g not vary with the optical conditions and all operationally defined measurements of g will remain consistent if the operationally defined α is used. On employing the same optical equipment as that used for analyzing test tracks, calibration tracks in the same emulsion can be used to measure α. An estimate can be obtained from any track segment by measuring:

$$(-L/B)\ln L \equiv \alpha \tag{9.7.7}$$

There are numerous other ways to determine α. As examples, from Table 9.7.1 one sees that for every L a value of αB is tabulated. Therefore, a measurement of L and the corresponding B provides an estimate of α. Similarly a measurement of $\bar{l}$ and L gives α from $\alpha = -\bar{l}\ln L$. A measurement of $\bar{b}$ and L yields another estimate because for every L, $\bar{b}/\alpha$ is tabulated.

It may also be noticed that B passes through its maximum, $B_{\max}$, when $g\alpha = 1$. Therefore,

$$\alpha = (eB_{\max})^{-1} \tag{9.7.8}$$

The product $(\alpha + l)H(l)$ is a universal function of $(\alpha + l)g$. Any observation of $H(l)$, therefore, can be used to estimate g.

There have been statements in the literature that the exponential law of gap lengths breaks down for small gaps. If α is not operationally defined, such a conclusion could, of course, be reached. The writer believes that such a result may be a consequence of failure to employ a consistent operational definition of α in the expression $H = ge^{-g(\alpha+l)}$. The basic difficulty is that the diffraction pattern of a grain in the microscope is not sharp-edged, and an ambiguity may exist as to what distance should be measured between two grains separated by a gap. Consistency, however, is all that is required. The apparent gap length depends on the color and on intensity of the light used, as well as on the numerical aperture of the objective lens. Of course, the lacunarity also varies with the emulsion development and with the characteristics of the emulsion itself. The observer must take care to check his ability to repeat measurements on a standard track, so that his calibration does not drift. After such precautions are taken, α is best calculated from $\alpha = -(L/B)\ln L$.

When the track is inclined so that in unprocessed emulsion it makes an angle $(\pi/2) - \delta$ with the normal to the emulsion surface, the projected image of the track contains an increased density of grains. The projected grain density then is what we call g. Its relation to g_0 is $g = g_0 \sec \delta$. The structure of the projected track image is the same as that of an uninclined

track of grain density $g_0 \sec \delta$. Since all track segments are inclined somewhat, we shall discuss g. The analysis must insure, however, that $g \cos \delta (\equiv g_0)$ remain invariant with dip. Of course, g_0 is the quantity ultimately to be determined.

In Fig. 9.7.1 are plotted measurements reported by Patrick and Barkas (PB 61) of g_0 as a function of particle velocity in K.5 emulsion. Several

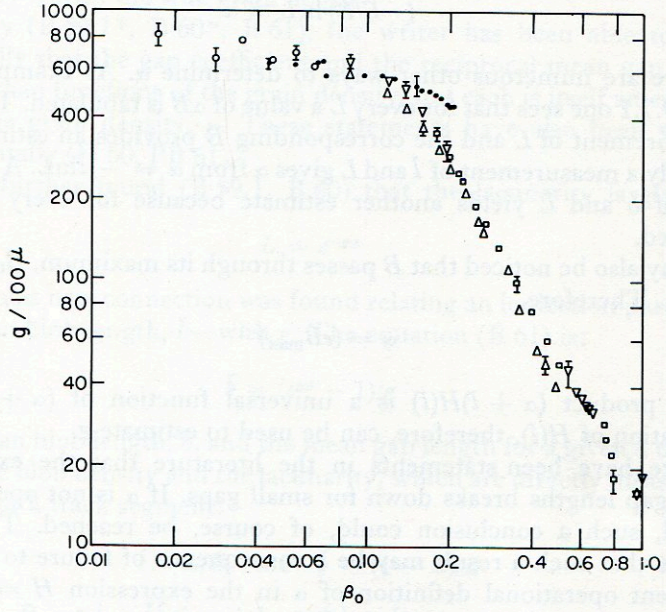

FIG. 9.7.1. The grain density as a function of particle velocity in a certain sample of K.5 emulsion. The different types of points correspond to different methods for measuring g_0. Solid points were obtained from alpha-particle tracks (IDLRL).

different particles and various objective measurement procedures were employed. The measurements were made by several individuals. A truly objective measurement cannot depend on the observer. It is seen that except in the region of saturation, below $\beta \approx 0.2$, that g_0 varies roughly with the inverse square of the velocity. The grain density of all tracks including alpha particles saturate below $\beta \approx 0.1$ at about the same value.

Fowler and Perkins have pointed out that much of the grain-density information in the gaps can be obtained without measurement—merely by counting. If the blobs (or gaps) are counted, and in addition the gaps exceeding a length, $l \approx 2.5/g$, these two points on the integral frequency curve determine g without knowledge of α. The length l is chosen to be an

integral number of eyepiece scale divisions when automatic track-analysis equipment is not used. If automatic equipment is used, it is often convenient to record the data for several values of l simultaneously.

Another technique that requires only counting was suggested by O'Brien to supplant or supplement blob counting in the region of the blob-count maximum (O 58.2). He proposed, in addition, to count the density of blobs consisting of single grains. From our analysis it is readily seen that the density B_1 of such blobs is $ge^{-2\alpha g}$, the maximum $(2\alpha e)^{-1}$ of which occurs when $2\alpha g = 1$. The density of blobs consisting of $(j + 1)$ grains is

$$B_{j+1} = ge^{-2\alpha g}(1 - e^{-\alpha g})^j \tag{9.7.9}$$

The weakness of O'Brien's proposal is the subjectivity involved in deciding whether or not a blob consists of a single grain.

The blob length is the diameter of one grain plus an average length β for each additional grain in the blob. Since the grains grow with development and overlap for other reasons, β is always less than $\alpha/2$. It approaches $1/g$ when the grain density is high. The mean number, ν, of grains in a blob is

$$\nu = e^{\alpha g} \tag{9.7.10}$$

Long blobs have an exponential distribution of lengths. The probability that the lengths exceed b is e^{-qb} with

$$q \to \frac{g(1 - e^{-\alpha g})}{e^{\alpha g} - 1 - \alpha g}$$

The average length $\bar{b}_{j+1}$ of a blob of $(j + 1)$ grains is

$$\bar{b}_{j+1} = \alpha + j\frac{(e^{\alpha g} - 1 - \alpha g)}{g(e^{\alpha g} - 1)} \tag{9.7.11}$$

Therefore, each additional grain in a blob adds an average additional length β with

$$\beta = \frac{e^{\alpha g} - 1 - \alpha g}{g(e^{\alpha g} - 1)} \tag{9.7.12}$$

When the number of grains in a blob is incorrectly set equal to the length of the blob in units of the mean grain diameter, the grain density is underestimated. The expectation value $\langle D \rangle$ of the corresponding ionization parameter, D, has the value $B(L - 1)/(L\ln L)$. The variability of individual blob lengths arises from the fluctuating numbers of grains

in a blob, and also from the variable grain spacing within the blob (subject to the constraint that no gap be left in the blob structure).

In very unsaturated tracks the bulk of the information in the linear structure of the track is obtained by measuring $B = ge^{-\alpha g}$ or $\bar{l} = 1/g$. In near-saturated tracks, on the other hand, the mean blob length—$\bar{b} = (e^{\alpha g} - 1)/g$—contains most of the information. It has recently been proven (B 61) that $\bar{l}$ contains *all* the information in the gap structure of a track segment. This is because in the terminology of Sir Roland Fisher it is a *sufficient* statistic (F 25). If many blobs are measured, $\bar{b}$ practically exhausts the information regarding g that is contained in the blob lengths. It was further shown that $\bar{l}$ and $\bar{b}$ are completely independent quantities.

Some years ago, before the mean blob length was given its present interpretation, Castagnoli *et al.* (CCM 55) found empirically that $\bar{l}$ was the best ionization parameter in the near minimum region. In the clogged region they concluded that L was the best parameter.

An elementary track cell consists of a blob and the adjacent gap. The track is generated by a repetition of this unit. The expectation value of the blob length is $\langle b \rangle = (e^{\alpha g} - 1)/g$, but theoretical values of the higher moments are only approximations that depend on the blob model used for the calculation. The variance of the blob length, σ_b^2, can be treated as a parameter of the emulsion—a number like α to be obtained by calibration. It varies, however, with $\bar{b}$.

The estimates g_1, derived from $g_1 = 1/(\bar{l})$, and g_2, derived from $\bar{b} = (e^{\alpha g_2} - 1)/g_2$, are particularly valuable because they are results of independent measurements. Between them is contained all the available information. No further independent measurements can be made on the linear structure of the track.

A method of maximum likelihood combines g_1 and g_2 into a single best estimate of the grain density. The likelihood function is written as follows (B 61):

$$P \doteq \frac{1}{\sigma_b}\left[\frac{N}{2\pi}\right]^{1/2} g^N \exp\left[-g\sum_1^N l_i\right] \exp\left[\frac{-N(\bar{b} - \langle b \rangle)^2}{2\sigma_b^2}\right] \qquad (9.7.13)$$

The likelihood $P(g)$ is the relative probability that any particular value of g is the true value.

The likelihood function is constructed from the configuration of gaps having lengths $l_1, l_2, \cdots, l_N$, and blobs of mean length $\bar{b}$ observed in a segment of track containing N elementary cells. The relative likelihood for different lengths b to occur not being known exactly, it is necessary to employ the likelihood distribution of $\bar{b}$ as the factor containing the blob observations. A particular value g' of g then maximizes P.

The best estimate of g' is the linear combination

$$g' = \omega g_1 + (1 - \omega)\, g_2 \tag{9.7.14}$$

The weighting factor ω is related to the blob-length variance as follows:

$$\frac{\omega}{1-\omega} = \frac{(L \ln L)^2}{(1 - L + \ln L)^2}\,(\sigma_b/\alpha)^2 \tag{9.7.15}$$

Although no exact blob model exists, the blob-length variance can be calculated fairly closely (B 61). Two extreme blob models limit it as follows:

Let $y_1, y_2, \cdots, y_n$ be the projections on the particle path of the distances between sucessive grain centers in a blob. The expectation value of y_i is $\langle y \rangle$, and its variance is σ_y^2. The mean square blob length is

$$\langle b^2 \rangle = e^{-g\alpha} \sum_{n=0}^{\infty} \langle (\alpha + y_1 + y_2 + \ldots + y_n)^2 \rangle\, (1 - e^{-g\alpha})^n$$

$$= \alpha^2 + (2\alpha \langle y \rangle + \sigma_y^2)\, e^{-g\alpha} \sum_{n=0}^{\infty} n(1 - e^{-g\alpha})^n + \langle y \rangle^2\, e^{-g\alpha} \sum_{n=0}^{\infty} n^2 (1 - e^{-g\alpha})^n$$

The mean blob length also can be calculated:

$$\langle b \rangle = e^{-g\alpha} \sum_{n=0}^{\infty} \langle (\alpha + y_1 + y_2 + \ldots + y_n) \rangle\, (1 - e^{-g\alpha})^n$$

$$= \alpha + \langle y \rangle\, e^{-g\alpha} \sum_{n=0}^{\infty} n(1 - e^{-g\alpha})^n$$

Then $\sigma_b^2 = \langle b^2 \rangle - \langle b \rangle^2$ can be found, and in general

$$\sigma_b^2 = e^{g\alpha}(1 - e^{-g\alpha})\, \sigma_y^2 + e^{2g\alpha}(1 - e^{-g\alpha})\, \langle y \rangle^2$$

The variance of the diameters of single grains could be added as another term, but this is hardly justified.

Now the minimum value of σ_y is zero, and when the grain spacing within a blob is completely random, $\sigma_y^2 = (1 - \alpha^2 g^2 e^{-\alpha g})/[g(1 - e^{-\alpha g})]^2$ Therefore limits are imposed on σ_b as follows:

$$\frac{1 - L^2 + 2L \ln L}{(L \ln L)^2} > \frac{\sigma_b^2}{\alpha^2} > \frac{(1 - L + L \ln L)^2}{(1 - L)(L \ln L)^2} \tag{9.7.16}$$

The residual error in g' is measured by its variance, $\sigma_{g'}^2$. If the grains in the track segment of length Λ were dimensionless and countable, then

σ_g^2, would be equal to g'/A. Some information is lost, however, because the individual grains in a blob are finite in size and are not resolved. Therefore, $A\sigma_g^2/g'$ is not unity, but is given by

$$A\sigma_g^2/g' = (1/p) = \omega/L \tag{9.7.17}$$

In Table 9.7.1 are tabulated the connections that exist between g and the ionization parameters L, B, and $\langle b \rangle$. Based on the two extreme models, models 1 and 2, between which all actual blobs must lie, the weights and errors in the evaluation of g' are also given.

TABLE 9.7.1

THE CONNECTIONS THAT EXIST BETWEEN g AND THE IONIZATION PARAMETERS L, B, AND $\langle b \rangle$

				Combined g_1 and g_2						g_1 alone
				(*a*) Model 1			(*b*) Model 2			(*c*)
L	αg	αB	$\langle b \rangle/\alpha$	ω	$A\sigma_g^2/g$	p	ω	$A\sigma_g^2/g$	p	$A\sigma_g^2/g$
0.00	∞	0.00	∞	0.000	∞	0.00	0.000	∞	0.00	∞
0.05	2.9957	0.1498	6.342	0.143	2.86	0.350	0.139	2.77	0.361	20
0.10	2.3026	0.2303	3.908	0.212	2.12	0.472	0.202	2.02	0.495	10
0.15	1.8971	0.2846	2.987	0.271	1.81	0.553	0.255	1.70	0.587	6.67
0.20	1.6094	0.3219	2.485	0.326	1.63	0.614	0.304	1.52	0.659	5.00
0.25	1.3863	0.3466	2.164	0.376	1.51	0.664	0.349	1.40	0.717	4.00
0.30	1.2040	0.3612	1.938	0.425	1.42	0.706	0.392	1.31	0.765	3.33
0.35	1.0498	0.3674	1.769	0.471	1.35	0.742	0.435	1.24	0.805	2.86
0.40	0.9163	0.3665	1.637	0.517	1.29	0.774	0.476	1.19	0.840	2.50
0.45	0.7985	0.3593	1.531	0.561	1.25	0.803	0.517	1.15	0.870	2.22
0.50	0.6932	0.3466	1.440	0.604	1.21	0.828	0.558	1.12	0.896	2.00
0.55	0.5978	0.3288	1.369	0.646	1.17	0.851	0.599	1.09	0.918	1.82
0.60	0.5108	0.3065	1.305	0.688	1.15	0.873	0.640	1.07	0.937	1.67
0.65	0.4308	0.2800	1.250	0.728	1.12	0.893	0.682	1.05	0.953	1.54
0.70	0.3567	0.2497	1.201	0.769	1.10	0.911	0.724	1.03	0.966	1.43
0.75	0.2877	0.2158	1.158	0.808	1.08	0.928	0.768	1.02	0.977	1.33
0.80	0.2231	0.1785	1.120	0.848	1.06	0.944	0.812	1.01	0.986	1.25
0.85	0.1625	0.1381	1.079	0.886	1.04	0.960	0.857	1.01	0.992	1.18
0.90	0.1054	0.0949	1.054	0.925	1.03	0.973	0.903	1.00	0.997	1.11
0.95	0.0513	0.0487	1.027	0.963	1.01	0.986	0.951	1.00	0.999	1.05
1.00	0.0000	0.0000	1.000	1.000	1.00	1.000	1.000	1.00	1.000	1.00

[a] The important track quantities are tabulated as functions of the track lacunarity. The table also relates them to each other. The quantity $A\sigma_g^2/g$ gives: (*a*) the error for the maximum likelihood solution using model 1 for σ_b; (*b*) the maximum likelihood solution using model 2; and (*c*) the error when g_1 alone is measured. The corresponding values of ω and p are also tabulated.

For most purposes it will matter little what model intermediate between the extremes is assumed for calculating the statistical reliability of measurements. On either model the weighting coefficient ω varies from zero to unity, and except at very high grain densities, neither differs much from L. In the high grain density region, most of the information regarding g resides in $\bar{b}$.

When g becomes very large, it reaches a limit which is a measure of the quality of the particular emulsion employed as an instrument. When g approaches 5000 per mm, according to Fowler and Perkins, it saturates in G.5 emulsion. On plotting g for relativistic particles as a function of z^2, they found a near proportionality until this value was approached. Finer grains raise this limit.

Fowler and Perkins attempted, with incomplete success, also to make allowance for variations in the emulsion sensitivity and development by normalizing g values to the plateau value in the same emulsion. For low grain densities this is satisfactory, but for proton ranges of less than 1 cm, corresponding to a lacunarity of less than about 0.5, it is not a reliable procedure.

When emulsion fog or other single-grain background is high, a correction to the measured grain density may be required. Some of the grains along the track locus would not have developed had not the defect that produces fog grains been present. Let ρ be the radius within which a grain is considered part of the track. Then the corrected grain density g is found from

$$g = \frac{g_u - k(\pi\rho^2 N)}{1 - k} \tag{9.7.18}$$

In this formula g_u is the grain density uncorrected for background, N is the number of grains per unit volume in the emulsion sample, and k is the fraction of all grains that develop as background in the absence of a track.

For many purposes no correction for background is necessary even if it is high. This is because applications of measured grain densities often merely require *equality* of grain densities. The amount of background hardly matters, and even the relationship of the measured quantity to the true grain density is not important when all the measurements are made in the same sample of emulsion.

The amount of data that must be taken to determine the grain density with any prescribed statistical uncertainty, of course, always can be determined by using an internal estimate of the error. The variance of each ionization parameter also can be estimated by the methods of this

chapter. For example, for a track segment of length Λ, the variance σ_B^2 of B is

$$\sigma_B^2 = \frac{BL^2}{\Lambda}[1 + (\ln L)^2 (\sigma_b^2/\alpha^2)] \tag{9.7.19}$$

Similarly the variance, σ_L^2, of the lacunarity is

$$\sigma_L^2 = \frac{L^2}{B\Lambda}[(1 - L)^2 + (L \ln L)^2 (\sigma_b^2/\alpha^2)] \tag{9.7.20}$$

It is often found in poorly processed emulsion that grain densities depend explicitly on the distance from the emulsion surface that the measurement is made. This effect can be caused by incorrect development, by nonuniform latent-image fading, by corrosion of developed silver grains, and perhaps in other ways. When the effect exists, grain-density measurements can be made more reliable by determining a correction curve as a function of depth. Unfortunately the per cent correction generally depends on the grain density. Correction curves for minimum tracks (tracks near the minimum of ionization) are often best obtained by using particles that traversed the emulsion layer at a small angle of dip, and at such a high velocity that no appreciable change in the energy-loss rate is incurred in the segment of track studied. Another method is to measure the grain densities in tracks found at various depths in the emulsion, but produced by a monoenergetic particle beam. To find depth corrections at high grain densities, the tracks of identified particles, stopping at various depths in the emulsion, may be compared at residual ranges where their ionizations are equal. Tracks of multiply charged minimum particles traversing the emulsion also may be studied. Bonetti, Dilworth, and Occhialini (BDO 51) have reported that the effect of nonuniform development increases with the grain density.

In general, the emulsion batch, the age of the track, and the processing each affect the measured grain density. All calibration tracks should be of the same age, they should be produced at the same temperature, and they should also be found in the same volume of emulsion as the tracks being measured. Grain-density measurements near the edge of a plate are unreliable. The development may be abnormal, the grains may have been presensitized by light or mechanical stress, and the tracks probably will have been distorted in processing. Occasionally a lack of homogeneity occurs in the body of the emulsion. In Fig. 9.7.2 is shown an extreme (and rare) case of greatly reduced emulsion sensitivity in the middle of a track segment. Accompanying the reduction of sensitivity in this instance was an abnormally low shrinkage, as if a bit of emulsion with a low silver halide concentration had been occluded.

An important question for multiply charged particles is whether or not tracks made by particles of different charges, but of the same restricted rate of energy loss, have the same primary grain density. The answer is yes in first approximation. Using proton and alpha-particle beams, the blob density, B, was determined by Bowker *et al.* (BGB 51) as a function of rate of energy loss in Ilford D.1 emulsion. In the region where the data overlapped, the proton blob density was $3 \pm 2\%$ higher than that for the

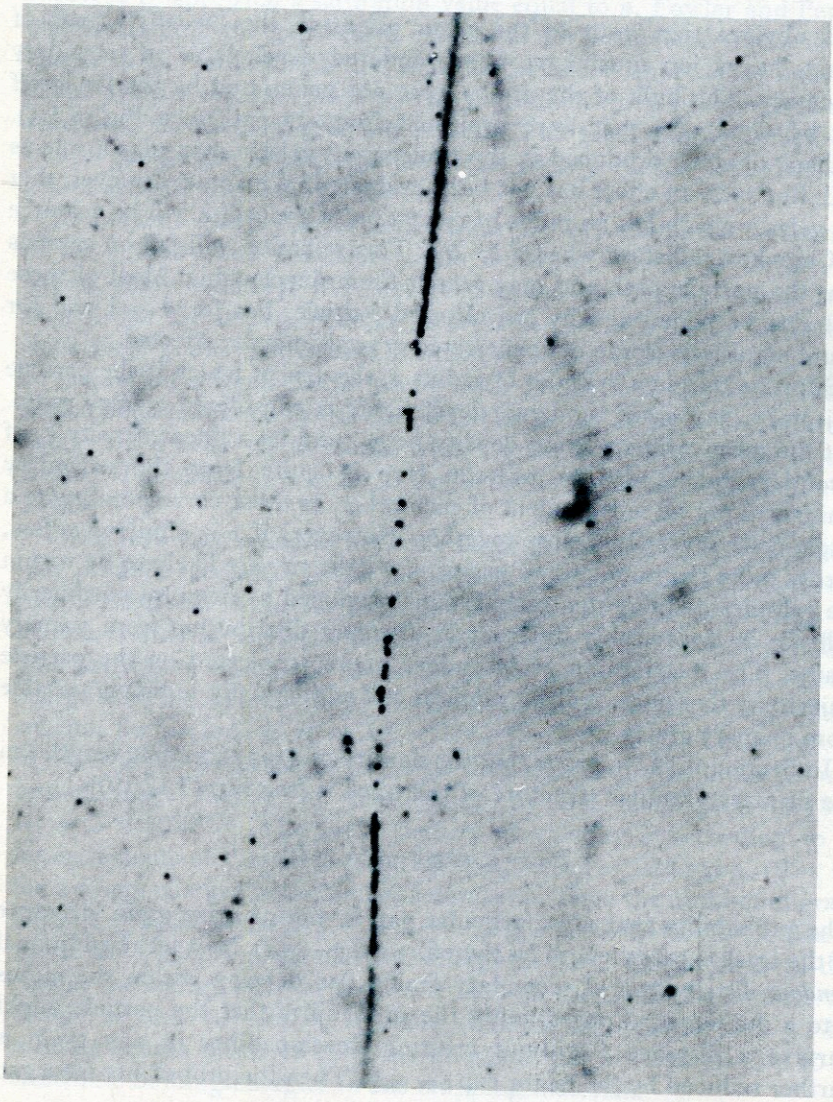

FIG. 9.7.2. An unusual example of suddenly reduced emulsion sensitivity in a region traversed by a strongly ionizing particle. (Photomicrograph by C. Cole.)

alpha particles. It must be remembered, however, that the delta-ray spectra are different when the velocities differ, and it is really effective energy-loss rates in AgBr that should be compared, so that exact agreement is not expected.

9.8 Secondary Grain Density

It is obvious that most of the silver grains in the "woolly" track of a fast, heavy ion must have been rendered developable in secondary processes. The bulk of the grains were not penetrated by the ion itself but by delta rays that were projected from its path (see Fig. 9.1.1). Perhaps photons produced in the transparent gelatin may play a role as well, but such an effect has not been evaluated. We know, however, that the gelatin which has an index of refraction of about 3/2 will be a source of Cerenkov radiation when $\beta > 2/3$. This radiation will fall on crystals near the particle path and may render them developable. Most of these will also be penetrated by the charged particle, but for $\beta \to 1$ and for dilute emulsions, some nonpenetrated crystals may be affected.

Suppose that in a cylinder of radius ρ, the axis of which is the particle trajectory, any grain rendered developable is considered a track grain. Let the mean primary grain density be g_p, and let a linear density g_s of secondary grains also be present. If ρ is quite large the secondary grains will not be independent of each other, as those corresponding to a single delta ray will be close together. However, if ρ is a micron or less, hardly more than one or two grains of a delta ray are likely to lie within the cylinder defining the track. Grains produced by delta rays ordinarily will not be appreciably different in diameter distribution from primary grains. The distribution of secondary grains, projected on the particle trajectory, therefore, will be random and individually indistinguishable from primary grains.

In Section 9.12 we prove that the density of gaps exceeding length l in the primary granular structure of the track is [see Eq. (9.12.19)]:

$$H_p = g_p \exp\left[-g_p(\alpha + l)\right]$$

The probability that any particular gap in the primary grain structure of the track exceeds length l is therefore $\exp(-g_p l)$. Now let an additional *random* distribution of secondary grains also develop within the radius ρ to a density g_s. Consequently the probability that the particle might survive a distance l without creating developability in any grain is further reduced by the factor $\exp(-g_s l)$. Then the probability for a gap

to exceed length l is $\exp[-(g_p + g_s)l]$. On setting $g = g_p + g_s$ we can write that the probability for a gap to exceed length l is $\exp(-gl)$, and the presence of the secondary grains gives no new character to the gap-length distribution. The gap-length coefficient then is g and $l = 1/g$. If, on the other hand, delta rays of several grains are included in the grain density, there could be an excess of small gaps.

When the effective rate of energy loss becomes very large, g_p is expected to approach a saturation value equal to n. Fowler and Perkins, on determining the gap-length coefficient for relativistic tracks of high charge in G.5 emulsion, found that the coefficient approached a value of about five per micron. Since n is no more than three per micron in G.5 emulsion, an excess of grains is present. The grain density contributing to the gap-length coefficient, therefore, clearly exceeds the density of grains actually traversed by the ion.

In a recent study, Patrick and Barkas (PB 61) attempted a separation of the primary and secondary grain densities. Tracks of oxygen ions having many delta rays were observed as the ion velocity varied. It was judged that the average observer accepts as part of a highly unsaturated track some grains that extend as much as 1.25 μ from the particle path. At points on oxygen tracks where such grains first appeared, the ion velocity corresponded to a maximum delta-ray of 22 Kev. The minimum energy for a delta ray to escape from a grain is ill defined, but it is not critical. The radius of a grain (0.1 μ) is the range of an electron of about 2 Kev.

Delta rays with energies between about 2 Kev and 22 Kev, therefore, may produce secondary grains all or most of which would be counted as part of the track. In the K.5 emulsion studied by Partick and Barkas such delta rays produce a density of secondary grains, $g_s = 3.9z^2/\beta_0^2$ per 100 μ. The particle to which the formula applies has velocity β_0 and carries a charge ze. This formula for g_s was deduced as follows: the range-velocity relation for protons is $R \approx 3.6 \times 10^5\beta^{10/3}\ \mu$ ($\beta < 0.3$). The range, R_e, of a low-velocity electron is obtained with satisfactory accuracy from the proton range merely by multiplying by the mass ratio (1/1800): $R_e \approx 2 \times 10^2\beta^{10/3}$. The grain density at velocity β according to the measurements of Patrick and Barkas is $g_0 \approx 9.2 - 32\beta$ per μ, ($\beta < 0.3$) for a singly charged particle in K.5 emulsion. Then the number of grains, $G(\beta) = \int_0^\beta g_0 dR_e = 2000/3 \int_0^\beta (9.2 - 32\beta)\beta^{7/3}d\beta = 0.18w^{5/3} - 0.03w^{13/6}$, where $w(= 256\beta^2)$ is the electron energy in Kev. The number of delta rays in the energy interval w to $(w + dw)$ on the track of a particle with charge ze and velocity β_0 is about $(0.0255z^2/\beta_0^2)\,(dw/w^2)$ per μ. This formula breaks down at delta-ray energies that are comparable to the electronic binding energies in the stopping material.

The number of grains, g_s, per micron produced by the delta rays along the path of a particle of charge ze and velocity β_0 then is found by integrating over w. It is

$$g_s = \frac{Az^2}{\beta_0^2} \tag{9.8.1}$$

with $A = 0.68\,(w_m^{2/3} - w_0^{2/3}) - 1.1 \times 10^{-2}\,(w_m^{7/6} - w_0^{7/6})$.

In this expression, w_0 represents the lowest average energy of delta rays contributing to the secondary grain density, and w_m is the maximum energy that a delta ray may have while its grains still are considered part of the track locus. $A = 3.9$ when $w_0 = 2$ Kev and $w_m = 22$ Kev.

The few track grains contributed by delta rays of higher energy may be compensated by the overestimate of w_m occasioned by its measurement on 0^{16} of low velocity.

9.9 Relativistic Rise of Grain Density

Experimental data on a rise of grain density in relativistic particle tracks beyond the ionization minimum, which occurs in the vicinity of $\tau = 3$ Bev, have demonstrated that an effect doubtlessly exists. Furthermore, its magnitude is about that expected were the grain density proportional to the restricted rate of energy loss (see Table 9.5.3), although the magnitude and even the existence of the effect was initially in doubt. A rise of the correct order of magnitude was found first by Pickup and Voyvodic (PV 50). An extensive study was carried out by Stiller and Shapiro (SS 53). They found agreement with that anticipated from their calculations of the restricted rate of energy loss, and a number of other workers have found substantial relativistic effects (V 51, DDMP 52, MV 53, FL 55, AJ 57, J 60).

A complete study of this effect, which may be influenced by the development or as yet unknown phenomena, has not been made. The limiting value of the restricted rate of energy loss is the plateau value that is approached asymptotically by Eq. (9.5.1) as $\beta \to 1$. Then the plasma frequency, ω_p, controls the energy loss. It's magnitude

$$\omega_p = \left(\frac{4\pi ne^2}{m}\right)^{1/2} = 7.36 \times 10^{16}/\text{sec}$$

for silver bromide is the limiting frequency. The restricted-energy-loss rate on the plateau is:

$$i'_{pl} = 0.067 \left[\ln 2\,\frac{\pi m^2 c^2}{nh^2 e^2}\,w'\right] \text{ Mev gm}^{-1}\text{ cm}^2 \tag{9.9.1}$$

$$\approx 0.98 \quad \text{Mev gm}^{-1}\text{ cm}^2 \text{ for } w' \approx 5000 \text{ ev}$$

$$\approx 0.92 \quad \text{Mev gm}^{-1}\text{ cm}^2 \text{ for } w' \approx 2000 \text{ ev}$$

Various experimental difficulties tend to obscure the rise. Cosmic-ray tracks are difficult to use because the particle velocity is hard to determine, and the age and amount of fading of an individual track usually is not known. The *temperature* of the emulsion at the time the latent image of the track was produced probably also is important. According to the data of Mme. Debeauvais-Wack the emulsion sensitivity rises about 2% per degree centigrade in the interval 20°-30°C, but this result has not been found by all observers in all emulsions. At the moment, the data on the temperature-dependence of the sensitivity of various emulsions is contradictory. Probably unrecognized interfering effects are present. Because there is evidence for a temperature effect, however, elementary prudence suggests that emulsion temperatures should be the same during exposures which are to be compared.

Long straight tracks of electrons on the plateau of ionization can be obtained, but at the minimum of ionization electrons scatter too much to be very useful. Tracks of mesons or protons, which have recently become available in accelerator beams, are best used to determine the grain density at the minimum. Ideally, the tracks to be compared should be produced simultaneously in the same sample of emulsion and at the same depth in the pellicle.

The shape of the grain density versus velocity curve in the relativistic region has potential importance for the study of elementary particle physics. In the stars produced by high-energy collisions, many of the relativistic particles emitted ionize above the minimum, but below the plateau of grain density. To identify such a particle, two quantities must be known. The multiple scattering is a quantity, in addition to the grain density, that may be measurable. Sternheimer (S 53.2) and others have shown that the Cerenkov radiation, which accounts for the rise of the energy-loss rate above the minimum, will be largely absorbed in the silver halide crystal and should contribute to the primary grain density. However, only the primary grain density is expected to be determined by the restricted rate of energy loss, and the secondary grain density can be appreciable. It was estimated by Patrick and Barkas (PB 61) to contribute as much as 25% at the ionization minimum. Admittedly the estimate is rather crude, so that it is difficult to place limits of error on it. At all high velocities the secondary grain density is expected to fall with the inverse square of the velocity, and therefore not to participate in the relativistic rise.

This previously unrecognized effect of the secondary grain density caused Patrick and Barkas to re-examine the whole problem of the relativistic rise of grain density. Precautions to avoid temperature-and-development-difference effects were taken, and fading was avoided.

Several independent measurements in the relativistic region were made.

If the mean excitation potential of AgBr is approximately 442 ev, the relativistic rise in the restricted rate of energy loss with a cut off of 2 Kev is about 18%. The secondary grain density was assumed to be given by Eq. (9.8.1) with $A = 3.9$ per 100 μ.

In Fig. 9.9.1 the solid curve is the calculated restricted energy-loss rate

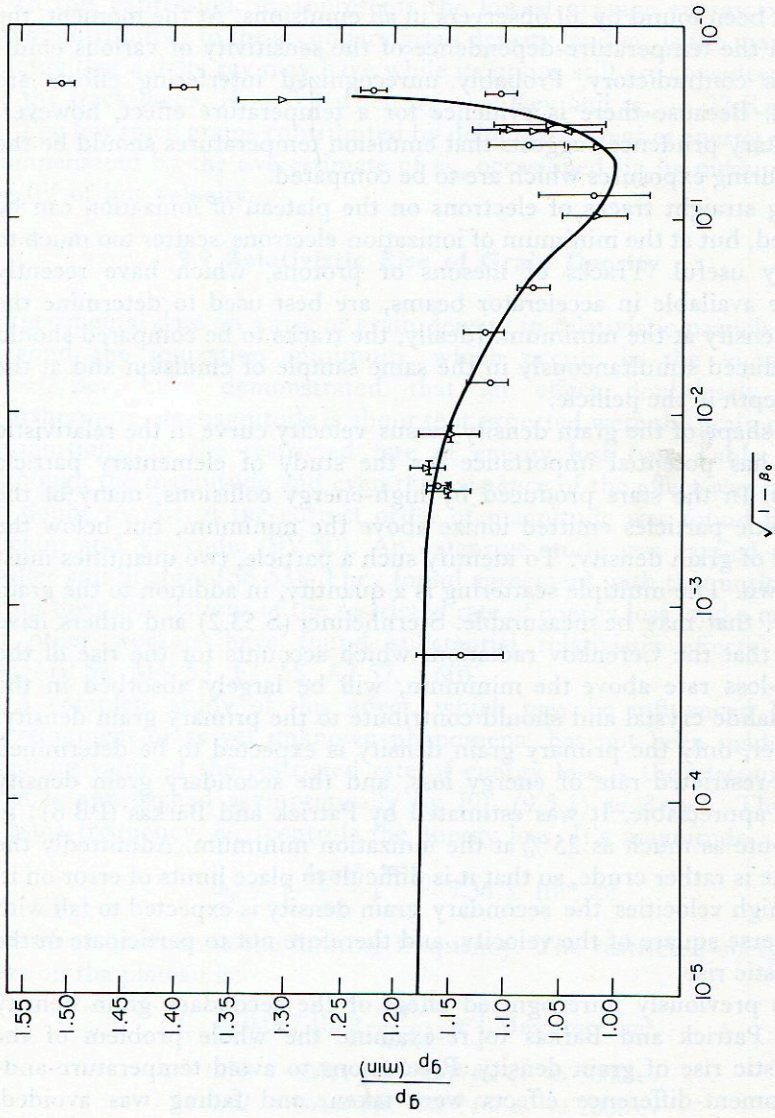

FIG. 9.9.1. The ratio of the primary grain density to that at the minimum of ionization derived from K.5 emulsion measurements of Patrick and Barkas (IDLRL).

relative to the minimum. The measurements of the primary grain density are shown as experimental points. There is apparent agreement, but it is obvious that much more exploration of the trans-minimum region of grain density will be required before velocity measurements beyond the ionization minimum can be made with confidence.

Since the primary grain density does not exceed n it tends to saturate even at the minimum of ionization when the particle is multiply charged. The secondary grain density does not saturate in this way, and it has no minimum. The minimum in the grain density is therefore expected to disappear for multiply charged particles.

It may be remarked that tracks of less than the "minimum" grain density are produced near the origin of very high-energy electron pairs. The coherent energy loss varies from zero upward as the two oppositely charged particles separate.

9.10 The Track Width

When the ionization is low, most of the information content of the track granularity can be obtained by blob counting or measurement of the gaps. If the ionization is somewhat higher, however, the blob lengths become a source of information, and near the blob density maximum the blob lengths contain more information than the gap lengths. At still higher rates of energy loss, the mean blob length provides most of the information in the linear structure of the track, but the absolute quantity of information still tends to vanish when the lacunarity approaches zero.

Fortunately, here another measurement technique becomes available. The width of the track rises with increasing grain density just in the region where little information remains in the linear track structure.

The "width" of a track depends in a complex way on the means employed for its measurement. It also depends on the characteristics of the emulsion, on the development the emulsion has received, as well as on the particle variables of velocity and charge. A formulation of the track width in terms of the particle variables alone cannot be made, and the correct determination of these quantities from measurements of the width is hardly a task for an amateur. Nevertheless, the particle variables do affect the track width, and this connection often can be usefully exploited.

Alvial *et al.* (A-O 56) made an extensive study of track widths by means of eyepiece micrometers. Measurements were made with cells of as little as 0.25 μ. It was found necessary to define carefully the conditions of measurement. The intensity of the light and the fatigue of the observer,

for example, are conditions that, in addition to development and depth in the emulsion, required close control.

It is not hard to think of ways in which the track can be widened by an increase of the particle ionization. Suppose that, when the ionization is low, only crystals traversed with the maximum sensitive path of the primary particle are likely to receive enough energy to be rendered developable. Such a track would have the minimum width. On the other hand, if the particle ionizes strongly, perhaps only a very small path in the crystal may be sufficient to produce developability. Then the track width may approach the sum of the processed and unprocessed grain diameters. When the emulsion sensitivity is high, of course, delta-ray grains displaced from the trajectory also develop (L 53.1). Photons produced by the Cerenkov effect and those from atomic excitations perhaps may also broaden the track.

Another reason for track broadening is a crowding out of grains as their number increases (A-O 56). This effect may be accentuated by the shrinkage when the track is dipping in the emulsion. A related effect was studied by Heckman *et al.* (H-B 60). Tracks of highly ionizing particles, in some strongly developed emulsions become crooked, as shown in Figs. 2.3.1 and 9.10.1. The growth of closely packed grains seems to produce such a crowding along the particle trajectory that the track buckles. There is apparently some cohesion between grains because the displacements of adjacent grains from the original particle trajectory are correlated, and loci are produced in which a characteristic wavelength appears to be defined.

On the other hand, minor development effects exist which tend to narrow the developed track. Suppose an ionizing particle passes through the edge of a grain. It is probable that the initiation of development would begin at the sensitivity centers on that side of the grain so that the reduced silver might be displaced from the grain center toward the particle trajectory. A slight decrease in the average diameter of grains that develop is also expected as the ionization increases.

Alvial *et al.* found a maximum width to occur in the tracks of singly charged particles at a velocity ($\beta \approx 0.1$) where one-grain delta rays first would be expected.

The track width is measured by accurate eyepiece micrometers, by tracing the projected track image and determining its area with a planimeter, by measuring its photoelectric opacity, from its Vidicon signal pattern, and in other ways (KMO 62).

In Table 9.10.1, the average widths in microns of the last 10 μ of proton tracks, and of the diameter of random grains in various emulsions as measured by W. F. Fry (F 57.2) using an eyepiece instrument, are given.

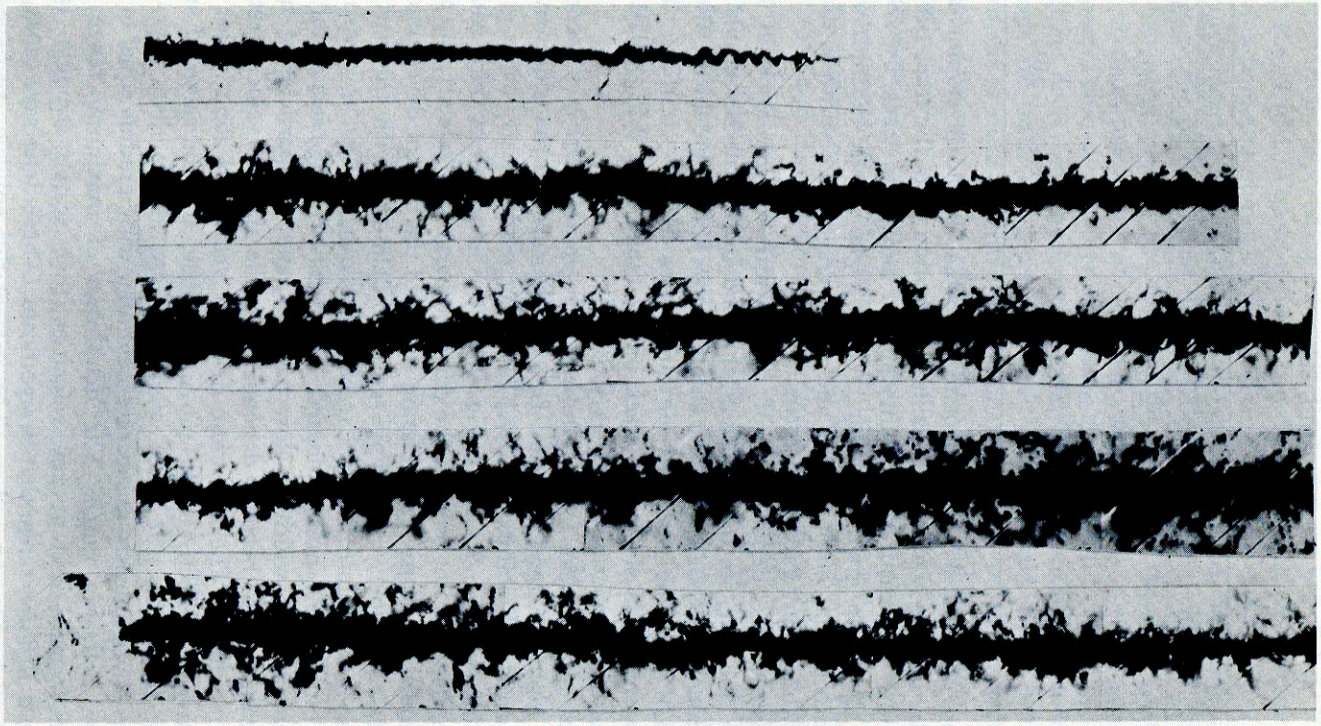

FIG. 9.10.1. A heavy primary cosmic-ray track crudely estimated to have an atomic number of 42 ± 4. Note the buckling near the end of the range. (Courtesy of M. M. Shapiro.)

TABLE 9.10.1

MEASURED TRACK WIDTHS

Emulsion type	Mean track width	Random grain diameter
RIAN PR	0.27 ± 0.017	0.35 ± 0.03
Ilford L.4	0.39 ± 0.017	0.42 ± 0.04
Ilford K.5	0.45 ± 0.017	
Ilford G.5	0.53 ± 0.034	
Ilford C.2	0.34 ± 0.02	0.427 ± 0.034

The values obtained doubtless depend somewhat on the development.

One obtains nearly all the available information from the track profile if the width is measured at points spaced along the track by about one-half the mean grain diameter. Where a gap exists, the measured track width at that point is zero and the average track width is much reduced when many gaps are present.

To indicate the dependence of track width on ionization at low velocities one can cite other results obtained by Fry in L.4 emulsion. Measurements on the last 8 μ of a single proton track gave for the width $0.42 \pm 0.017\ \mu$. The standard deviation was $0.084 \pm 0.017\ \mu$. The measurements on a single Li^8 track of 8 μ range gave $0.50 \pm 0.018\ \mu$ with a standard deviation of $0.07 \pm 0.018\ \mu$.

According to Eq. (9.1.1) the number of low-energy delta rays becomes large for highly charged particles. In a cylinder around the trajectory of such a particle, therefore, the delta rays may render nearly every grain developable (see Fig. 9.1.1 and Fig. 9.10.1). The apparent track width, therefore, depends not only on the particle charge and velocity, but also on the emulsion sensitivity, the grain size, and the type of development. The delta-ray velocity and range go up indefinitely with the particle energy, so no absolute limit on track width exists. What is measured depends on the conventions adopted. The delta-ray range sets a limit on the observed track width of slow particles, and, for particles of high charge, causes it to become dependent on the particle velocity rather than on its charge. The maximum delta-ray velocity is about twice the (nonrelativistic) velocity of the moving particle, and the range of such electrons determines the track width as long as the delta rays are numerous enough nearly to saturate a cylinder with a radius equal to the maximum delta-ray range. The delta rays of maximum range are projected forward, but at low velocities they scatter strongly. It is therefore a *diffusion* range that is significant. These delta rays cause the tracks of all highly charged particles in sensitive emulsion to have the

characteristic tapered appearance illustrated in Fig. 9.1.3, Fig. 9.1.4, and Fig. 9.10.1. The so-called "thin-down" length (see Section 9.4) has no fundamental significance, however, and it is not, as once thought, a range interval where the particle net charge and ionization are falling because the particle slows down and captures electrons. The ionization, in fact, continues to rise through the region of maximum track width to reach a maximum at residual range usually much less than the apparent thin-down length in a sensitive emulsion.

It has been found by Ammar (A 60) that when closely spaced measurements are made along a track, not the mean track width but its third moment is most sensitive to the charge of the particle producing the track. This may be an effect of "sub δ rays" which roughen the track profile.

Physical development and extrusion of reduced silver from the silver halide crystal cause the grains to enlarge on development. The amount of the enlargement depends on the kind of development. Della Corte (BD 58) and his collaborators studied the track width as a function of development, and concluded that the main influence is additive to the effect of velocity and charge. They also found that the difference in width of tracks of alpha particles and carbon ions is the same function of

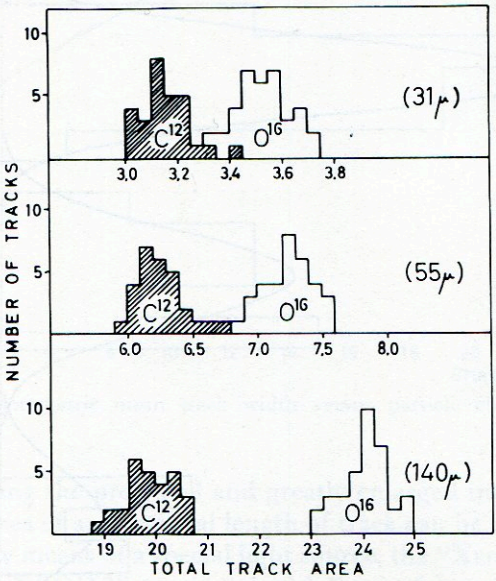

FIG. 9.10.2. Resolution of carbon and oxygen obtained from measurements of the track area when 31 μ, 55 μ, and 140 μ, respectively, of residual range were used for the measurements. (Courtesy of S. O. Sörensen.)

residual range in plates of the same type that have been developed differently.

Gegauff (G 59) studied development effects in some detail. She found that alpha-particle track widths in G.5 emulsion always increased as the time of development increased. The curves for ID-19, amidol, and glycin each had the same general behavior. These track widths remained about in proportion respectively to 1 : (3/4) : (3/5). Ascobic acid and Fe^{2+},

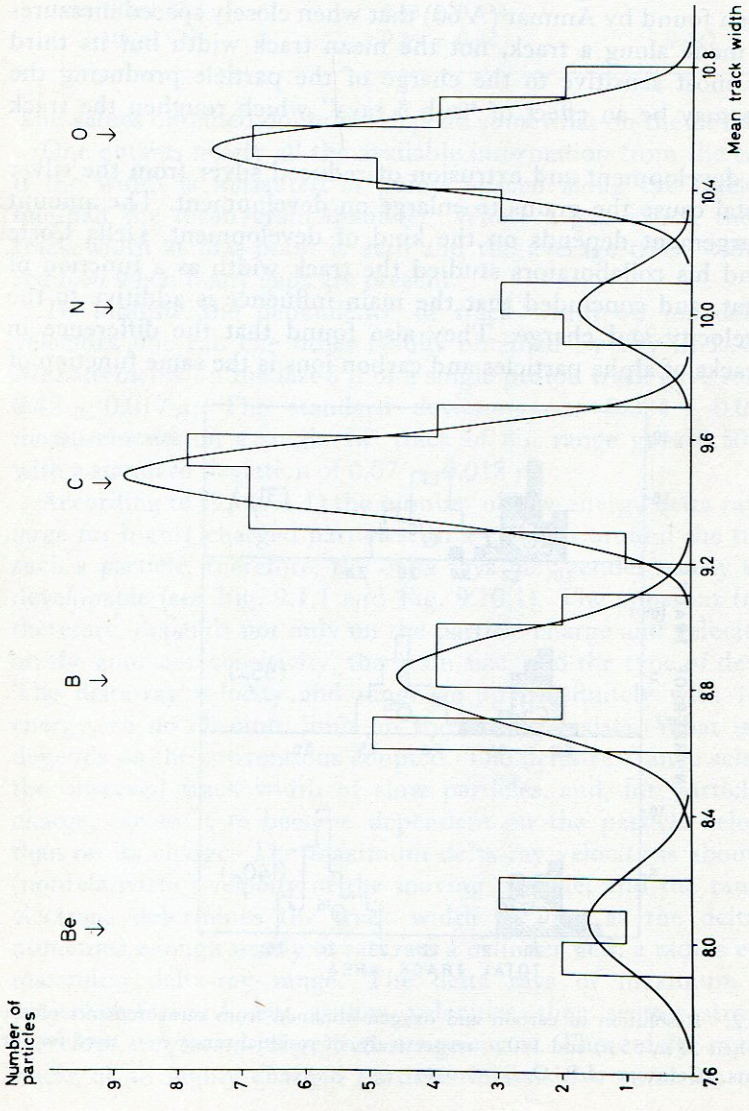

FIG. 9.10.3. Mean track widths of the light elements as measured by a track photometer. (Courtesy of S. von Friesen.)

Fe^{3+} after 30 min of development produced tracks of about the same width as amidol and glycin, respectively. After 90 min, however, they had widened only about an additional 10%, whereas the tracks developed with ID-19, amidol, or glycin were broadened by 50% or more.

A very simple method of track-width measurement that gives excellent results is employed by S. O. Sörensen and his collaborators in Oslo.

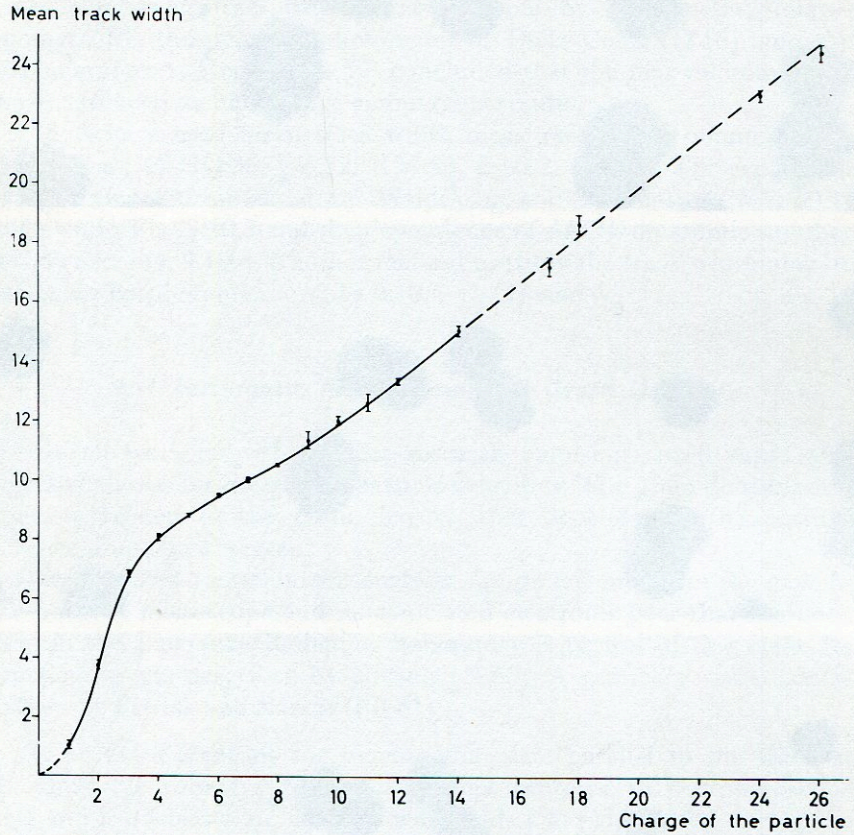

FIG. 9.10.4. Photometric mean track width versus particle charge. (Courtesy of S. von Friesen.)

Merely by tracing the projected and greatly enlarged image of the track on paper, the area of any residual length of track can be determined with a planimeter. By means of a special light source, the "Xenon-Hochdruckbrenner 150W, XBO162" combined with 7 cm of water filter, a magnification of 6000 can be used in a projection microscope. Successive segments of the track are brought into focus and then traced.

No corrections for loss of contrast deep in thick emulsions are required.

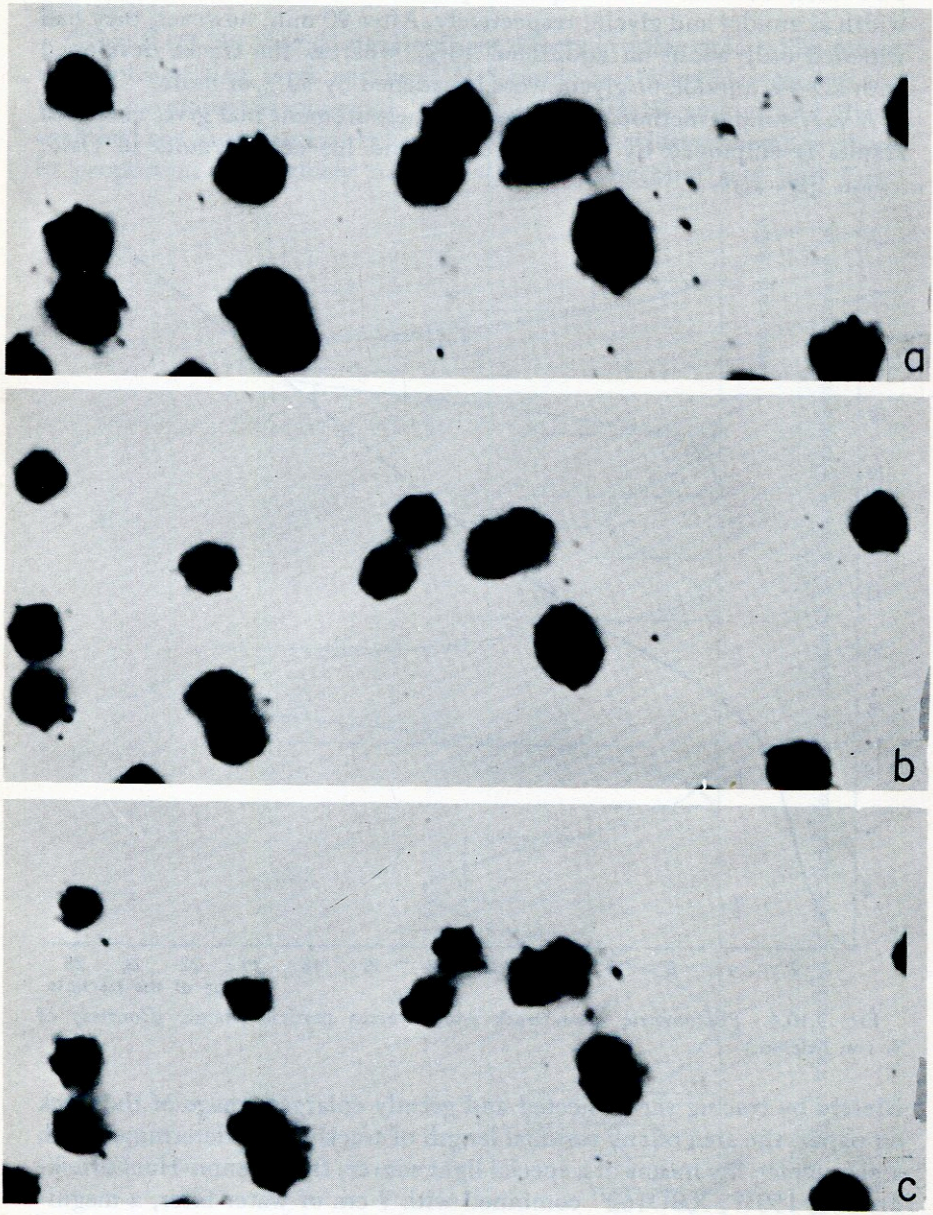

FIG. 9.10.5. (*a*) Argon ion tracks viewed end-on in C.2 emulsion when the residual range is about 90 μ. (*b*) The same field of view at a smaller residual range. (*c*) The same near the end of the range. Notice the change in track diameter as the end of the range is approached. (Photomicrographs by C. Cole.)

The area divided by the length is a measure of the mean track width that serves effectively to separate nuclear fragments of different atomic numbers. Figure 9.10.2 shows the resolution obtained using tracks of varying lengths. Track widths of light nuclei are well resolved when a track length of 140 μ is available in G.5 emulsion, but even 55 μ provides a separation that is satisfactory for many purposes.

On comparing track-width measurements by photometry, microphotography, the dynamic photometer of Della Corte (D 56), and the filar micrometer, Gegauff (G 59) concluded that the filar micrometer is the least objective, but all give comparable results.

Others have used mean track-width measurements to obtain similar resolutions (NTHO 56, CZ 52, KM 53, C 60.2, P 59.1). The separation of light elements obtained by Waldeskog and Mathiesen (WM 60.1) is shown in Fig. 9.10.3 and the dependence of MTW on atomic number is shown in Fig. 9.10.4. Another method to study the track width may be suggested by photomicrographs 9.10.5(*a*), (*b*), and (*c*).

9.11 Automatic Measurement of Grain Density

Nearly all workers with nuclear research emulsions need rapid and objective means for measuring particle velocities. The grain density, or a quantity related to the grain density that depends on the particle velocity, must be observed.

One type of automatic track-analysis equipment measures the gaps in the track. A microscope and its associated electronic gear that has been used in the Lawrence Radiation Laboratory is typical of this class. Its functioning was described by Nickols (N 60). A summary was made as follows by Patrick and Barkas (PB 61):

"It provides a means for moving the plate parallel to the track at an adjustable velocity. The track is kept centered in the microscope field and in focus by an observer who holds a key depressed during the time that a fine reticle line perpendicular to the track crosses the track in a gap. He releases the key when the end of each gap is reached, and depresses it when each new gap first reaches it. The lengths of track and gap, the number of gaps, and the distribution of gaps in ten intervals of length are tabulated electronically. For reliable work the stage velocity must be decreased until no changes in results are produced by a further reduction in speed."

Subsequent improvements have included photomultiplier measurements of the gaps, automatic track centering, and accurate rotation

of the plate about the objective-lens axis. These features permit more rapid tabulation of the gaps, and are steps toward completely automatic operation. Quite a large number of devices built for a similar purpose have been described. See, for example, references (R 53, BC 54, HS 54, M 55, KB 56, E 57).

An improvement in objectivity and a saving in time is effected by an automatic focusing device such as that of Castagnoli *et al.* (CFLP 59). Such a feature is also incorporated into the scanning system of Voronokov *et al.* (VMSS 60), described in Section 7.4. The objective lens is mounted flexibly so that it can be moved up and down electromagnetically. By feedback, the signal itself then can be used to maintain the objective at the position of maximum signal, or a cycle of focusing motions can be imparted to the objective so that it sweeps through the correct focal position periodically.

Another type of automation was carried out at Strasbourg. On coupling a Poohstrolino eyepiece micrometer to a linear potentiometer, Gegauff (G 59) was able to make rapid track-width measurements that were automatically recorded as pen displacements on tape. Another somewhat similar device has been described by Stiller and Louckes (SL 58).

Tests have been made with commercial components, and a complete television system for track granularity analysis is currently being constructed at the Lawrence Radiation Laboratory. This model has an electronic resolution distance of 0.1 μ at a magnification of 2000. By means of a tilting stage and long working distance optics it accepts tracks with dip angles of up to 25° in the processed emulsion, so that only about one-fourth of randomly directed tracks are too steep to be measured with it. The track segment is oriented generally perpendicular to the sweep which is gated for an adjustable period as it crosses the track. The presence of a signal corresponding to a track grain is recorded along with the signal duration, measured in cycles of a 20-megacycle oscillator. These basic bits of information can be used to obtain a detailed analysis of the granularity of any track segment. As designed, the blob density, the mean blob length, the mean gap length, the mean track width, the depth of the track segment in the emulsion, and the dip angle are displayed and punched into IBM cards. The data can be entered on the cards either for individual track segments as short as desired, or as averages over longer portions of the track. In the IBM program provision for depth and dip calibrations are included.

Weighting of the blob and gap data is made according to the solution of maximum likelihood (Section 9.7).

The television equipment has several obvious advantages. It is very

fast. Its output can be programmed to calculate and read out any geometrical feature of the track. Electronic control can be utilized so that the track contrast does not vary with depth in the emulsion. The signal pulses also can be shaped so that grain edges become objective discontinuities.

An interesting subject, but one that has not yet been well developed, is the description of a track entirely by the Fourier transform of the electrical signal generated when a photometer scans the track. An initial attempt to describe a track segment by a Fourier series has been reported by Ahmad *et al.* (ACDD 58). Very rapid track analysis by such a method may be possible using modern electronic techniques.

The photometric track width, and the application of this quantity to particle mass and charge determination, have been studied extensively by Prof. S. von Friesen and his collaborators in Lund. The measuring instrument for this work, several variations of which exist, is illustrated by Fig. 9.11.1. Operational and constructional details have been given by von Friesen and Kristiansson (VK 52) and by von Friesen and Stigmark (VS 54). In the model illustrated, a real image of the track is

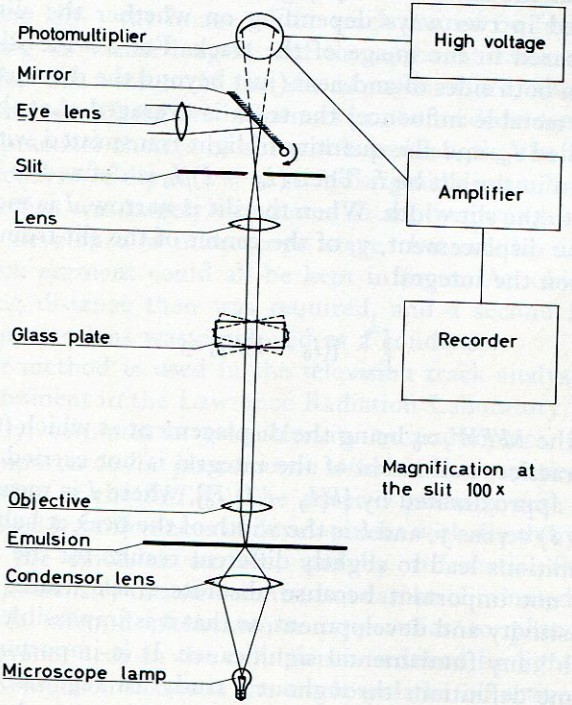

FIG. 9.11.1. Schematic arrangement of von Friesen-type track photometer (IDLRL).

produced at the plane of the slit. It can be examined by means of the eye lens utilizing light reflected from a face of the mirror through which most of the light passes to the photomultiplier. The diameter of the photocathode is much greater than the length of the slit. The slit dimensions are typically 10 mm by 0.5 mm. A plane parallel glass plate 4.5 mm in thickness causes the image of a track to move across the slit as the plate is tilted. Periodic tilting is effected by a synchronous motor. A speed of displacement is selected that is not too high for faithful recording by equipment that registers the output of the photomultiplier tube. This equipment consists of a dc amplifier and a recorder. The effective speed of the track in the object plane is about 0.1 μ per second. The initial tilt of the plate is about 10°, and small changes of tilt do not much affect the amount of light transmitted by it.

Tests for constancy of the battery-powered light, reproducibility of the measurements, linearity of the amplifier, and consistency of the background measurements are made while putting the instrument into correct adjustment.

With this instrument is obtained a rather objective measure of the grain density of the track as the photometric mean track width (*MTW*). This is defined in two ways depending on whether the slit is narrow or wide compared to the image of the track. For a wide slit, the light transmitted on both sides of and near (just beyond the distance where the track has a detectable influence) the track is averaged. Let this quantity of light be called I_0, and the quantity of light transmitted with the track image centered in the slit be I. Then $(I_0 - I)/I_0$ is defined to be the ratio of the *MTW* to the slit width. When the slit is narrow, I is measured as a function of the displacement, y, of the center of the slit from the axis of the track. Then the integral

$$\int_{-x_0}^{x_0} [(I_0 - I)/I_0]\, dy$$

is defined as the *MTW*, x_0 being the displacement at which $(I_0 - I)$ falls to zero. In practice, evaluation of the integral is not carried out, but its magnitude is approximated by $[b(I_0 - I)/I_0]$, where I is measured at the peak of $(I_0 - I)$ versus y, and b is the width of the peak at half maximum. The two definitions lead to slightly different results for the *MTW*. The difference is not important because absolute track widths depend on emulsion sensitivity and development, so that it is impossible to attribute to the "width" any fundamental significance. It is important merely to retain the same definitions throughout a study. In Fig. 9.10.4 the mean track width of heavy cosmic-ray primaries is given as the percentage

of the slit width (4.3 μ projected on the emulsion plane), and in Fig. 9.10.3 the separation obtainable between light nuclei is illustrated when 10 to 30 mm of each track has been measured. Individual charges up to the region of iron can now be resolved if several centimeters of track are available for measurement. Iron itself is conspicuous in the primary cosmic radiation. Elements immediately below iron in atomic number are found and presumed to be spallation products of iron produced in interstellar collisions, while little or nothing heavier than iron was found (KMW 60).

Many other track photometers have been built that are more or less similar to the Lund equipment. Some are described in the following references: (V 55, MD 53, I 57).

A difficulty that is not limited to photometric measurements of the *MTW* is encountered in studying tracks that are inclined in the emulsion. In general, two tracks of the same ionization but different dip angles will not have the same measured *MTW*. Fortunately it has been found that this effect can be largely eliminated in photometric work by the correct choice of slit dimensions. The apparent mean track width tends to be increased on a steep track because gaps are obscured. On the other hand —with a long slit— the image of the track cannot be focused simultaneously along its whole length, and the apparent track width will be decreased for this reason. If the slit is made wider, the out-of-focus effect is decreased. These two influences can be made to compensate each other with practical choices of slit width and length; the *MTW* can be made independent of dip to 1% or so for original dip angles of up to 30°.

The dip effect was largely eliminated in another way by Van Rossum (V 55). He developed a microscope stage that would tilt so that an inclined track segment could all be kept in focus. An objective lens of long working distance then was required, and a second long working distance objective lens was employed as a condenser.

(A similar method is used in the television track-analysis equipment under development in the Lawrence Radiation Laboratory.)

A difficulty, common in grain-density measurements, but having a particular importance for photometric work, is the variation with depth in the emulsion of the *MTW*. The effect is partially real. A change in *MTW* is caused by differences in development with depth by corrosion of grains near the emulsion surface, and by differential fading. These affect all grain-density measurements, but can be eliminated more or less perfectly. The second phenomenon is peculiar to photometry. The contrast of grains deep in the emulsion is reduced by light scattered in the layer of emulsion between the track and the objective, so that the measured value of $(L_0 - L)/L_0$ from identical tracks falls as the depth

of the track in the emulsion increases. Allowance for this effect must be made, and for each plate, or at least for each emulsion stack, a correction curve for the MTW as a function of depth in the emulsion must be constructed. Fortunately it usually is almost independent of the track width.

9.12 Theory of the Primary Grain Density

This section is an exposition of a theory developed by the writer (B 59.1, B 60), and it follows portions of the original documents closely. It relates only to the primary grain density, the density of developed grains that were penetrated by the primary particle as it traversed emulsion. The secondary granularity produced by delta rays was discussed in Section 9.8. The elementary process which produces developability in delta-ray grains is doubtless the same. The delta ray is then considered the primary particle. In this treatment we assume the independence of crystals, their approximate spherical shape, a distribution of crystal diameters, and other postulates mentioned in Section 3.9.

9.12.1 Creation of Developability

All current theory of the latent image contemplates the initial creation of a free electron-hole pair in the crystal lattice. This is the primary act, and it is immaterial for this treatment whether the electron is captured in an impurity center or whether imperfections in the crystal lattice, as proposed by Mitchell (MM 57), serve as points where free silver atoms aggregate. The details will, however, affect the coefficients A_{ijk}, introduced below, and it is to be hoped that the fundamental mechanisms of silver halide sensitivity may become better understood by a study of the influence on the A_{ijk} of physical and chemical conditions, for example the temperature.

In this treatment it is assumed that the effect of a moving charged particle is as follows: the virtual photons of its electric field disturb the electrons of a silver halide crystal and induce transitions between their energy states. This produces electron-hole pairs in the crystal lattice, as free photons do. Some of the electrons released are given sufficient energy to produce further electron-hole pairs in the crystal, just as an X-ray photoelectron is capable of doing.

Let $(d\sigma/dw)dw$ be the cross section for a moving charged particle to transfer energy in the interval dw to the electron in the crystal, and let n_e be the electron density. Then

$$\mathscr{I}_h = n_e \int_0^{w_{\max}} w \frac{d\sigma}{dw}\, dw \qquad (9.12.1)$$

is the average energy loss per unit path in the crystal. (For the purpose of this discussion one need not distinguish between the different classes of electrons—a separate integral over each class would be required in general.)

In the above formula $w_{\max}$ is the maximum energy that the electron can absorb from the field of the moving particle. This may be so large that the range of the electron far exceeds the dimensions of the crystal. For this reason Messel and Ritson (MR 50) suggested that the upper limit of w be cut off at some value w' corresponding to the electron energy required for escape from the crystal.

$$\mathscr{J}' = n_e \int_0^{w'} w \frac{d\sigma}{dw}\, dw \tag{9.12.2}$$

This quantity, the restricted rate of energy loss, was calculated in Section 9.5. The effectiveness of a charged particle in creating developability should be largely determined by $\mathscr{J}'$, but it is still an approximation. It is suggested that one cannot weight equally all transfers of similar amounts of energy regardless of how it is distributed. There is certainly an optimum packet of energy for which per unit of energy a highest probability of development occurs. A relative efficiency $E(w)$ for energy utilization can be defined. [$E(w)$ should be calculable from the spectral sensitivity curve for the emulsion obtained by measuring its sensitivity to photons of all energies.] It is obvious that the particle energy is used very inefficiently in producing developability. Whereas a charged particle in a sensitive emulsion loses $\approx$ 1000 ev per developed grain, photons of the optimum energy require only the order of 10 ev per grain. To be quite exact therefore,

$$\mathscr{J}'' = n_e \int_0^{w_{\max}} w \frac{d\sigma}{dw} E(w)\, dw \tag{9.12.3}$$

is the function affecting the probability of development of a crystal traversed by a charged particle. This, one may call the *effective* rate of energy loss.

The function $E(w)$, however, is probably peaked well below w', and since the velocity dependence of $d\sigma/dw$ occurs chiefly as a factor, one expects a large range of high velocities over which $\mathscr{J}''$ is proportional to $\mathscr{J}'$. The distinction between them nevertheless should be retained.

A theory that does not take account of the statistical nature of the energy-loss process can have no fundamental validity. The energy dissipation when a charged particle traverses a grain, as has been emphasized by Barkas (B 51), Brown (B 53.5), Fowler and Perkins

(FP 55), and Bogomolov (B 57), is a highly stochastic process. The mean rate of energy loss has little direct connection with the energy loss in a particular grain. Suppose one considers a 100 μ path of a 3 Bev proton in an emulsion of standard composition and with a root mean square grain diameter of 0.17 μ (Ilford L-type emulsion). The average energy loss in a grain will be about 100 ev, and the proton will encounter about 440 grains in this element of path. Now, whereas in about 190 such traversals the proton will lose more than 100 ev in about 19, the energy loss will exceed 1000 ev. Therefore, at least in fine-grain emulsions, a large fraction of the grains rendered developable at the minimum of ionization can be attributed to the relatively rare traversals with large energy transfers.

When a charged particle penetrates a silver halide crystal it transfers energy to electrons until, after a certain such collision, the crystal may for the first time be in a developable condition. Further transfers only strengthen the latent image. We assume that in any element of path the probability for an act that of itself is sufficient to render the crystal developable depends on the product of three factors: s, a measure of the local sensitivity; $\mathcal{J}''$, the effective rate of energy loss; and, dy, the element of path length. First one treats the simplest model that may have some validity: a probability ψ is defined that a crystal of diameter D remain undevelopable after being penetrated a distance y by a charged particle with an effective rate of energy loss $\mathcal{J}''$. One assumes:

$$d\psi = -\psi s\mathcal{J}'' \, dy \quad \text{or} \quad \psi = \exp(-s\mathcal{J}''y) \tag{9.12.4}$$

The probability, G, that the crystal be completely traversed without being rendered developable then is $G = \exp(-s\mathcal{J}''\delta)$, where δ is the length of the track segment in the crystal.

In effect, this model assumes that there is a mean free path, $(s\mathcal{J}'')^{-1}$, for developability. It is unlikely, however, that matters are that simple. A mean free path for developability will exist only if the rendering of a crystal developable by an interaction is solely determined by this event, and is not influenced by a cumulative conditioning effect in the crystal brought about by the prior passage of the charged particle through sensitive parts of that crystal or surrounding matter.

It is also unlikely that s can be independent of position in the crystal. Bogomolov (B 57) has put forward evidence that the sensitive volume of a crystal is a thin surface layer. Certainly surface sensitivity centers are more accessible to the reducing action of the developing agent, and such centers probably are more abundant on the surface. The migration distances of electrons and silver are not known.

The true physical situation regarding these questions cannot be stated precisely at present, and in a general theory one must simply make appropriate allowance for any reasonable form the facts ultimately may be found to assume. This is done by the introduction of free parameters, the presence of which in the theory will offer the possiblity of their experimental evaluation.

If a radial variation of sensitivity is to be taken into account, then the traversal of a crystal of diameter D with a path segment in the crystal of length δ would lead to a probability, $\exp\{-\mathscr{J}''s\delta f[(D-\delta)/b, \delta/b]\}$, that the crystal would not be rendered developable. Here b is a characteristic length describing how rapidly the sensitivity varies with radius, and the function f is unknown except that it is expected to increase when $(D-\delta)/b$ rises. Since one cannot in general overlook the possibility of cumulative effects, as mentioned above, the quantity $\mathscr{J}''s\delta f[(D-\delta)/b, \delta/b]$ must be multiplied by still another function of δ.

One should also introduce a second characteristic length, a, which has the significance that the effect of the passage of a charged particle through a segment of the crystal will have little effect on points more remote than the distance a.

Then to allow for all these possibilities one expresses the probability of nondevelopability, G, by the following series:

$$G = 1 - \sum_{i=1}^{\infty}\sum_{j=0}^{\infty}\sum_{k=0}^{\infty} A_{ijk}(D/b)^j(\delta/a)^k(\delta s\mathscr{J}'')^i \tag{9.12.5}$$

Here a is assumed large compared to crystal dimensions. Equation (9.12.5) may be compared with the simpler form obtained using the mean-free-path model. This is:

$$G = \exp(-\delta s\mathscr{J}'') = 1 - \sum_{i=1}^{\infty}\frac{(-1)^{i-1}}{i!}(\delta s\mathscr{J}'')^i \tag{9.12.6}$$

From Eq. (9.12.5) the total cross section, Ω, for developability of a crystal can be calculated

$$\Omega = (\pi/2)\int_0^D (1-G)\,\delta\,d\delta \tag{9.12.7}$$

or

$$\Omega = \frac{\pi}{2}\sum_{i=1}^{\infty}\sum_{j=0}^{\infty}\sum_{k=0}^{\infty}\frac{A_{ijk}}{i+k+2}D^{i+j+k+2}b^{-j}a^{-k}(s\mathscr{J}'')^i \tag{9.12.8}$$

The primary grain density, g_p, in a track then is

$$g_p = N\int_0^{\infty}\Omega F(D)\,dD = \frac{\pi N}{2}\int_0^{\infty}F(D)\,dD\int_0^D(1-G)\,\delta\,d\delta \tag{9.12.9}$$

or

$$g_p = \frac{3C}{\langle D^3 \rangle} \sum_{i=1}^{\infty} \sum_{j=0}^{\infty} \sum_{k=0}^{\infty} \frac{A_{ijk} \langle D^{i+j+k+2} \rangle \, a^{-k} \, b^{-j} (s\mathcal{J}'')^i}{i + k + 2} \tag{9.12.10}$$

For a particular emulsion type, the moments $\langle D^\mu \rangle$ of the diameter distribution are established by a grain-diameter analysis. The coefficients A_{i00} can be identified with the quantities $[(-1)^{i-1}]/i!$. The product $(s\mathcal{J}'')$ must be expressed in reciprocal length units; s is therefore a reciprocal energy.

The remainder of the coefficients is to be determined from experiment, but they are dimensionless and assumed to be independent of D and $\mathcal{J}''$; s and $\mathcal{J}''$ appear only in the product relationship. The coefficients can be studied by measuring g_p while varying $\mathcal{J}''$, s, and the $\langle D^\mu \rangle$ separately. The sensitivity s is maintained constant when the crystal precipitation, sensitization, and development procedures are fixed. It is not known how varying these procedures affects the quantities a, b, and A_{ijk}. In the Ilford G, K, and L series of emulsions the standard composition remains the same in all, and the grain-size distribution in each series is kept constant, but is different for each series. The sensitivity varies through each series, being maximum for sensitivity 5-emulsion and decreasing as one goes through the K series, for example, from K.5 to K.4 to K.3, etc. The concentration of each emulsion type can also be varied. It appears that such emulsions, especially in low concentrations, might be suitable for investigations on the cross section for developability of a silver halide crystal. The variable $\mathcal{J}''$ is under the control of the investigator, as is the physical and chemical environment. The primary grain density, of course, is obtained from the measured value of g by subtracting the secondary grain density. At present only crude data can be found for comparison with the theoretical form of Eq. (9.12.10), and no conclusions have been reached regarding its usefulness.

9.12.2 Structure of the Developed Track

Let $G = G(\delta, D, b, a, s\mathcal{J}'')$ be the probability that crystal C (see Section 3.9) be not developable after it is traversed by a charged particle, but for the following we need not specify the form of G. The quantity

$$\frac{\pi N (1 - G) \, \delta \, d\delta \, F(D) \, dD}{2 g_p} \tag{9.12.11}$$

is the probability that any particular crystal encountered will be of class C and will be rendered developable by the charged particle.

Now the probability that a crystal of class C' in the interval of particle path $d\mu$ be also rendered developable is

$$\frac{\pi^2 N^2}{4g_p}\,\delta\delta'\,d\delta\,d\delta'(1-G)\,(1-G')\,F(D)\,F(D')\,dD\,dD'\,d\mu \qquad (9.12.12)$$

Then the probability is q that the particle render crystal C developable and traverse the emulsion a distance exceeding μ *without* rendering developable a crystal of class C'. This probability is found from:

$$\frac{1}{q}\frac{dq}{d\mu} = -\frac{\pi^2 N^2}{4g_p}\,\delta\delta'\,d\delta\,d\delta'(1-G)\,(1-G')\,F(D)\,F(D')\,dD\,dD' \qquad (9.12.13)$$

One now is in a position to calculate the probability, Q, that the particle, after rendering a crystal developable, may go a distance exceeding μ without creating developability in any other crystal. This is formulated:

$$\frac{1}{Q}\frac{dQ}{d\mu} = -\frac{\pi^2 N^2}{4g_p}\iiiint \delta\,\delta'\,d\delta\,d\delta'(1-G)\,(1-G')\,F(D)\,F(D')\,dD\,dD' \qquad (9.12.14)$$

so that, as P_1 was calculated in Eq. (3.9.17),

$$Q = \exp\left[-\frac{\pi^2 N^2}{4g_p}\iiiiint \delta\,\delta'\,d\delta\,d\delta'(1-G)\,(1-G')\,F(D)\,F(D')\,dD\,dD'\,d\mu\right] \qquad (9.12.15)$$

We adopt the convention that a gap can exist between two developed grains C and C' only when $\mu > (D + D' + e + e')/2$. The quantities e and e' are the respective amounts by which the optical diameters $(D + e)$ and $(D' + e')$ of the developed grains exceed the unprocessed crystal diameters. (It is to be noted that the grains are projected on the trajectory of the particle before it is asked whether or not a gap is present. In case of an inclined track, everything is first projected on the horizontal plane. Then the circles representing the grains are projected on the particle trajectory.)

The probability that the charged particle may go a distance exceeding $(D + D' + e + e')/2 + l$ after rendering crystal C developable, and without rendering developable a crystal of class C', is:

$$\exp\left\{-\frac{\pi^2 N^2}{4g_p}\left(l + \frac{D}{2} + \frac{D'}{2} + \frac{e}{2} + \frac{e'}{2}\right)[\delta(1-G)\,d\delta\cdot\delta'(1-G')\,d\delta' \cdot F(D)\,F(D')\,dD\,dD'\right\}$$

Considering crystals of all classes, the density H_p of gaps with lengths exceeding l is:

$$H_p = g_p \exp\left\{-\frac{\pi^2 N^2}{4g_p}\left[\int_0^\infty (D+e)F(D)\,dD\int_0^D \delta(1-G)\,d\delta\right]\right. \tag{9.12.16}$$
$$\left.\times\left[\int_0^\infty F(D)\,dD\int_0^D \delta(1-G)\,d\delta\right] - \frac{\pi^2 N^2 l}{4g_p}\left[\int_0^\infty F(D)\,dD\int_0^D \delta(1-G)\,d\delta\right]^2\right\}$$

Using Eq. (9.12.9) this becomes

$$H_p = B_p \exp(-g_p l) \tag{9.12.17}$$

with

$$B_p = g_p \exp\left\{-\frac{\pi^2 N^2}{4g_p}\left[\int_0^\infty (D+e)F(D)\,dD\int_0^D \delta(1-G)\,d\delta\right]\right.$$
$$\left.\times\left[\int_0^\infty F(D)\,dD\int_0^D \delta(1-G)\,d\delta\right]\right\}$$

If

$$\alpha = \frac{\int_0^\infty (D+e)F(D)\,dD\int_0^D \delta(1-G)\,d\delta}{\int_0^\infty F(D)\,dD\int_0^D \delta(1-G)\,d\delta} \tag{9.12.18}$$

the density of gaps exceeding length l can be written

$$H_p = g_p \exp[-g_p(\alpha + l)] \tag{9.12.19}$$

The particular average over the grain diameters that we call α is identified with the similar quantity α defined by Fowler and Perkins. It should be noted, however, that it has not a purely geometric meaning unless the grain-size distribution is very narrow. In general it is slightly dependent on g, and, as we have seen above, its operational definition involves the optical resolution. No dependence of α on g can be detected in the data of Alvial *et al.* (A-O 56), and in view of the form of Eq. (9.12.18) it generally will be very insensitive to g. It is recommended, nevertheless, that this parameter of the emulsion be determined independently on tracks similar in grain density to those in which g is to be measured.

The structure of a particle track is illustrated by Fig. 3.9.1. The path of a particle through the unprocessed emulsion is shown in (*a*) including a typical deta-ray path. The projection of this path and crystal configuration on the (x, y) plane is shown as (*b*), and in (*c*) the projected configuration of developed grains relative to the particle's path is illustrated.

Ranges and Range Straggling in Emulsion

10.1 Particle Ranges in Matter

If a particle has initial kinetic energy T_0 and in penetrating matter loses energy at a space rate, $\mathscr{J}(T)$ per unit path, then the distance it will go before coming to rest is

$$R_0 = \int_0^{T_0} \frac{dT}{\mathscr{J}} \tag{10.1.1}$$

The stopping is actually brought about by collisions between the moving particle and obstructions (chiefly electrons) in the stopping medium. The quantity $\mathscr{J}$ is therefore a statistical variable which is dispersed about its mean value. The expression (10.1.1) with $\mathscr{J}$ interpreted as the mean value of the energy-loss rate is consequently only an approximation to the mean range, and individual ranges will fluctuate about a mean value, R.

As first pointed out by Lewis (L 52), R exceeds R_0 because the mean value of the reciprocal of the energy loss in unit path exceeds the mean value of the path length per unit energy loss. In addition, individual ranges will differ from R in a random way. The distribution of ranges is approximately a Gaussian. Lewis has calculated the moments of the distribution for nonrelativistic particles. The variance of the distribution (the straggling) was first given by Bohr (B 15). The standard deviation of the range divided by the range is slowly varying with particle velocity. It is inversely proportional to the square root of the particle mass, and does not depend on its charge.

When the particle path is not visible in the stopping material the "range" may be given other meanings. Because the particle scatters, the path length will exceed the depth that it penetrates the absorber. The depth of penetration when the particle is normally incident on the absorber, we designate R_p. The straggling of R_p exceeds that of R. A complication occurs when the geometry is ill-defined so that some, but

not all, scattered trajectories are eliminated. The situation is still further complicated by the detecting instrument if the particle-path terminus is not observed visually. The instrument always has a finite resolution, and may, for example, respond to total ionization. Then secondary particles also may interfere with one's attempt to define the range. For these reasons, emulsion in which the whole particle path can be seen is superior to nonvisual instruments for precise determination of the particle energy from range measurements.

10.2 The Residual Range and Its Measurement

The concept of the *residual range* is one that is quite generally employed in emulsion work. The residual range, R, is the average distance that a particle with a given velocity has yet to go before coming to rest. It is a track variable that rises with the velocity, momentum, and energy. For a given charge and velocity, the residual range is quite precisely proportional to the particle mass. The length of a track, or the range, can be measured accurately in emulsion, and it is an estimate of the residual range that the particle had at the beginning of the track. The measured quantity, however, is subject to straggling, and is, therefore, a statistical variable. The residual range, on the other hand, is an ideal distance. It is the expectation value of the path length required to bring the particle to rest.

Since the distance to the terminus of a track from any point on it is usually an easily measured quantity, it is often employed as an independent variable in track measurements. Except for electrons the variance of the range is small, and often one need not distinguish between the residual track length and the residual range. In the literature the symbol R is used interchangeably for them.

Ranges of low-energy particles are conventionally measured in microns (10^{-6} meters), while longer ranges are expressed in millimeters or centimeters. The range, when expressed as a length, refers to emulsion of standard density which we define to be 3.815 gm/ml. Ranges are also expressed in grams per square centimeter. Conversion of ranges from nonstandard conditions is discussed in Section 10.7.

The particle range is, of course, the length of its path in emulsion before the emulsion has been processed. In processing it shrinks and undergoes other distortions (Chapter 6). Unmounted pellicles may suffer both lateral and vertical shrinkage. Shrinkage factors S_x, S_y, S_z may be defined along the principle axes of the ellipsoid into which a small sphere of the emulsion is distorted in processing. Usually

$S_x \approx S_y \approx 1$, and $S_z \equiv S$ for mounted pellicles. One makes the range calculation by evaluating the sum

$$R = \sum_{i=1}^{u} (S_x^2 \Delta x_i^2 + S_y^2 \Delta y_i^2 + S_z^2 \Delta z_i^2)^{1/2} \tag{10.2.1}$$

To carry out this summation one breaks up the track, which is not straight owing to scattering (Chapter 8), into n essentially straight segments. Then Δx_i, Δy_i, Δz_i are the three projections of the length of the ith track segment on the coordinate axes. The segment length chosen depends on the accuracy demanded. One may decide to approximate track segments by chords in such a way that the resultant error in the range remains less than 0.1 %. This requires that the root-mean-square space angle between the track and the chords remain less than 1.7°. In the *coordinate method* of range measurement, the x, y, and z coordinates of points on the track connected by such chords are measured. Suppose they are (x_0, y_0, z_0) $(x_1, y_1, z_1) \cdots (x_i, y_i, z_i) \cdots (x_n, y_n, z_n)$. Then, when the emulsion shrinks only in the z direction, the range is calculated from the formula

$$R = \sum_{i=1}^{u} [(x_i - x_{i-1})^2 + (y_i - y_{i-1})^2 + S^2(z_i - z_{i-1})^2]^{1/2} \tag{10.2.2}$$

which is equivalent to Eq. (10.2.1) when lateral distortions are not present (see Fig. 10.2.1). Increments of x, y, and z also are occasionally measured by micrometer dial gauges which record relative displacements of the stage and objective.

Tracks become straighter as the particle velocity and mass increase, so that long cells or segments can be used. When measuring short tracks, effects of the emulsion granularity also must be taken into account (H-B 60). It is probably best to measure the length of the track between the extremities of the first and last track grain, unless there is a definite point of origin such as a star center. One then applies corrections as follows: in a sensitive emulsion the terminal grain density is saturated, and it may be assumed that, on the average, the particle stopped at the last grain. If the particle entered the emulsion through a free surface and the surface has not been wiped or otherwise disturbed, one assumes that the particle will have traversed a distance in emulsion equal to the local mean gap length multiplied by the local track lacunarity before passing the center of the first developed grain. Now the mean grain diameter α is given by $\alpha = -(L/B)\ln L$ (Chapter 9). Therefore, to obtain the true range for this case, the length $(L/B)(L + \ln L)$ is to be

added to the track length measured between the extremities of the first and last grains. The track parameters L and B are to be measured at the high-velocity end of the track. The same correction applies to tracks known to start in the gel, such as those of protons recoiling from neutron collisions. On the other hand, tracks known to start in a silver halide

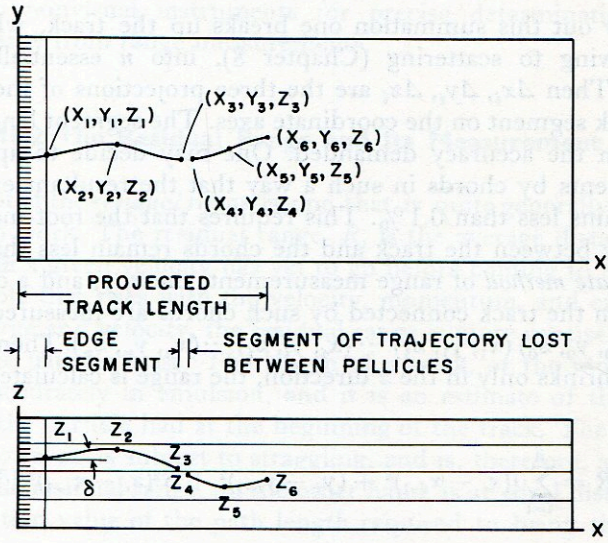

FIG. 10.2.1. Diagram to illustrate the geometric analysis of a particle track to determine the range in an emulsion stack. A small edge-segment may not be seen, but allowance must be made for it if the track entered the stack through the edge. Milling of the stack face is recommended. The track must be broken into relatively straight segments, and the range calculated using Eq. (10.2.2). The most serious uncertainty often arises in connection with a segment of trajectory lost between pellicles (between the points 3 and 4 indicated) (IDLRL).

crystal require a different correction. If the reaction is a violent one, almost certain to render the crystal developable, the quantity α is to be subtracted. In other circumstances, the correction may have to be calculated from the known characteristics of the emulsion, and the type and conditions of origin of the particles. For example, it was found (H-B 60) that heavy ions occasionally project a delta ray backward from their point of entrance into the emulsion. If the particle entry is at a small angle to the surface of the emulsion, this may add to the apparent range. When tracks that seemed to be influenced by this effect were eliminated, and the end corrections described above were applied, equal ranges were found by von Friesen (H-B 60) in emulsions of various sensitivities and grain sizes.

In emulsion stacks tracks that traverse several or many pellicles often must be measured. Then corrections usually are required for portions of the particle path that were overlooked or that have been completely lost from the surface. The finite grain spacing as well as possible surface corrosion and insensitivity lead to such losses. On the other hand, a layer of surface grains also may cause track sements to be missed if the track enters or leaves the surface at a grazing angle, and especially if the surface is not perfectly flat. For a fast particle that completely traverses a pellicle, the end corrections in each pellicle are made by adding the quantity $(L/B)\,(2L + \ln L)$ to the length measured between the extremities of the first and last developed grain.

Emulsion distortion can cause both systematic errors, requiring correction, or random errors that contribute to the apparent straggling of ranges (Section 6.12).

Neglect of scattering in the vertical plane, of course, causes as much error as its neglect in the horizontal plane, but for psychological reasons it is harder to make correct allowance for it. While measuring ranges great care should be exercised to detect changes of the dip angle. The dip is often best monitored by observing the length of the segment of track that is in focus.

The shrinkage factor of a group of plates cannot be assumed to be the same unless they are all of the same emulsion batch, and they have been processed identically. Variation of the fixing and washing times, as well as the drying, affects the shrinkage factor. An especially important effect arises from the glycerin soaked into the plate when the emulsion is immersed in a bath of glycerin and water or of glycerin and alcohol. Then the ambient relative humidity, the time of immersion, and the glycerin concentration all affect the emulsion thickness at the time of observation. One must remember also that the z calibrations of the microscope depend on the numerical aperture of a dry objective. If the surface of a plate is completely covered with immersion oil, it is protected from the atmosphere and changes of relative humidity affect the emulsion thickness hardly at all. Unless a very intense light source is used, the time of illumination (under oil) of a given area of the emulsion does not affect its thickness appreciably, but moist emulsion under a dry objective can be seriously affected.

A type of range error that often is not taken into account is that caused by distortion from compression of the emulsion in a stack. Emulsion is not strong and rigid. When pellicles are squeezed together to eliminate air gaps between them, they may be forced out laterally. The effect is partially elastic, so that on relieving the pressure the emulsion tends to return to its original dimensions. The correction for

this effect sometimes can be as high as 0.5% (B-T 58). The correction was determined as follows: after the stack was made up and tightened, opposite edges were milled so that they were parallel. The pellicle dimension was measured to 0.1% or better. Then after the pellicles were mounted, they were measured again to the same accuracy. This measurement was carried out on a measuring microscope stage. The edge where the emulsion was attached to the glass could best be observed when the plate was turned over and the emulsion-glass interface viewed through the glass with an objective of long working distance.

If one has an accurately moveable microscope stage which translates the plate along the x axis (conventionally to the left), and the y axis (conventionally toward the observer), this offers a satisfactory means for making range measurements. Displacements must be measurable to an accuracy of about 1 μ for many range measurements. Vertical displacements in the emulsion can be measured to this accuracy by means of a calibrated fine-focus scale. The z axis is conventionally taken to be positive when it is the distance in the emulsion above the glass-emulsion interface. Vertical displacements are measured with z increasing for a practical reason. The objective usually is raised against gravity to vary z. If it is lowered it tends to hang up, because of friction; therefore, such readings have reduced reliability. The z-coordinate readings should be taken in the opposite order when it is the stage that is moved.

Short ranges often are measured by means of an eyepiece reticle (Section 7.6). As mentioned elsewhere in this book, the magnification sometimes varies with the portion of the microscope field that is used. For precise range measurements, one should test for the presence of this effect by observing the length of a test body as a function of the distance from the center of the field.

In using a reticle it is generally best to keep the track length within one field of view, if possible. Thus, for example, an objective-ocular combination yielding a power of 500 and a reticle scale of 200 μ is preferable to a higher power for measuring 190 μ tracks. If the magnification were higher, the field would have to be shifted to measure the track length.

When it is necessary to shift the field, one examines the track and the region near the track to find recognizable landmarks. With the scale rotated so as to be parallel to the track, he may try to find a conspicuous grain exactly on the line at the end of the scale, or tangent to it. Alternatively there may be a small gap in the track near where it is crossed by the line. Such features are utilized to translate the track by accurately observable distances. This may be a distance equal to the length of the scale or the distance from a point where the particle scatters to the end

of the scale. The z coordinates of the ends of such a segment are also observed so that the true segment-length can be obtained from the composition of the horizontal and vertical components.

Unless unusual care is taken, there tends to be an error of a micron or so in shifting the field. One may expect a resultant error of about $n^{1/2}\,\mu$ in a track measurement requiring n shifts of the field. While the statistical error can be reduced by repeated measurements, it is seldom profitable to make the reading many times because the error normally is negligible compared to the range straggling. An important reason, however, for repeated independent range measurements is to eliminate gross errors, which may easily occur.

It is obvious that for accurate range measurements fine screw-motions must be used and backlash must either be taken up first or eliminated by good mechanisms. It should not be forgotten either that the calibration of the reticle depends on the tube length. This varies with the interocular separation on most microscopes. The tube length is altered in focusing some microscopes.

When one has a choice, as when there is a large flux of particles, he avoids the edge of a plate and measures only tracks which are not dipping and which do not scatter appreciably. If no bias is introduced in this way, complications are avoided. When dipping tracks are measured, errors may be looked for by plotting ranges that are expected to be equal against the dip angle. If no systematic effect is revealed in such a test, there is no reason to suspect bias in the data. Similarly, the lengths of scattered tracks may be compared with those of unscattered tracks of the same initial particle momentum. This will detect differences, either real or introduced by the method of measurement.

Suppose a coordinate frame is chosen with the origin at the beginning of a track and the x axis coincident with its original direction. Let the track terminus be at (x, y, z).

Then the range R is:

$$R = \int_0^x \left[1 + \left(\frac{dy}{dt}\right)^2 + S^2\left(\frac{dz}{dt}\right)^2\right]^{1/2} dt \qquad (10.2.3)$$

where the derivatives are taken on the track locus. The *direct range*, R_d, is simply $(x^2 + y^2 + z^2)^{1/2}$. Another measure of the range, mentioned above, is R_p, the projection of the particle path on its original direction of motion. This is simply equal to x.

The range can also be written: $R = \int_0^x \sec\theta\, dt$, where θ is the angle in unprocessed emulsion between the track segment and its initial direction of motion, and t is a variable running from 0 to x.

Now θ is the net angle through which the particle will have scattered on going a distance t in its original direction, and $dR/dt = \sec\theta$. Then if θ is small: $dR/dt = 1 + \langle\theta^2\rangle/2 + \cdots$ or $R \approx R_p + 1/2 \int_0^{R_p} \langle\theta^2\rangle dt$. In connection with the measurement of particle scattering, $\langle\theta^2\rangle$ was calculated as a function t in Section 8.11. Using this estimate, we find

$$R \approx R_p + \frac{\alpha}{8}(R_p/z^{1/2}M)^{4/5} \tag{10.2.4}$$

where $\alpha \approx 1/3$.

The correction term $(\alpha/8)(R_p/z^{1/2}M)^{4/5}$ was measured by William Simon using proton tracks in emulsion. He observed approximately a four-fifths power dependence on range. On tracks from which were eliminated those having sharp deflections, he found $\alpha = 0.28$, and K_0 to be 0.105 in the units employed in Section 8.11.

The direct range R_d now also can be calculated. We evaluated $\langle y^2\rangle$ in Section 8.11. Now $\langle z^2\rangle$ of the track terminus is equal to $\langle y^2\rangle$. Therefore, $R_d^2 = R_p^2 + 2\langle y^2\rangle$ or

$$R_d \approx R_p + \frac{\alpha}{18}(R_p/z^{1/2}M)^{4/5} = R - \frac{5\alpha}{72}(R_p/z^{1/2}M)^{4/5} \tag{10.2.5}$$

Simply by measuring the straight-line distance R_d between the ends of a track, the expectation value of the true range can be found. One merely adds a correction term, $\approx 5\alpha/72(R_d/z^{1/2}M)^{4/5}$.

While applicable over a wide range of energies, these formulas should be amended for the tracks of relativistic particles. A formula for $p\beta$ of wider applicability* and a better experimental evaluation of $\langle y^2\rangle$ are required. The statistical uncertainties of R_p and R_d, of course, exceed those of the measured R. Range straggling is treated in Section 10.8.

Since emulsion is a visual instrument, R can be observed directly. The same is not true of the range in most other materials. Usually the only measured quantity is R_p. The difference ΔR between R and R_p for any material, however, can be estimated using the emulsion results. Suppose, for a given energy T, $\Delta R/R_p$ is measured or calculated for emulsion. This value we designate $(\Delta R/R_p)_e$. Then for any other material of radiation length X_0 in which at energy T the particle has a projected range R_p, we can write $\Delta R/R_p = (\Delta R/R_p)_e(X_0/R_p)_e(R_p/X_0)$,

* An empirical formula for $p\beta$ that is not as good at low velocities as the one we have adopted, but which has a much wider interval of applicability was fitted to the range data by J. W. Patrick. It is $(p\beta)^{-2} = 2.60M^{-0.89}z^{-2.22}R^{-1.11}$. From the tracks of approximately 8-cm pions, he found $K_0 = 0.138 \pm 0.014$ in the units given above.

where $(X_0/R_p)_e$ is the ratio of radiation length to range in emulsion. All factors in this expression are to be dimensionless.

Some of the most important variables associated with the track are conventionally measured so that they rise as one traverses the track *counter* to the direction of particle motion. Where the particle comes to rest, its velocity, kinetic energy, momentum, and residual range vanish. If one follows the track, starting from this point, he will traverse it backward in time and in a direction opposite to the particle motion. All the above quantities increase monotonically with the distance.

An important concept is that of *equivalent track points*. Consider point O_1 on the track of a particle of mass M_1 and charge z_1 (in proton units). At this point it has velocity β (in light units), kinetic energy T_1, momentum p_1, residual range R_1. On the track of another particle there is a point O_2 equivalent to O_1, at which the second particle also has the velocity β. To every point on the track of a given particle, there exist equivalent points on the tracks of each other particle.

The importance of equivalent points is that simple, but very important, connections exist between the particle and track variables at the points O_1 and O_2. Any quantities that are solely dependent on the particle velocity will be equal at these points. Thus, for example, $T_1/M_1 = T_2/M_2$ and $P_1/M_1 = P_2/M_2$. Many more similar connections exist.

When $z_1^2 = z_2^2$, the tracks at the points O_1 and O_2 are similar in appearance, the grain densities are the same, and the rates of energy loss of the particles are equal. Then, also, the residual ranges will be in *proportion* to the masses; or $R_1/R_2 = M_1/M_2$.

Often a segment of track is available for study which is not the terminal portion of a particle path. Then its length is considered to be the difference between the residual ranges corresponding to the end points. These and all intermediate points have equivalents on tracks of particles that stop in the emulsion. The grain densities being the same at equivalent points, and the scattering sagittas here being inversely proportional to the masses, it is often possible to identify the particle that produced the track segment.

10.3 Ranges of Slow Protons and Alpha Particles

Of the measurements that can be made on the track of a slow hydrogen or helium nucleus in emulsion, the range provides by far the most reliable estimate of its energy. At low velocities no theory of stopping is accurate enough for this purpose, however, and empirical range-energy tables are used. Lattes, *et al.* (LFC 47) measured the ranges of nuclear

disintegration products of known energies and provided the first reliable data of this sort. Further measurements were made by Bradner, *et al.* (BSBB 50), Cüer and Jung (CJ 51), Rotblat, Catala, and Gibson (RCG 51), and others. Webb (W 48) calculated ranges for Eastman Kodak emulsion. Early range measurements were summarized by Vigneron (V 53). An especially careful study of alpha-particle ranges, which also aided the preparation of proton-range tables, was made by Wilkins (W 51).

It is fortunate that at low velocity the range is somewhat insensitive to the emulsion density because, with the exception of Wilkins', few early experiments were done with good knowledge of the emulsion density. At low velocities the tightly bound electrons of silver and bromine are ineffective in stopping, so that the lighter elements of the gel and water are relatively more effective. As the water content of the emulsion varies, the range changes by a smaller percentage when the velocity is low than when it is high.

In another respect early range measurements were incomplete. Again, with the exception of Wilkins', the methods of making end corrections, if any were made, have not usually been fully disclosed. To obtain the accuracy that is theoretically possible from emulsion measurements, most of the empirical data are not very satisfactory. However, additional information is available. The rates of energy loss at low velocities that are tabulated in Section 9.2 can be used to calculate particle ranges if the constant of integration is evaluated. This has been done (H-B 60) by measuring the range of 0.585 Mev protons. On making the corrections for end effects and density, this range was found to be $6.69 \pm 0.12\ \mu$.

The low-velocity portion of Table 10.4.1 is based on this measurement and on the rates of energy loss that are given in Table 9.2.2. The residual range, λ, of an ideal proton (Section 10.4) of energy τ_0 is then calculated from:

$$\lambda(\tau_0) = \int_{0.585}^{\tau_0} \frac{d\tau}{\iota(\tau)} + 6.69\ \mu \qquad (10.3.1)$$

where $\iota(\tau)$ is the rate of energy loss expressed as a function of the proton kinetic energy.

Ranges of slow protons are accurately known in air, and the simple ratio of air ranges to emulsion ranges is of interest. Air is composed of light elements. The comparison may be expected to show that emulsion is relatively less effective for stopping at low velocities than at high. The integral stopping power of standard emulsion is given in Table 10.3.1; such an effect is demonstrated.

TABLE 10.3.1

INTEGRAL STOPPING POWER OF STANDARD EMULSION

Proton energy (Mev)	Emulsion λ (microns)	Air (at 760 mm, 15°C) R (cm)	Integral stopping power of emulsion
0.1	0.99	0.127	1285
0.2	1.78	0.253	1420
0.3	2.76	0.410	1486
0.4	3.91	0.598	1530
0.6	6.69	1.06	1588
1.0	13.92	2.31	1660
1.5	25.63	4.43	1725
2.0	39.98	7.13	1785
2.5	57.06	10.4	1825
3.0	76.7	14.2	1852
3.5	98.3	18.5	1883
4.0	122.3	23.3	1903

It is useful to know, too, that at low velocities the energy is expressed with an uncertainty of as little as 1% by the three-fifths power of the range. In the interval $\tau = 2$-20 Mev, one can write $\tau = 0.220\lambda^{3/5}$.

As pointed out long ago by Livingston and Bethe (LB 37), the range-energy relation for an alpha particle can be derived from that of a proton by a simple transformation. In Section 10.6 we evaluate the range extension produced by capture of electrons. The observed (end-corrected) range R is related to λ as follows: $R = (M/z^2)(\lambda + B_z)$. For an alpha particle with $\beta > 0.03$

$$R = 0.993\lambda(\beta) + 1.3\ \mu \qquad (10.3.2)$$

This formula is valid for an alpha particle when it has the same velocity as the ideal proton (Section 10.4) of range λ. Wilkins (W 51) made range measurements of ThC′ alpha particles having an energy of 8.776 Mev. On converting his measured ranges to ranges at standard emulsion density (Section 10.7) the mean value is 48.2 μ, in precise agreement with Eq. (10.3.2). These long-range alpha particles often occur in radioactive "stars." They provide a convenient means for density and shrinkage-factor calibration.

At low velocities the asymptotic value 1.3 μ, of B_2 must be replaced by the estimate given in Section 10.6.

10.4 Ranges of Singly Charged Particles

While Eq. (10.3.1) is a good approximation to the range of a proton in emulsion, several small effects must be discussed that affect the relative ranges of singly charged particles of different masses. The effect of the sign of the charge also must be considered.

While the rate of energy loss is nearly independent of the particle mass, there exists a slight dependence in virtue of the appearance of the particle mass in $w_{\max}$ (Eq. 9.1.2). The quantity ι given in Table 9.2.2 is the rate of energy loss by a particle so heavy that the electron mass can be neglected in comparison to it. Furthermore, as mentioned in Section 10.1, ι is an average rate of energy loss brought about by collisions with electrons. Since this fluctuates, the reciprocal of its average value is not identical with the mean distance traversed per unit energy loss. For these reasons Eq. (10.3.1) is approximate. The two effects mentioned above taken together we have called the Lewis effect (L 52, BBS 56).

For emulsion this effect increases the residual range of a particle of mass M (in units of the proton) approximately by the factor $(1 + 0.41/M\iota\tau)$, where one takes for ι and τ the initial values of these quantities (BSB 55).

As a positive particle approaches the end of its range, it tends to become neutralized by electrons that it captures. For heavy ions the reduction of charge produces a substantial increase of range which is treated in more detail in Section 10.6. For singly charged particles, however, it usually is negligible. The range increment is about $0.2M$ in microns (B 53, H-B 60). There is also a slight tendency for negative particle ranges to be reduced relative to those of positive particles because of their greater probability for interacting with nuclei while yet in flight. The probability, of course, depends on the interaction behavior of the particle. Its maximum value, in order of magnitude, can be estimated by putting the cross section for capture by a nucleus equal to $\pi\lambda\!\!\!^{-2}$ where $\lambda\!\!\!^{-}$ is $1/(2\pi)$ times the particle wavelength. With this assumption the maximum fraction of slow negative particles with residual range R that are captured before they come to rest is

$$1 - \exp\left(-\frac{1.8 \times 10^{-4}}{M^{4/3}} R^{1/3}\right)$$

The residual range here is to be expressed in microns. This formula implies that the mean range is reduced no more than about 1.35×10^{-4} $(R/M)^{4/3}\,\mu$. As an example, suppose that for ranges less than $10\,\mu$ the capture in flight of a negative pion is undetectable. Then the measured

mean range of negative pions is reduced by their capture in flight by $\approx 0.037\ \mu$ or less.

Slow particles in emulsion radiate energy in an amount of $3.1 \times 10^{-5}/M$ Mev/cm (B53.1). For mesons and heavier particles, this is quite negligible, but it may be noted that it is mass-dependent, whereas the ionization loss rate does not depend on the mass.

In an elaborate experiment to measure pion and muon masses, a small difference appeared in the apparent relative masses of negative and positive pions (SBB 53). The difference was rather large to dismiss as a statistical fluctuation. It was suggested that it might be an effect of a difference in the stopping power of emulsion for positive and negative particles. E. Fermi (BBS 56) pointed out a specific reason for a difference and calculated this effect. Although not large enough to account completely for the measurements, this correction made the equality of the masses statistically compatible.

Fermi recalled that the scattering cross section (W 33) for a particle, such as an electron describable by Dirac wave functions, contains a relativistic term that depends on the sign of the scatterer's charge. Therefore, if the energy transfer to electrons is evaluated by calculating the electron scattering in the rest frame of the particle, as we have done in Section 9.2, a difference in the energy-loss rate is found. It has subsequently been noticed that the formula Fermi employed for the difference in cross section was incorrect (see Volume II, Eq. 5.1.6), but a difference of the same order of magnitude is still expected.

All of these effects are small for singly charged particles that are heavy compared to an electron. We therefore defined a particle of protonic mass for which none of these small corrections apply. This is called an *ideal proton*. Its range, λ, is given in Table 10.4.1, and its energy-loss rate, ι, is given by Table 9.2.2. The ranges and energy-loss rates of all real particles are then expressible in terms of those for the ideal proton, through mass and charge normalization and by correction terms and factors. Some of the most frequently needed ranges are given as a nomogram in Fig. 10.4.1.

At the time this is written only one range-energy experiment in emulsion has included both precise particle-range and absolute momentum measurements of high-energy particles (B-T 58). Some of the ranges measured were at particle velocities much higher than those for which any previous data existed. A number of precautions such as accurate density determinations also were included in the plan of the measurements.

The experiment was carried out with the 184-inch cyclotron at Berkeley. The primary proton beam of 340 Mev bombarded a

TABLE 10.4.1

Ideal PROTON RANGE-ENERGY RELATION

τ (Mev)	λ (microns)	τ (Mev)	λ (microns)
0.1	0.99	32.5	4347
0.2	1.78	35.0	4952
0.4	3.91	37.5	5591
0.6	6.69	40.0	6264
0.8	10.06	42.5	6970
1.0	13.92	45	7709
1.2	18.26	50	9275
1.4	23.06		
1.6	28.30		
1.8	33.94		
2.0	40.0	τ (Mev)	λ (cm)
2.5	57.0		
3.0	76.4		
3.5	97.9	55	1.097
4.0	121.9	60	1.278
4.5	148.0	65	1.471
5.0	175.9	70	1.675
5.5	206.0	75	1.891
6.0	237.9	80	2.117
6.5	271.5	85	2.353
7.0	307.8	90	2.600
7.5	345.6	100	3.124
8.0	385.3	110	3.686
8.5	426.8	120	4.286
9.0	470.3	130	4.923
9.5	515.4	140	5.594
10	562.5	150	6.298
11	662.0	160	7.034
12	769.1	170	7.800
13	882.0	180	8.596
14	1002	190	9.421
15	1129	200	10.27
16	1262	220	12.06
17	1402	240	13.95
18	1548	260	15.92
19	1700	280	17.99
20.0	1858	300	20.14
22.5	2283	320	22.37
25.0	2744	340	24.67
27.5	3243	360	27.04
30.0	3777	380	29.48

TABLE 10.4.1 *(contd)*

τ (Mev)	λ (cm)	τ (Mev)	λ (cm)
400	31.98	1600	229.9
420	34.53	1800	266.1
440	37.14	2000	302.4
460	39.81	2200	338.8
480	42.52	2400	375.3
500	45.28	2600	411.7
520	48.08	2800	448.0
540	50.93	3000	484.2
560	53.81	3200	520.4
580	56.73	3400	556.4
600	59.69	3600	592.3
620	62.68	3800	628.1
640	65.71	4000	663.7
660	68.76	4200	699.2
680	71.84	4400	734.6
700	74.96	4600	769.9
720	78.09	4800	805.0
740	81.26	5000	840.0
760	84.44	6000	1013
780	87.65	7000	1184
800	90.88	8000	1352
820	94.13	9000	1518
840	97.40	10,000	1682
860	100.7	11,000	1844
880	104.0	12,000	2005
900	107.3	13,000	2164
920	110.7	14,000	2323
940	114.0	15,000	2479
960	117.4	20,000	3249
980	120.8	25,000	4000
1000	124.2	30,000	4735
1200	158.7	35,000	5059
1400	194.1		

polystyrene target with a vertical dimension of 1/2 inch, a radial dimension of 1/16 inch, and a width of 3/8 inch. Nuclear disintegration products and positive mesons that emerged from the target in the forward direction, and with a slight downward component of velocity, were bent by the magnetic field through approximately 180°, and were intercepted by emulsion. Plates and stacks of emulsion were placed along the radial line connecting the cyclotron center and the target. The observed position and entrance angle of each track as it entered the

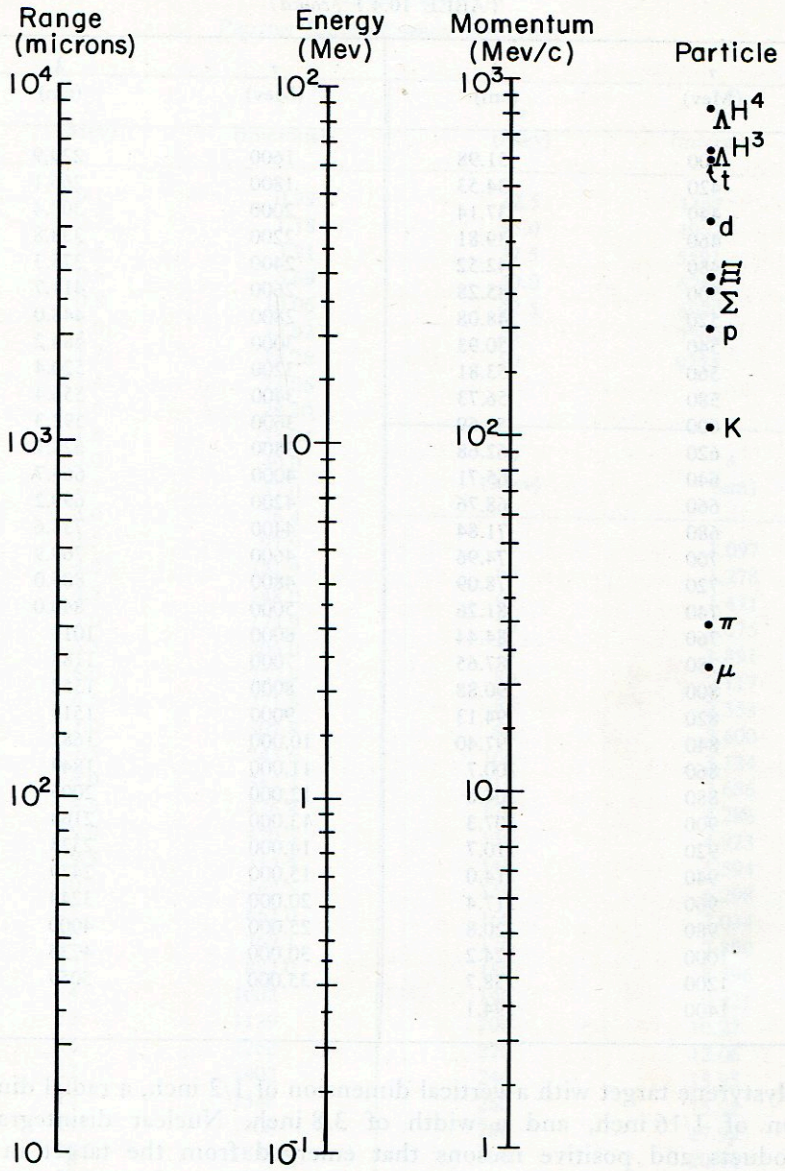

FIG. 10.4.1. Nomogram giving the connection between range, energy, and momentum for singly charged particles. A straight edge passed through the point indicated for each particle cuts the range, energy, and momentum lines at related points. Points corresponding to the masses of the known singly charged particles, excepting electrons, are plotted.

emulsion sufficed for calculating the particle momentum to better than a part in a thousand. Careful allowance for precession of the orbits in the somewhat nonuniform field and for the finite source size was, of course, necessary.

A feature of the exposure technique was the maintenance of the water content of the emulsion near the standard value while it was in the cyclotron vacuum chamber. In the case of pellicles to be exposed to particles entering though a free face of the pellicle, this was done by keeping the emulsion sheets clamped tightly together up to the instant of exposure. Clamped stacks of emulsion were exposed to long-range particles that entered the stack through an edge. That face of the stack previously had been machined flat.

TABLE 10.4.2

PARTICLE RANGE MEASUREMENTS

Particle	τ (Mev)	λ (cm)
α	1.295	$20.7 \pm 0.2 \times 10^{-4}$
p	2.421	$53.9 \pm 0.6 \times 10^{-4}$
t	2.450	$55.67 \pm 0.34 \times 10^{-4}$
d, t, He^3, α	5.00	$175.1 \pm 2.0 \times 10^{-4}$
d	5.477	$204.6 \pm 0.6 \times 10^{-4}$
α	5.477	$205.5 \pm 1.1 \times 10^{-4}$
He^3	10.00	$562.7 \pm 2.6 \times 10^{-4}$
p	13.96	$988.3 \pm 7.4 \times 10^{-4}$
p	21.21	$2056 \pm 5 \times 10^{-4}$
μ^+	36.55	$5345 \pm 22 \times 10^{-4}$
π^+	200	10.31 ± 0.07
π^+	340	24.74 ± 0.10
π^+	540	51.15 ± 0.45
π^+	700	74.97 ± 0.36

In Table 10.4.2 the experimental results are given. The particles measured; the kinetic energy, τ, which has been normalized to the proton; and the range, λ, normalized to the ideal proton, are listed. Also given are the standard deviations of the ranges. The ranges have also been adjusted to emulsion of standard density (3.815 gm/cm^3) (Section 10.7) and a number of small corrections for systematic effects have been made. There is a certain arbitrariness in the corrections, and they may be improved in the future. To quote the original paper on this point: "It is well to remember that small differences in the technique of measurement can easily affect the measured ranges by 1 % or so. For the

greatest accuracy, therefore, this range-energy relation must be used in conjunction with the range-measurement procedure and the corrections described above." The corrections to which reference was made were: (*a*) The depth of penetration into the stack (the x coordinate of the track terminus was compared with the sum $\Sigma\Delta x_i$ of the x components of the segments in each pellicle). The correlation between the unaccounted-for difference, $x - \Sigma\Delta x_i$, and the track length, for a fixed momentum, was used to evaluate the bits of track length that were unseen or otherwise lost between pellicles. Alternatively all tracks with $x - \Sigma\Delta x_i$ amounting to more than $0.007x$ were discarded, and for the accepted tracks, half the difference, $x - \Sigma\Delta x_i$ was added to the sum of the segment lengths. (*b*) The long ranges required a 0.2 % correction because the stack was small and the longer ranges had a lower probability of remaining in the stack to their termini. (*c*) A correction of 0.2 % to the longest ranges was required because the stack was compressed in assembly and the pellicles contracted when the compressive force was released. (*d*) Correction for nonstandard emulsion density was made.

The experimental data were sufficiently complete and accurate that an attempt was made to find a theoretical curve that would fit them (B 58.3). The K- and L-shell tight binding corrections of Walske (W 56) were applied. The data were then found to be best represented by a mean excitation potential of 331 ev. The high-energy portions of Tables 9.2.2 and 10.4.1 correspond to this choice of mean excitation potential. The low-energy portion of the empirical range-energy relation was fitted by permitting a smooth deviation from the Bethe-Bloch theory, the lowest part being purely empirical. In Tables 9.2.2 and 10.4.1 this portion has been further adjusted so as to reflect the best current information.

In the time that has passed since reference (58.3) was published a number of pieces of evidence have tended to the conclusion that a mean excitation potential of 331 ev may be higher than the true value. The precise amount that it may have been overestimated to is too uncertain, however, for an adjustment of the range table to be attempted.

Some of the evidence regarding the mean excitation potential is derived from the ranges in emulsion of K meson and hyperon decay products (BV 61). These data suggest that the theoretical range may be as much as 1 % too high at high velocities, but radiative effects in the decay processes have not been fully evaluated, nor have all the observers adhered to the conventions regarding the corrections. Another kind of evidence comes from stopping power ratios to aluminum, the mean excitation potential of which is thought to have the well-established value of 163 ev (BV 61).

On the other hand, some measured absolute ranges are in excellent accord with the range table (BV 61, F 57), but there is no substantial body of experimental data to imply that the mean excitation potential of emulsion might have been underestimated.

10.5 Electron Ranges

The measurement of an electron range in emulsion offers difficulties because the scattering is so great that it is hard to rectify the track. The measurement is easier if the emulsion sensitivity is very high. Range straggling of at least four sorts also is present. The first is human and instrumental caused by the difficulty in measuring the ranges. Lonchamp and Gegauff (LG 56) have pointed out that for an 8 Kev electron the ratio of silver halide stopping power to that of gel is as high as 2.24. This leads to a large heterogeneity range-straggling effect (see Section 10.8), especially when the track is so short that only a few silver halide crystals have been traversed. Electrons in collision with other electrons also suffer much more violent energy losses in proportion to their total energy than do heavy particles. The finite grain size and variable grain sensitivity cause fluctuations in the points marking the beginning and end of the particle trajectory. This may be a serious cause of straggling when the electron range is only a few microns. At high energies radiation straggling is present also.

These fluctuations of energy-loss rate slightly affect even the electron mean range. A well-known difference between positrons and electrons also exists (RC 54). The energy-loss rate in emulsion for an electron of a low velocity, βc, is less than that of a proton of the same velocity. The difference is about

$$\frac{0.656}{\beta^2} - 0.20 - 0.19\beta^2 \text{ Mev/cm} \qquad (10.5.1)$$

when the velocity is so low that radiation is negligible. The difference is estimated from the difference in the Møller cross section for electron-electron scattering, and the Mott cross section for scattering of an electron by a structureless point charge, which for this purpose is used to represent the proton. The difference in stopping behavior of positrons and electrons similarly is accounted for by the difference in the positron-electron and electron-electron scattering cross sections (Chapter 5, Volume II).

The ranges of electrons and positrons in standard emulsion have been calculated and are presented in Table 10.5.1 along with the range

estimate one obtains from the λ-τ relation. The energy loss by radiation was taken from Table 5.1.1 (see Volume II) in order to make this calculation.

TABLE 10.5.1

CALCULATED ELECTRON AND POSITRON RANGES IN EMULSION OF DENSITY 3.815 GM/CM^3

Kinetic energy (Kev)	Range[a] (microns)	Calculated range (microns)	
		Electron	Positron
10	0.9	1.2	1.0
20	2.9	3.8	3.3
30	6.0	7.6	6.7
40	9.9	12.5	11.3
50	14.6	18.2	16.5
60	20.0	24.8	22.6
70	26.2	32.2	29.7
80	33.1	40.2	37.1
90	40.4	49.0	45.4
100	48.8	58.3	54.2
120	66.0	78.5	73.1
150	94.5	112	105
170	117	137	129
200	151	178	169
250	214	252	242
300	286	329	318
350	359	411	399
400	437	497	486
450	518	586	576
500	600	676	667
550	688	768	761
600	770	861	856
650	851	954	949
700	939	1049	1049
750	1020	1144	1144
800	1117	1240	1247
850	1207	1335	1343
900	1298	1432	1442
950	1388	1528	1539
1000	1480	1625	1639
1200	1840	2008	2034
1400	2220	2387	2424
1600	2580	2762	2814
1800	2935	3133	3200
2000	3295	3500	2581
2200	3660	3861	3958
2400	4005	4420	4332

[a] Estimated from Table 10.4.1.

Measured ranges are in part a matter of definition, because the end corrections and the method of track rectification vary with the observer, but only the short ranges are affected seriously.

Sacton (S 56) has measured four range points and compiled other data. His best curve through the measurements (RZ 48, RZ 49, H 49, B 49, B 51.3) fits the calculated electron range of Table 10.5.1 reasonably well at low velocities, but the measured ranges drop below the theoretical range by 20% before an energy of 200 Kev is reached. The data of Violet (V 53) is also low by roughly 11%. Since Violet's electrons were delta rays, the energies of which were estimated from the angles at which they were projected, an ambiguity caused by the binding energy of the electron complicates the interpretation of his data. The appearance of such a delta-ray track is illustrated by Fig. 9.5.1.

Only about 4% of the range deficiency can be attributed to the common use of dry emulsion of high density for making the measurements. It appears, therefore, that either there is something wrong with the theory, or the track rectification is so difficult that the range is usually underestimated. The latter explanation is preferred. For comparison with typical measurements, electron ranges are possibly better obtained from the λ-τ relation than from the presumably more accurate calculations made specifically for electrons.

Most of the differences between the *theoretical* range-energy relations for electrons and positrons and the λ-τ relation are caused by improbable large energy transfers, which also cause the extreme range straggling characteristic of electrons. Energy transfers of over 20 Kev are easily seen as delta rays, and it may be legitimate either to ignore tracks producing energetic delta rays, or to allow for the delta-ray energy in the measurement. If only "clean" tracks are measured it would be logical to calculate the energy-loss rate using $w_{\max}$ equal to 10 or 20 Kev instead of $(1/2)T$ or T as is usual for electrons or positrons, respectively. This would make the calculated ranges even larger than those of Table 10.5.1, however.

To avoid rectifying the range one may merely count the grains in a track. Ross and Zajac (RZ 48, RZ 49) gave data for NT-4 emulsion, and Lonchamp and Gegauff, for G.5. The statistical error of any measure of the grain count, however, is normally not as low as the range straggling. In addition, one must normalize the emulsion sensitivity and adopt an objective procedure for grain counting (see Chapter 9), if the energy measurement is to be absolute. To count delta rays exceeding a given energy, it may frequently be convenient to count tracks consisting of N or more grains, N being perhaps 4 for $T \approx 20$ Kev. The relative advantage of grain-counting electron tracks over range

measurement is greater for fine-grain emulsions, and very fine-grain highly sensitive emulsions would be good for this purpose. Besides the rectified track length, and the grain number, other measures of the electron range have been studied by Sacton (S 56).

The range of an electron with less than 10 Kev kinetic energy is almost meaningless, but in connection with the study of track structure it is of some importance to describe the behavior of delta rays of a few Kev. The number of such monoenergetic electrons that attain a distance R from the source falls almost linearly with R, and a linear extrapolation of this curve from its point of maximum slope to the point where the tangent cuts the axis is a well defined range. This is very close to the practical maximum range when the number of electrons considered is finite. For example, the number of delta rays determining the width of a heavy-ion track is not large and the electron projected range probably is applicable.

For the elements of atomic number up to about 50, Feldman (F 60) has found that the practical maximum range (not mean range) is given by an expression of the form $R \approx bW^{1.8}$, where b is a constant and W is the electron kinetic energy. In AgBr he computes a range of 0.93 μ at 10 Kev. Thus for AgBr,

$$R = 1.47 \times 10^{-2} W^{1.8} \mu \tag{10.5.2}$$

where W is in Kev. Using the ratio (2.24) of silver bromide to gel stopping power suggested by Lonchamp and Gegauff, the maximum range of electrons from 1 to 10 Kev becomes

$$R = 2 \times 10^{-2} W^{1.8} \mu \tag{10.5.3}$$

for standard emulsion. This range, of course, is to be compared with measured emulsion ranges to which the end corrections have been made.

10.6 Ranges of Multiply Charged Nuclei

As discussed in Chapter 9, when an atom of atomic number z penetrates matter at a high speed, it is divested of its low-velocity electrons. It does not retain those whose root-mean-square velocities are considerably less than its own velocity, but it will keep electrons whose root-mean-square velocities exceed perhaps twice its velocity relative to the stopping medium. Electrons with intermediate velocities are held part of the time. If the atom is completely stripped of electrons, its rate of energy loss is z^2 times that of a proton of the same velocity: $\mathscr{J} = z^2\iota$. At lower velocities, we define an effective charge z^* for energy loss such that $z^{*2} = \mathscr{J}/\iota$. The

quantity z^{*2} is close to the actual mean-square-charge carried by the ion but must not be identified with it. Were the electron-capture effect not present, the end-corrected range of an ion of mass M and charge z in units of the proton would be $(M/z^2)\lambda(\beta)$. However, an additional term, the range extension, must be added to allow for the reduced rate of energy loss caused by the neutralization of its charge. This effect was studied in cloud chambers by Blackett and Lees (BL 32). The effect profoundly influences the range and energy loss of fission fragments, and in this connection it was studied theoretically by Bohr (B 40), Lamb (L 40), and by Knipp and Teller (KT 41). Efforts to evaluate it for emulsion were made by Wilkins (W 51), Lonchamp (L 53.1), and by Papineau (P 56). The range extension was first measured for carbon by Miller (M 52). Early measurements of the ranges of N^{14} ions in emulsion were made by Reynolds and Zucker (RZ 54).

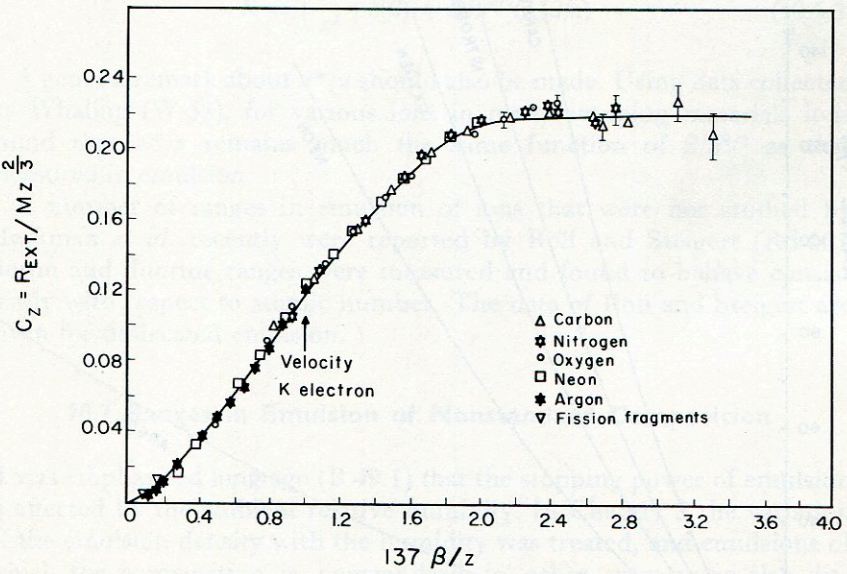

FIG. 10.6.1. The experimental curve of the quantity C_z for emulsion (IDLRL).

When the extension of the range is writen $(M/z^2)B_z$, B_z is the same function of velocity for all isotopes of an element. The quantity B_z was introduced in a study of the range extension of helium, lithium, and boron. Its asymptotic value was measured for these elements (B 53). It is zero for $\beta = 0$. It rises with β monotonically to about $\beta = 2z/137$

(about twice the K-electron velocity), by which time it has reached the asymptotic constant value. Its expression is

$$B_z(\lambda_1) = \int_0^{\lambda_1} \left[\left(\frac{z}{z^*}\right)^2 - 1\right] d\lambda \qquad (10.6.1)$$

An approximate z^3-dependence of the asymptotic value was derived

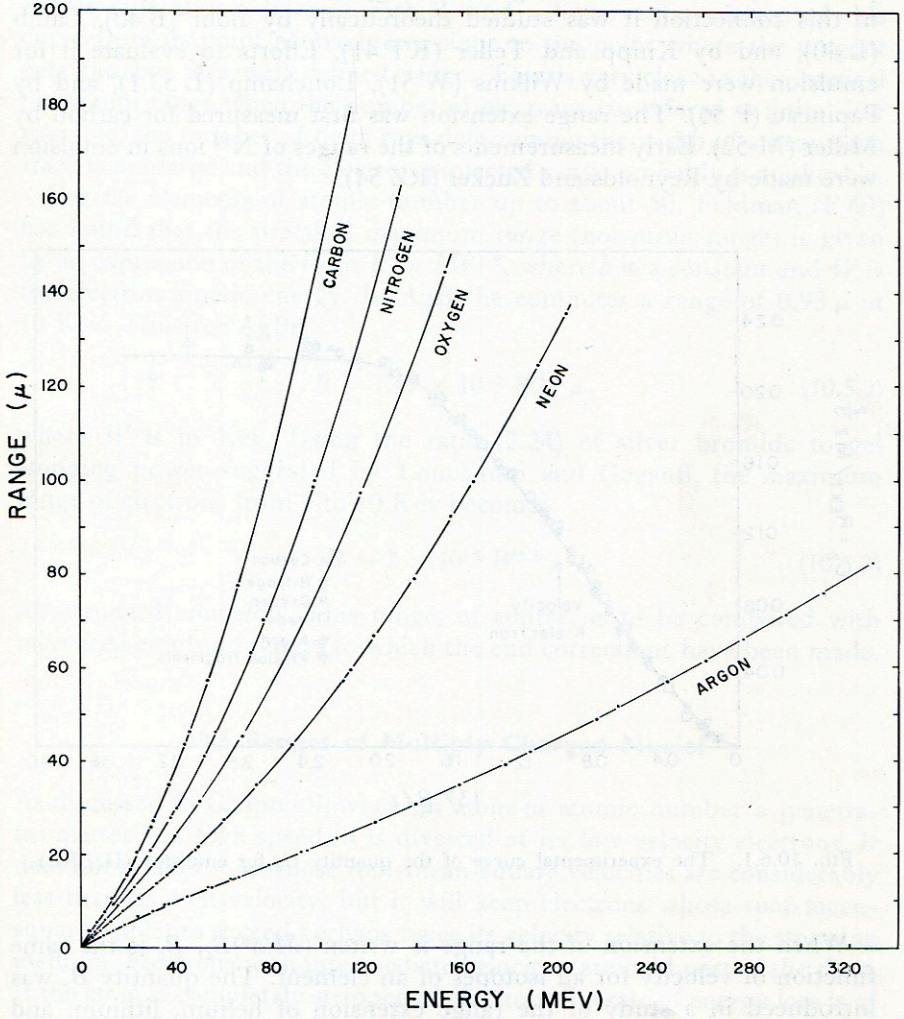

FIG. 10.6.2. Range-energy curves in emulsion for C, N, O, Ne, and A measured by Heckman *et al.* (IDLRL).

(B 53). Later more precise data obtained by Heckman *et al.* (H-B 60) were fitted by

$$B_z \text{ (asymptotic)} = 0.2z^{2.72}\,\mu \tag{10.6.2}$$

The data of Heckman *et al.* were so extensive and accurate, moreover that quite detailed information could be obtained. The quantity $C_z = B_z/z^{8/3}$ was studied as a function of β/z. It was found that in a practical sense it is a universal function of this variable for z at least up to 18. The data are shown in Fig. 10.6.1 for carbon, nitrogen, oxygen, neon, argon, and fission fragments. The measured ranges are graphed in Fig. 10.6.2.

To obtain the end-corrected range in standard emulsion of an atomic nucleus or ion with velocity βc, therefore, one can employ the following formula of Heckman *et al.*

$$R = \left(\frac{M}{z^2}\right)\lambda(\beta) + Mz^{2/3}C_z(\beta/z) \tag{10.6.3}$$

A general remark about z^*/z should also be made. Using data collected by Whaling (W 58), for various ions in many stopping materials it is found that z^*/z remains much the same function of $\beta/z^{2/3}$ as that measured in emulsion.

A number of ranges in emulsion of ions that were not studied by Heckman *et al.* recently were reported by Roll and Steigert (RS 60). Boron and fluorine ranges were measured and found to behave consistently with respect to atomic number. The data of Roll and Steigert are given for desiccated emulsion.

10.7 Ranges in Emulsion of Nonstandard Composition

It was emphasized long ago (B 49.1) that the stopping power of emulsion is affected by the ambient relative humidity. In Chapter 3 the variation of the emulsion density with the humidity was treated, and emulsions of which the composition is nonstandard in other ways were also discussed.

Often a range-energy relation is desired for emulsion that has been loaded with water, for one in which the silver halide concentration has been changed, or for one in which neither are present in the standard proportions.

If the emulsion can be described by concentrations C_e, C_h, and C_w of normal emulsion, silver halide, and water, respectively, expressed as fractions by weight, and the respective rates of energy loss are U_e, U_h, U_w

TABLE 10.7.1

RANGE OF PROTONS IN $AgBr$[a]

τ (Mev)	R_h (gm/cm²)	τ (Mev)	R_h (gm/cm²)	τ (Mev)	R_h (gm/cm²)	τ (Mev	R_h (gm/cm²)	τ (Mev)	R_h (gm/cm²)
0.2	0.00115	15	0.5071	150	26.90	700	315.4	4000	2752
0.4	0.00230	16	0.5661	160	30.01	720	328.6	4200	2898
0.6	0.00371	17	0.6277	170	33.26	740	341.8	4400	3044
0.8	0.00539	18	0.6920	180	36.63	760	355.1	4600	3188
1.0	0.00730	19	0.7591	190	40.12	780	368.6	4800	3333
1.2	0.00941	20	0.8288	200	43.72	800	382.1	5000	3476
1.4	0.01172	22.5	1.014	220	51.26	820	395.7	6000	4187
1.6	0.01423	25	1.216	240	59.22	840	409.4	7000	4885
1.8	0.01692	27.5	1.433	260	67.58	860	423.1	8000	5573
2.0	0.01977	30	1.665	280	76.30	880	436.9	9000	6252
2.5	0.02961	32.5	1.912	300	85.36	900	450.8	10,000	6922
3.0	0.03644	35	2.174	320	94.75	920	464.8	11,000	7586
3.5	0.04629	37.5	2.450	340	104.4	940	478.8	12,000	8242
4.0	0.05719	40	2.740	360	114.4	960	492.9	13,000	8892
4.5	0.06899	42.5	3.044	380	124.7	980	507.0	14,000	9537
5.0	0.08172	45	3.362	400	135.2	1000	521.2	15,000	10,180
5.5	0.09532	50	4.036	420	145.9	1200	665.4	20,000	13,310
6.0	0.1098	55	4.763	440	156.9	1400	812.8	25,000	16,370
6.5	0.1251	60	5.539	460	168.1	1600	961.9	30,000	19,360
7.0	0.1413	65	6.365	480	179.4	1800	1112	35,000	22,310
7.5	0.1584	70	7.239	500	191.0	2000	1263		
8.0	0.1763	75	8.159	520	202.8	2200	1415		
8.5	0.1950	80	9.125	540	214.7	2400	1564		
9.0	0.2144	85	10.13	560	226.8	2600	1714		
9.5	0.2347	90	11.19	580	239.1	2800	1864		
10	0.2557	100	13.42	600	251.5	3000	2014		
11	0.3001	110	15.82	620	264.0	3200	2163		
12	0.3475	120	18.37	640	276.6	3400	2311		
13	0.3978	130	21.07	660	289.5	3600	2459		
14	0.4511	140	23.91	680	302.4	3800	2606		

[a] In this table and in some others in this book, the calculated entries have not been rounded off to the reliable number of significant figures. First differences and derivatives then can be obtained without rounding errors.

TABLE 10.7.2

CALCULATED RANGE ENERGY RELATION FOR PROTONS IN WATER

τ (Mev)	R_w (gm/cm²)	τ (Mev)	R_w (gm/cm²)
0.2	0.00023	64	3.480
0.4	0.00058	68	3.880
0.6	0.00105	72	4.299
0.8	0.00163	76	4.737
1.0	0.00234	80	5.192
1.2	0.00314	84	5.666
1.4	0.00406	88	6.156
1.6	0.00507	92	6.664
1.8	0.00619	96	7.189
2.0	0.00740	100	7.730
2.4	0.01010	120	10.68
2.8	0.01316	140	14.00
3.2	0.01657	160	17.68
3.6	0.02033	180	21.69
4.0	0.02442	200	26.00
4.4	0.02885	240	35.47
4.8	0.03359	280	45.95
5.2	0.03866	320	57.33
5.6	0.04404	360	69.50
6.0	0.04973	400	82.38
6.8	0.06202	500	117.2
7.6	0.07553	600	155.1
8.4	0.09021	700	195.4
9.2	0.1061	800	237.5
10.0	0.1230	900	281.1
12	0.1704	1000	325.9
14	0.2246	1200	418.3
16	0.2855	1400	513.4
18	0.3529	1600	610.3
20	0.4266	1800	708.5
24	0.5927	2000	807.4
28	0.7829	4000	1805
32	0.9965	6000	2785
36	1.233	8000	3745
40	1.491	10,000	4686
44	1.771	14,000	6527
48	2.073	18,000	8325
52	2.394	22,000	10,092
56	2.736	26,000	11,834
60	3.098	30,000	13,556